BAROCLINIC INSTABILITY AND FRONTOGENESIS

A.J. Simmons

European Centre for Medium
Range Weather Forecasts,
England

and

B.J. Hoskins

Department of Meteorology
University of Reading,
England

Seminar 1979

1. INTRODUCTION - THE GOVERNING EQUATIONS

In these lectures, we shall review some fundamental theory and controlled numerical experimentation relating to the dynamics of baroclinic wave development and frontogenesis in middle latitudes of the earth's atmosphere. The understanding that resulted from the early development of this theory was a valuable aid to the improvement of manual forecasting techniques, while with the widespread use of objective numerical forecasting methods, theoretical understanding has become a prerequisite for the diagnosis and correction of many types of deficiency in numerical forecasting systems. The theory of frontogenesis may also be useful for evaluating numerical products, particularly as regards weather on the frontal scale.

Dynamical meteorology has progressed largely by thorough mathematical and numerical analyses of specific phenomena in simplified situations. A significant part of this simplification has been achieved by a systematic reduction in the complexity of the governing equations of fluid dynamics in which attention is restricted to motion of a certain scale, and much current theory has resulted from reduction to a set, known as the quasi-geostrophic equations, particularly amenable to analytic or simple numerical study. We thus begin with a derivation of these equations. We also derive a Boussinesq form of the primitive equations which will be used in later lectures.

The Quasi-Geostrophic Equations

There have been a number of derivations of the quasi-geostrophic equations given in the literature. Here we take as our starting point the adiabatic, frictionless primitive equations of motion written in general vector form with geometric height as the vertical coordinate.

Horizontal momentum equation

$$(\frac{\partial}{\partial t} + \underset{\sim}{u}_h \cdot \nabla_h)\underset{\sim}{u}_h + w\frac{\partial}{\partial z}\underset{\sim}{u}_h + f\underset{\sim}{k} \times \underset{\sim}{u}_h + \frac{1}{\rho}\nabla_h p = 0 \qquad (1.1)$$

Hydrostatic equation

$$\frac{\partial p}{\partial z} + g\rho = 0 \qquad (1.2)$$

Continuity equation

$$(\frac{\partial}{\partial t} + \underset{\sim}{u}_h \cdot \nabla_h)\rho + \rho\nabla_h \cdot \underset{\sim}{u}_h + \frac{\partial}{\partial z}(\rho w) = 0 \qquad (1.3)$$

Thermodynamic equation

$$(\frac{\partial}{\partial t} + \underset{\sim}{u}_h \cdot \nabla_h)\ln\theta + w\frac{\partial}{\partial z}(\ln\theta) = 0 \qquad (1.4)$$

Equation of state

$$\ln\theta = \frac{1}{\gamma}\ln p - \ln\rho - \ln(Rp_s^{-(1-\frac{1}{\gamma})}) \qquad (1.5)$$

Here $\underset{\sim}{u}_h$ is the two-dimensional horizontal velocity vector, $\underset{\sim}{u}_h = (u,v,o)$, w is the vertical velocity, p the pressure, ρ the density and θ the potential temperature. t is time, z is geometric height and ∇_h the two-dimensional horizontal gradient operator. f is the Coriolis parameter, twice the vertical component of the earth's angular rotation, $\underset{\sim}{k}$ is the unit vertical vector, g the acceleration due to gravity, γ the ratio of the specific heat of air at constant pressure to that at constant volume, R the gas constant and p_s the mean reference surface pressure used in the definition of θ:

$$\theta = T\,(p/p_s)^{-(1-\frac{1}{\gamma})}$$

where T is temperature.

We now introduce the horizontal and time-mean pressure, $p_o(z)$, and density $\rho_o(z)$, and write

$$p = p_o(z) + p'' \quad \text{and} \quad \rho = \rho_o(z) + \rho''.$$

$\theta_o(z)$ is defined by

$$\ln\theta_o = \frac{1}{\gamma}\ln p_o - \ln\rho_o - \ln(Rp_s^{-(1-\frac{1}{\gamma})})$$

with

$$\theta = \theta_o(z) + \theta''$$

Defining T_o to be the mean temperature corresponding to potential temperature θ_o, we also write

$$T = T_o(z) + T''$$

The mean static stability, $N^2(z)$, is defined by

$$N^2 = g\frac{d}{dz}\ln\theta_o = g(-\frac{g\rho_o}{\gamma p_o} - \frac{1}{\rho_o}\frac{d\rho_o}{dz})$$

$$= \frac{g}{T_o}(\frac{dT_o}{dz} + \frac{g}{c_p}) \qquad (1.6)$$

N is known as the buoyancy, or Brunt-Väisälä, frequency.

Given the above equations and basic definitions, we now assign the following characteristic scales for a particular atmospheric motion under study:

Time scale	-	T
Horizontal length scale	-	L
Height scale for the motion	-	H
Density height scale	-	H_s
Horizontal velocity scale	-	U
Static stability scale	-	N_o^2

It should be noted that we have already tacitly assumed $H/L \ll 1$ by our use of the primitive equations. If the radius of the earth is denoted by a, the second scaling assumption is

$$\frac{L}{a} \ll 1 \tag{1.7}$$

We may then map that portion of the earth's surface over which the motion of interest takes place onto a plane with x eastward and y northward:

$$\nabla_h = \left(\frac{\partial}{\partial x}, \frac{\partial}{\partial y}, 0\right)$$

Furthermore, we may assign a characteristic value f_o to the Coriolis parameter, although it should be noted that variations in f over the length scale L cannot be neglected in <u>all</u> terms in the governing equations. This will become evident in Equation (1.23).

The following scale assumptions are then additionally made:

$$U/f_o L \ll 1 \tag{1.8}$$

$$\frac{1}{T} \lesssim \frac{U}{L} \tag{1.9}$$

$$f_o UL/N_o^2 H^2 \ll 1 \tag{1.10}$$

$$N_o^2 H/g \ll 1 \tag{1.11}$$

$$H/H_s \lesssim 1 \tag{1.12}$$

Assumption (1.11) may, in fact, be relaxed without introducing much additional complication, but we include it here for simplicity and for direct comparison with most classical studies. For further discussion of this point see White (1977). Taking $U = 20\ ms^{-1}$, $f_o = 10^{-4}\ s^{-1}$, $L = 10^6 m$, $T = 10^5\ s$, $H = 10^4\ m$, $H_s = 10^4\ m$ and $N_o^2 = 10^{-4}\ s^{-2}$, the largest numbers that are assumed to be small compared with unity are $U/f_o L$ and $f_o UL/N_o^2 H^2$, both of which have a value of 0.2. The combination of $U/f_o L$ is known as the Rossby number, Ro.

The balance of terms in the thermodynamic Equation (1.4) implies that

$$|w|_s \lesssim \frac{UH}{L} \tag{1.13}$$

where $|w|_s$ denotes a scale value for the vertical velocity w. Scale assumptions (1.8) and (1.9) may then be used to show that the approximate balance in (1.1) is geostrophic:

$$f_o \underset{\sim}{k} \times \underset{\sim}{u}_h \approx \frac{1}{\rho} \nabla_h p \tag{1.14}$$

Using Equations (1.2), (1.5) and (1.14), and scale assumptions (1.1) and (1.11), we find

$$\left|\frac{\theta''}{\theta_o}\right|_s \sim \left|\frac{p''}{p_o}\right|_s \sim \left|\frac{\rho''}{\rho_o}\right|_s \sim \frac{f_o UL}{gH} = \left(\frac{N_o^2 H}{g}\right)\left(\frac{f_o UL}{N_o^2 H^2}\right) \ll 1 \quad (1.15)$$

Equations (1.1) to (1.5) may now be simplified.

Horizontal momentum equation

To lowest order, the horizontal geostrophic velocity, $\underset{\sim}{u}_g$, is defined by

$$f_o \underset{\approx}{k} \times \underset{\sim}{u}_g = \frac{-1}{\rho_o} \nabla_h p'' \quad (1.16)$$

This allows the introduction of a streamfunction, ψ, for this geostrophic motion

$$\psi = \frac{p''}{\rho_o f_o} \quad (1.17)$$

with $\underset{\sim}{u}_g = \underset{\approx}{k} \times \nabla_h \psi$.

Thermodynamic equation

Since $\left(\frac{\theta''}{\theta_o}\right)_s \ll 1$, Equation (1.4) becomes

$$\left(\frac{\partial}{\partial t} + \underset{\sim}{u}_g \cdot \nabla_h\right) \frac{g\theta''}{\theta_o} + N^2 w = 0 \quad (1.18)$$

showing potential temperature to change at a point as a result of the horizontal advection of perturbation potential temperature by the geostrophic velocity and the vertical advection of the basic potential temperature, θ_o.

Continuity equation

By virtue of (1.18),

$$|w|_s \sim \frac{UH}{L} \quad \frac{f_o UL}{N_o^2 H^2} \tag{1.19}$$

so $$\left|\frac{1}{\rho}\left(\frac{\partial}{\partial t} + \underset{\sim}{u}_h \nabla_h\right)\rho\right|_s \sim \frac{f_o UL}{gH} \cdot \frac{U}{L} \sim \frac{N_o^2 H}{g} \left|\frac{\partial w}{\partial z}\right|_s$$

Equation (1.3) thus reduces to

$$\nabla_h \cdot \underset{\sim}{u}_h + \frac{1}{\rho_o} \frac{\partial}{\partial z}(\rho_o w) = 0 \tag{1.20}$$

It should be noted that if a strict mapping is made from the equations of motion in spherical geometry, with ∇_h as defined previously for the Cartesion geometry, an additional term $v\tan\theta_o/a$ should be added to $\nabla_h \cdot \underset{\sim}{u}_h$ in (1.20), where θ_o is the reference latitude at which $f = f_o$. However, an identical term should also be added to the divergence in (1.23) in this case, and the vorticity equation (1.24) is thus unchanged.

Equation of state

Using (1.15), Equation (1.5) reduces to

$$\frac{\theta''}{\theta_o} = \frac{1}{\gamma}\frac{p''}{p_o} - \frac{\rho''}{\rho_o} = \frac{f_o \rho_o \psi}{\gamma p_o} + \frac{1}{\rho_o g} \frac{\partial}{\partial z}(\rho_o f_o \psi)$$

$$= \frac{f_o}{g}\left(\frac{\partial \psi}{\partial z} + \frac{N^2}{g}\psi\right)$$

using (1.2) and (1.6).

We then use scale assumption (1.8) to obtain

$$\frac{g\theta''}{\theta_o} = f_o \frac{\partial \psi}{\partial z} \tag{1.21}$$

Vorticity equation

Equations (1.17), (1.18), (1.20) and (1.21) still do not yield a prognostic set of equations. To obtain such a set we must consider the next approximation to (1.1) above that of purely geostrophic balance, namely

$$\left(\frac{\partial}{\partial t} + \underset{\sim}{u}_g . \nabla_h\right)\underset{\sim}{u}_g + f\underset{\sim}{k} \times \underset{\sim}{u}_h + \frac{1}{\rho_o}\nabla_h p'' = 0 \tag{1.22}$$

where we have used (1.19) to neglect the vertical advection term. Taking the vertical component of the curl of Equation (1.22), we then obtain the quasi-geostrophic vorticity equation

$$\left(\frac{\partial}{\partial t} + \underset{\sim}{u}_g . \nabla_h\right)\nabla^2\psi + f_o \nabla_h . \underset{\sim}{u}_h + \beta v_g = 0 \tag{1.23}$$

or, using (1.20)

$$\left(\frac{\partial}{\partial t} + \underset{\sim}{u}_g . \nabla_h\right)\nabla^2\psi + \beta v_g - \frac{f_o}{\rho_o}\frac{\partial}{\partial z}(\rho_o w) = 0 \tag{1.24}$$

where $\beta = \frac{df}{dy}$ evaluated at the reference latitude θ_o and v_g is the northward component of the geostrophic wind: $\underset{\sim}{u}_g = (u_g, v_g, o)$. Here

$\nabla_h^2 \psi, = \frac{\partial v_g}{\partial x} - \frac{\partial u_g}{\partial y}$, is the vertical component of the relative vorticity associated with the geostrophic motion, and in the quasi-geostrophic approximation it

changes by the geostrophic advection of relative and planetary vorticity, the second and third terms in (1.24), and by the "stretching" or "shrinking" of the strong vertical vortex tubes associated with the planetary rotation by the ageostrophic vertical motion, the final term in (1.24).

Potential vorticity equations

We may now readily obtain a single prognostic equation. The vertical velocity is eliminated between the thermodynamic and vorticity Equations (1.18) and (1.24), using (1.21) to give

$$\left(\frac{\partial}{\partial t} + \underset{\sim}{u}_g.\nabla_h\right)\left\{ f_o + \beta y + \nabla_h^2\psi + \frac{f_o^2}{\rho_o}\frac{\partial}{\partial z}\left(\frac{\rho_o}{N^2}\frac{\partial \psi}{\partial z}\right)\right\} = 0 \quad (1.25)$$

or

$$\left(\frac{\partial}{\partial t} + \underset{\sim}{u}_g.\nabla_h\right)q = 0 \quad (1.26)$$

where

$$q = f_o + \beta y + \nabla_h^2\psi + \frac{f_o^2}{\rho_o}\frac{\partial}{\partial z}\left(\frac{\rho_o}{N^2}\frac{\partial \psi}{\partial z}\right) \quad (1.27)$$

q is known formally as the quasi-geostrophic quasi-potential vorticity. It is conserved under advection by the horizontal geostrophic velocity field alone, the effect of vertical motion now appearing only implicitly. Having solved (1.24) for ψ using appropriate boundary conditions, horizontal velocities and potential temperature are determined from Equations (1.16), (1.17), and (1.21), while the vertical velocity is given by rewriting (1.18) in the form

$$w = -\frac{f_o}{N^2}\left(\frac{\partial}{\partial t} + \underset{\sim}{u}_g.\nabla_h\right)\frac{\partial \psi}{\partial z} \quad (1.28)$$

The quantity q is related, but not equal to, the quasi-geostrophic approximation to Ertel's potential vorticity, Q, a quantity conserved by three-dimensional adiabatic, frictionless motion (Ertel 1942). In the hydrostatic approximation

$$Q = \frac{1}{\rho}\{(f + \frac{\partial v}{\partial x} - \frac{\partial u}{\partial y})\frac{\partial}{\partial z}\ln\theta - \frac{\partial v}{\partial z}\frac{\partial}{\partial x}\ln\theta + \frac{\partial u}{\partial z}\frac{\partial}{\partial y}\ln\theta\} \quad (1.29)$$

for a plane geometry, and its quasi-geostrophic approximation is

$$Q_g = \frac{N^2}{\rho_o g}\{f_o + \beta y + \nabla_h^2\psi + \frac{f_o^2}{N^2}\frac{\partial^2\psi}{\partial z^2}\} \quad (1.30)$$

with

$$(\frac{\partial}{\partial t} + \underset{\sim}{u}_g.\nabla_h + w\frac{\partial}{\partial z})Q_g = 0.$$

However,

$$w\frac{\partial Q_g}{\partial z} \simeq -\frac{f_o^2}{N^2}\{\frac{\partial}{\partial z}(\frac{N^2}{\rho_o g})\}\{(\frac{\partial}{\partial t} + \underset{\sim}{u}_g.\nabla_h)\frac{\partial\psi}{\partial z}\}$$

from which (1.24) may be directly obtained.

For brevity, any future references to "potential vorticity" in discussing quasi-geostrophic motion will assume the definition (1.27).

The quasi-geostrophic omega equation

The quasi-geostrophic vorticity and thermodynamic equations, (1.24) and (1.18) may be written

$$(\frac{\partial}{\partial t} + \underset{\sim}{u}_g.\nabla_h)\zeta - \frac{f_o}{\rho_o}\frac{\partial}{\partial z}(\rho_o w) = 0 \quad (1.31)$$

and

$$\left(\frac{\partial}{\partial t} + \underset{\sim}{u}_g \cdot \nabla_h\right) \frac{g\theta''}{\theta_o} + N^2 w = 0 \qquad (1.32)$$

while (1.16), (1.17) and (1.21) may be combined to give the thermal wind equation:

$$f_o \frac{\partial \zeta}{\partial z} = \nabla_h^2 \left(\frac{g\theta''}{\theta_o}\right) \qquad (1.33)$$

where ζ is the absolute vorticity $f_o + \beta y + \nabla_h^2 \psi$.
Equation (1.33) may be used to eliminate time derivatives between (1.31) and (1.32):

$$N^2 \nabla_h^2 w + f_o^2 \frac{\partial}{\partial z}\left\{\frac{1}{\rho_o} \frac{\partial}{\partial z}(\rho_o w)\right\} = f_o \frac{\partial}{\partial z}(\underset{\sim}{u}_g \cdot \nabla_h \zeta) - \frac{g}{\theta o} \nabla_h^2 (\underset{\sim}{u}_g \cdot \nabla_h \theta'') \qquad (1.34)$$

Equation (1.34) is one version of what is known as the omega equation after the corresponding form of the equation in pressure coordinates for the "vertical velocity" $\omega \equiv \frac{Dp}{Dt}$. It is a diagnostic equation relating the vertical velocity to the horizontal geostrophic velocity and temperature fields, and may be used in conjunction with (1.33) and either (1.31) or (1.32) as a prognostic system. In this form of the equation, vertical motion is seen to be forced by the vertical derivative of the vorticity advection, the first term on the righthand side of (1.34) and by the horizontal Laplacian of the thermal advection, the second term on the righthand side.

Evaluation of the right hand side of (1.34) can, in fact, be cumbersome, and may involve significant cancellation. Alternative forms of this forcing term have been detailed by Hoskins et al (1978). The "Sutcliffe" form

$$f_o\beta\frac{\partial v_g}{\partial z} + 2f_o\left(\frac{\partial u_g}{\partial z}\cdot\nabla_h\right)\nabla^2\psi \qquad (1.35)$$

involves the neglect of some deformation terms but is comparatively simple to visualise. An exact form with no cancellation problems is

$$f_o\beta\frac{\partial v_g}{\partial z} + 2\nabla_h\cdot\underset{\sim}{Q} \qquad (1.36)$$

where

$$\underset{\sim}{Q} = -\frac{g}{\theta_o}\left(\frac{\partial \underset{\sim}{u}_g}{\partial x}.\nabla_h\theta'',\ \frac{\partial \underset{\sim}{u}_g}{\partial y}.\nabla_h\theta'',0\right)$$

Interpretation of this form, and a number of examples, have been given by Hoskins et al and further applications will be given in later lectures.

The omega equation may be used for qualitative synoptic reasoning as follows. Since it is of Poisson type, if the righthand side is predominantly positive in a particular region, we may expect negative w, i.e. descent, and vice versa. Thus from a given synoptic situation, we may estimate the righthand side, and thus the sign of the vertical motion. Since the vertical velocity is zero at a flat lower surface, and small in the stratosphere, we may then deduce the sign of the stretching term, $\frac{1}{\rho_o}\frac{\partial}{\partial z}(\rho_o w)$, in the vorticity equation, and thus the development of the synoptic pattern. This may be particularly useful for surface development for which the vorticity advection, $\underset{\sim}{u}_g.\nabla_h\zeta$, in (1.31) may be relatively weak.

The ratio of horizontal and vertical scales

In large-scale motion there is commonly a close relationship between the horizontal and vertical length scales L and H. The horizontal advection of vorticity is characteristically of the same order of magnitude as the stretching term in the vorticity equation, and reference to equation (1.25) shows that this implies

$$f_o L \sim N_o H.$$

The effective horizontal length scale $N_o H/f_o$ is known as the "Rossby radius of deformation", L_R. Although this scaling can break down locally for long zonal length scales for which the β-effect becomes important, it will apply to many of the examples considered in subsequent lectures.

The Boussinesq equations

For many of the phenomena to be discussed, the compressibility of the atmosphere is of little importance. Baroclinic waves and frontogenesis occur in the ocean and in laboratory experiments using incompressible liquids. Therefore, it will sometimes be convenient to use a "Boussinesq" set of equations for the atmosphere which are formally equivalent to the full equations for a hydrostatic, incompressible liquid.

One approach to the Boussinesq equations has been given in Hoskins and Bretherton (1972) where a modified pressure coordinate was introduced. From our starting point, it is perhaps simpler to follow Ogura and Phillips (1962) and Williams (1967) and introduce

$$\phi = 2gz + c_p \theta_{oo} (p/p_s)^{\kappa} \qquad (1.37)$$

where θ_{oo} is a constant reference potential temperature.

It is easily shown that

$$\nabla_h \phi = \frac{\theta_{oo}}{\theta} \cdot \frac{1}{\rho} \nabla_h p, \tag{1.38}$$

and

$$\frac{\partial \phi}{\partial z} = 2g - g\frac{\theta_{oo}}{\theta} \tag{1.39}$$

Given the validity of (1.11) then θ differs little from θ_{oo} in the region of interest (typically 10% in the troposphere). Therefore the factor θ_{oo}/θ may be approximated by unity in (1.38) and using $\theta = \theta_{oo} + \theta'$, (1.39) gives

$$\frac{\partial \phi}{\partial z} = 2g - g(1 - \theta'/\theta_{oo} + \ldots)$$

$$\simeq \frac{g}{\theta_{oo}}\theta \tag{1.40}$$

In the continuity equation (1.3), the horizontal advection of density is quite generally less than the vertical advection and

$$w \frac{\partial \rho}{\partial z} / \rho \frac{\partial w}{\partial z} \sim H/H_s \tag{1.41}$$

Thus if the height scale of the vertical motion is small compared with the density scale height, even the vertical advection of density may be neglected.

Using the approximated form of (1.38) and (1.40) and the latter approximation, the primitive equations reduce to their "Boussinesq" form:

$$\frac{D}{Dt}\,\underset{\sim}{u}_h + f\,\underset{\sim}{k} \times \underset{\sim}{u}_h + \nabla_h\phi = 0 \qquad (1.42)$$

$$\nabla.\underset{\sim}{u} = 0 \qquad (1.43)$$

$$\frac{D\theta}{Dt} = 0 \qquad (1.44)$$

$$\frac{\partial\phi}{\partial z} = \frac{g}{\theta_{oo}}\theta \qquad (1.45)$$

where $\underset{\sim}{u} = \underset{\sim}{u}_h + w\underset{\sim}{k}$.

These equations still conserve an Ertel potential vorticity but it has the modified form

$$Q = (f + \frac{\partial v}{\partial x} - \frac{\partial u}{\partial y})\frac{\partial\theta}{\partial z} - \frac{\partial v}{\partial z}\frac{\partial\theta}{\partial x} + \frac{\partial u}{\partial z}\frac{\partial\theta}{\partial y} \qquad (1.46)$$

The streamfunction for the horizontal geostrophic motion is

$$\psi = \phi/f_o \qquad (1.47)$$

and the quasi-geostrophic potential vorticity is

$$q = f_o + \beta y + \nabla_h^2\psi + f_o^2\frac{\partial}{\partial z}(\frac{1}{N^2}\frac{\partial\psi}{\partial z}) \qquad (1.48)$$

This is conserved in horizontal geostrophic motion as in (1.26) and the vertical velocity w is given by (1.28) where now

$$\frac{\partial\psi}{\partial z} = \frac{g\theta}{f_o\theta_{oo}}$$

or by (1.34) with the density terms dropped

2. THE STABILITY OF QUASI-GEOSTROPHIC FLOW: SOME GENERAL CONSIDERATIONS

The earth's atmosphere is characterized by marked horizontal gradients in temperature between the equator and the poles, with zonal-mean westerly winds increasing with height in the troposphere and vertical shears of either sign in the stratosphere and mesosphere. The atmospheric mean state thus possesses significant kinetic and available potential energy.

In the following lectures, we examine under what circumstances such a mean state might be unstable, that is, under what circumstances initially-small perturbations will grow at the expense of either the kinetic or the potential energy of the mean state. We also discuss the structure of the resulting disturbances. Attention is concentrated on baroclinic instability, in which the predominant energy transfer is from zonal-mean to eddy potential energy. This is the process largely responsible for the growth of synoptic-scale disturbances in middle latitudes of the troposphere.

The Hydrodynamic Instability Problem

In examining large-scale instability in the atmosphere, we adopt the usual approach of hydrodynamic instability, seeking linearized solutions for a perturbation of normal-mode form. We let an overbar denote a zonal average (an average around a latitude circle) and a prime denote a deviation from this average. Then

$$\underset{\sim}{u} = \bar{\underset{\sim}{u}} + \underset{\sim}{u}' \ , \ \psi = \bar{\psi} + \psi' \ , \ q = \bar{q} + q' \ , \text{ etc.}$$

Assuming primed quantities to be small, the quasi-geostrophic potential vorticity equation (1.26) becomes

$$\left(\frac{\partial}{\partial t} + \bar{u}\,\frac{\partial}{\partial x}\right)q' + v'\,\frac{\partial \bar{q}}{\partial y} = 0 \qquad (2.1)$$

and if the perturbation has normal mode form:

$$\psi' = \mathrm{Re}\ \{\phi(y,z)e^{ik(x - ct)}\} \tag{2.2}$$

then (2.1) becomes

$$(\bar{u} - c)\left(\frac{f_o^2}{\rho_o}\frac{\partial}{\partial z}\left(\frac{\rho_o}{N^2}\frac{\partial \phi}{\partial z}\right) + \frac{\partial^2 \phi}{\partial y^2} - k^2\phi\right) + \bar{q}_y\phi = 0 \tag{2.3}$$

where

$$\bar{q}_y = \beta - \frac{\partial^2 \bar{u}}{\partial y^2} - \frac{f_o^2}{\rho_o}\frac{\partial}{\partial z}\left(\frac{\rho_o}{N^2}\frac{\partial \bar{u}}{\partial z}\right), \equiv \frac{\partial \bar{q}}{\partial y} \tag{2.4}$$

We assume rigid horizontal boundaries at $z = 0$ and $z = H$, and rigid vertical boundaries at $y = 0$ and $y = Y$. Boundary conditions on the motion are thus

$$\phi = 0 \quad \text{at} \quad y = 0,\ Y \tag{2.5}$$

and

$$w = 0 \quad \text{at} \quad z = 0,\ H \tag{2.6}$$

The latter condition at $z = H$ approximates the increase in static stability at the tropopause, but may be replaced by a condition of bounded energy as $z \to \infty$ with no additional complication to the discussion given here. Equation (2.6) may be rewritten

$$(\bar{u} - c)\frac{\partial \phi}{\partial z} - \frac{\partial \bar{u}}{\partial z}\phi = 0 \quad \text{at} \quad z = 0,\ H \tag{2.7}$$

Equations (2.3), (2.4), (2.5) and (2.7) comprise an eigenvalue problem for c as a function of zonal wavenumber k and the mean state. Instability occurs if there exists a complex eigenvalue c with $k\mathrm{Im}(c) > 0$, since (2.2) may then be written

$$\psi' = e^{kIm(c)t}\ Re\{\phi(y,z)e^{ik(x - Re(c)t)}\},$$

showing the initially small perturbation to grow in time.

The quantity kIm(c) is known as the growth rate of the instability, while Re(c) is the phase speed. Attention is usually concentrated on the solution at the value of k for which the growth rate is a maximum, since given a sufficiently small arbitrary initial perturbation, this most unstable mode is that which would be dominant after a long time interval. It must, however, be stressed that in reality it may not be the most unstable mode which dominates, since there may be a specific scale to the triggering of the instability and more generally differences in non-linear behaviour for different scales. Further discussion is given in later lectures.

A final introductory point is that if (ϕ,c) is a solution of the eigenvalue problem posed above, then so also is (ϕ^*,c^*), where $(\ )^*$ denotes a complex conjugate. Thus corresponding to each growing mode with kIm(c) > 0 there exists a conjugate decaying mode with kIm(c) < 0, and the same phase speed.

The Energetics of the Instability

Some general results concerning the stability of quasi-geostrophic flow may be introduced by considering the equation which describes the growth of the energy associated with the eddy motion. The perturbation momentum and thermodynamic equations for linearized quasi-geostrophic motion are

$$\frac{\partial u'}{\partial t} + \bar{u}\frac{\partial u'}{\partial x} + v'\frac{\partial \bar{u}}{\partial y} - fv' + \frac{1}{\rho_o}\frac{\partial p'}{\partial x} = 0 \qquad (2.8)$$

$$\frac{\partial v'}{\partial t} + \bar{u}\frac{\partial v'}{\partial x} + fu' + \frac{1}{\rho_o}\frac{\partial p'}{\partial y} = 0 \qquad (2.9)$$

$$\frac{\partial \theta'}{\partial t} + \bar{u}\frac{\partial \theta'}{\partial x} + v'\frac{\partial \bar{\theta}}{\partial y} + \frac{N^2}{g}\theta_o w' = 0 \qquad (2.10)$$

and the corresponding expressions for the kinetic (KE) and available potential (AE) energies associated with the perturbation are

$$KE = \int_o^Y \int_o^H \tfrac{1}{2}\rho_o (\overline{u'^2} + \overline{v'^2})dzdy \qquad (2.11)$$

and

$$AE = \int_o^Y \int_o^H \tfrac{1}{2}\rho_o \frac{g^2}{N^2}\overline{(\frac{\theta'}{\theta_o})^2}\, dzdy \qquad (2.12)$$

Multiplication of (2.8) by u', (2.9) by v' and (2.10) by θ', followed by integration by parts and use of the continuity and hydrostatic equations, yields:

$$\frac{\partial}{\partial t}(KE + AE) = \int_o^H \int_o^Y \rho_o \bar{u}\frac{\partial}{\partial y}(\overline{u'v'})dydz + \{-\int_o^H \int_o^Y \rho_o \frac{g^2}{N^2\theta_o^2}\frac{\partial \bar{\theta}}{\partial y}\overline{v'\theta'}\, dydz\} \qquad (2.13)$$

Equation (2.13) describes the rate of change of the energy associated with the eddy motion. The first term on the right-hand side represents the conversion from zonal to eddy kinetic energy that occurs, for example, when there is an eddy transfer of zonal momentum ($\overline{u'v'}$) such as to reduce a jet maximum. The second (bracketed) term is the conversion from zonal to eddy potential energy that occurs when there is a net horizontal eddy heat transfer ($\overline{v'\theta'}$) that tends to reduce the zonal-mean meridional temperature gradient.

Barotropic and Baroclinic Instability

The eigenvalue problem for pure barotropic instability, as studied by Kuo (1949), is obtained from (2.3), (2.4) and (2.5) by setting vertical derivatives equal to zero. The energy equation corresponding to (2.13) is then

$$\frac{\partial}{\partial t}KE = \int_0^Y \rho_o \bar{u} \frac{\partial}{\partial y} (\overline{u'v'}) \, dy$$

and if the zonal flow $\bar{u}$ is unstable, eddy kinetic energy grows at the expense of the zonal-mean flow:

$$\int_0^Y \bar{u} \frac{\partial}{\partial y} (\overline{u'v'}) dy > 0$$

For the classical case of an easterly jet ($\bar{u} < 0$) this energy conversion is accomplished by an eddy transfer of westerly momentum towards the jet maximum, in which case $\frac{\partial}{\partial y}(\overline{u'v'}) < 0$ in the region of strongest zonal-mean flow, as is discussed in Lecture 4.

Writing quite generally

$$\phi(y, z) = Ae^{i\eta} \qquad (2.14)$$

with A and η real,

$$u' = - \mathrm{Re} \{ (\frac{\partial A}{\partial y} + iA\frac{\partial \eta}{\partial y}) \, e^{i(\eta + k(x - ct))} \}$$

and

$$v' = \mathrm{Re} \{ ikAe^{i(\eta + k(x - ct))} \},$$

giving

$$\overline{u'v'} = - \tfrac{1}{2}kA^2 \frac{\partial \eta}{\partial y} . \quad e^{2k\mathrm{Im}(c)t} \qquad (2.15)$$

Thus $\frac{\partial \eta}{\partial y} < 0$ when there is a northward eddy transfer of westerly momentum, and this corresponds to a south-west to north-east tilt of the lines of constant phase of the stream function. In particular, for the case of barotropic instability discussed above, the eddy momentum transfer is associated with a horizontal tilt of troughs and ridges of opposite sign to the horizontal shear of the zonal flow, that is with phase tilts in directions opposite to those which would be produced purely by differential advection of the wave pattern by the horizontal shear flow (Fig. 2.1).

Pure baroclinic instability is obtained by setting $\frac{\partial \bar{u}}{\partial y} = 0$. Eddy kinetic and potential energy grow at the expense of mean-flow energy through the conversion from zonal to eddy potential energy

$$\int_0^H \int_0^Y \frac{\rho_o}{N^2 \theta_o^2} \frac{\partial \bar{\theta}}{\partial y} \overline{v'\theta'} dy dz < 0$$

If the zonal-mean temperature decreases towards the pole, with westerly winds correspondingly increasing with height, this energy conversion implies a largely poleward heat flux. Since from (2.14)

$$\overline{v'\theta'} = \tfrac{1}{2}(k f_o \theta_o / g) A^2 \frac{\partial \eta}{\partial z} e^{2k\,\mathrm{Im}(c)t} \qquad (2.16)$$

this corresponds to a westward tilt of the lines of constant phase with increasing height. This tilt is again in a direction opposite to that which would result from differential advection by the (now vertical) shear flow. Such a westward tilt is a common characteristic of developing disturbances in middle latitudes.

It should also be noted that in the above case of pure baroclinic instability the growth of eddy kinetic energy must occur as a result of a conversion from eddy available potential energy:

$$\int_0^H \int_0^Y \rho_o \frac{g}{\theta_o} \overline{w'\theta'} \, dy dz > 0$$

There is thus a net upward flux of heat.

Generally, when $\bar{u}$ is a function of both latitude and height we may not be able to talk of an exclusively baroclinic or barotropic instability. Clearly if a wave which is growing exhibits a conversion from eddy to zonal kinetic energy it is appropriate to speak of baroclinic instability. In a case in which both conversions are from zonal to eddy forms the general term mixed baroclinic-barotropic instability is appropriate, although if one or other conversion is of dominant magnitude it may be used to label the instability.

Necessary Conditions for Instability

The easterly zonal shear flow in the mid-latitude summer stratosphere is remarkably undisturbed compared with typical tropospheric flows, and the question thus arises as to what configuration of the zonal-mean state is required for instability. By way of introduction, we have noted above that a characteristic of unstable waves is a tendency for their stream function to tilt in a direction opposite to that which would be produced by differential advection by the vertical or horizontal shear flow that gives rise to the instability. Examination of the linearized potential vorticity equation (2.1) shows that either meridional gradients ($\bar{q}_y$) of the potential vorticity associated with the zonal-mean state or constraints due to boundary conditions on the motion, must play an important role in the instability. This is confirmed by the derivation of precise necessary conditions for instability.

Such conditions have been obtained for baroclinic motion by Green (1960), Charney and Stern (1962) and Pedlosky (1964a), and generalized for perturbations of non normal-mode form by Blumen (1968).

Equation (2.3) is multiplied by $\rho_o\phi^*/(\bar{u} - c)$ to give

$$f_o^2\,\phi^*\frac{\partial}{\partial z}\left(\frac{\rho_o}{N^2}\frac{\partial\phi}{\partial z}\right)+\rho_o\phi^*\frac{\partial^2\phi}{\partial y^2}\;\rho_o k^2|\phi|^2+\frac{\rho_o\overline{q_y}(\bar{u}-c^*)|\phi|^2}{|\bar{u}-c|^2}=0 \tag{2.17}$$

Integrating from y = 0 to y = Y, and z = 0 to z = H, and using integration by parts:

$$-\int_o^H\int_o^Y \rho_o\left\{k^2|\phi|^2+\left|\frac{\partial\phi}{\partial y}\right|^2+\frac{f_o^2}{N^2}\left|\frac{\partial\phi}{\partial z}\right|^2\right\}dydz$$

$$+\int_o^H\int_o^Y\frac{\rho_o\overline{q_y}(\bar{u}-c^*)|\phi|^2}{|\bar{u}-c|^2}dydz+\int_o^Y\left[\rho_o\frac{f_o^2}{N^2}\phi^*\frac{\partial\phi}{\partial z}\right]_o^H dy=0 \tag{2.18}$$

and using (2.7)

$$\left[\rho_o\frac{f_o^2}{N^2}\phi^*\frac{\partial\phi}{\partial z}\right]_o^H=\left[\rho_o\frac{f_o^2}{N^2}\frac{\partial\bar{u}}{\partial z}\frac{(\bar{u}-c^*)|\phi|^2}{|\bar{u}-c|^2}\right]_o^H$$

Consider first the case of zero vertical shear at the boundaries. The last term in Equation (2.18) then vanishes. Since the first term is real, taking the imaginary part yields

$$\mathrm{Im}(c)\int_o^H\int_o^Y\frac{\rho_o\overline{q_y}|\phi|^2}{|\bar{u}-c|^2}dydz=0 \tag{2.19}$$

As $\frac{\rho_o|\phi|^2}{|\bar{u}-c|^2}$ is everywhere non-negative, a necessary condition for an unstable wave, for which $\mathrm{Im}(c)\neq 0$, is that $\bar{q}_y$ change sign somewhere within the fluid. Setting $f_o = \beta = 0$, this reduces to Rayleigh's classical criterion that $d^2\bar{u}/dy^2$ change sign for instability of a shear flow. (Indeed, many of the results reviewed in this lecture are generalizations of results of hydrodynamic stability theory reviewed by Drazin and Howard (1966)).

More generally, (2.19) becomes

$$\mathrm{Im}(c) \int_0^Y \{ \int_0^H \frac{\rho_o \bar{q}_y |\phi|^2}{|\bar{u}-c|^2} \, dz + \left(\frac{f_o^2 \rho_o}{N^2} \frac{\partial \bar{u}}{\partial z} \frac{|\phi|^2}{|\bar{u}-c|^2} \right)_{z=H} - \left(\frac{f_o^2 \rho_o}{N^2} \frac{\partial \bar{u}}{\partial z} \frac{|\phi|^2}{|\bar{u}-c|^2} \right)_{z=0} \} \, dy = 0 \qquad (2.20)$$

Instability can thus arise for $\bar{q}_y$ of one particular sign if either

a. the vertical shear of the zonal flow at the lower boundary is of the same sign,

or b. the vertical shear of the zonal flow at the upper boundary is of the opposite sign.

If $\bar{q}_y \equiv 0$, the necessary condition for instability is that the vertical shear be of the same sign at the two boundaries.

As discussed by Bretherton (1966), these conditions may be simplified by defining a generalized potential vorticity gradient

$$\tilde{q}_y = \bar{q}_y + \left(\frac{f_o^2}{N^2} \frac{\partial \bar{u}}{\partial z} \right)_{z=H} \delta(z-H) - \left(\frac{f_o^2}{N^2} \frac{\partial \bar{u}}{\partial z} \right)_{z=0} \delta(z) \qquad (2.21)$$

where $\delta(z)$ is the Dirac delta function. The necessary condition for instability is then that $\tilde{q}_y$ be two-signed.

To picture $\tilde{q}_y$, consider the zonal flow shown in Fig. 2.2a. The corresponding distribution of $\tilde{q}_y$ may be viewed as that of $\bar{q}_y$ for the flow shown in Fig. 2.2b in the limit as the height scale h of the region of curvature decreases to zero.

A further condition is obtained from the real part of (2.18).

This gives

$$\int_0^Y \int_0^H \frac{\rho_o \tilde{q}_y (\bar{u} - \mathrm{Re}(c)) |\phi|^2}{|\bar{u} - c|^2} \, dz dy > 0$$

or, by virtue of (2.20)

$$\int_0^Y \int_0^H \frac{\rho_o \tilde{q}_y (\bar{u} - U_o) |\phi|^2}{|\bar{u} - c|^2} \, dz dy > 0 \quad \text{for any } U_o.$$

It is thus required for instability that

$$\tilde{q}_y (\bar{u} - U_o) > 0 \quad \text{somewhere, for any } U_o.$$

If $\tilde{q}_y$ and $\bar{u}$ are monotonic functions of z, independent of y, choosing U_o to be the value of $\bar{u}$ at the height where $\tilde{q}_y = 0$ shows the condition to become that the sign of the vertical shear of the zonal flow be the same as that of the vertical gradient of $\tilde{q}_y$. In other words, if westerly winds increase with height at the level at which $\tilde{q}_y = 0$, then for instability $\tilde{q}_y$ must be negative at lower levels and positive at higher levels.

These criteria can be given a more physical basis for simplified systems. In the linearized, quasi-geostrophic system perturbation potential vorticity changes at a point due to advection of perturbation potential vorticity by the mean zonal flow and due to advection of mean-state potential vorticity by the perturbation motion (eq . 2.1). Examination of how these two advections may balance to give a coherent wave structure with similar growth and movement at all heights and latitudes suggests the necessary conditions for instability. For an example of such an approach, see Bretherton (1966).

We now consider specific examples from the atmosphere where the instability criterion is satisfied.

a. The mid-latitude troposphere

Here the interior potential vorticity gradient $\bar{q}_y$ is largely positive, due to the β-effect reinforced by both the horizontal and vertical curvature of the mean flow at the jet maximum, and the increase in static stability at the tropopause. The conjunction of this interior distribution and westerly shear of the mean low-level wind provides the classical occurrence of baroclinic instability. It is this case that will be studied in the following lectures.

b. Easterly jets

Flow in the tropics is generally associated with positive $\bar{q}_y$, but commonly comprises an easterly jet, for which the curvature terms $-\partial^2\bar{u}/\partial y^2$ and $\partial^2\bar{u}/\partial z^2$ negative at the jet maximum. For a sufficiently strong jet this too may give rise to a region of negative $\bar{q}_y$. Although the geostrophic approximation may be less accurate in this case, primitive equation calculations such as described by Simmons (1977a) indicate results much as expected from quasi-geostrophic theory.

c. Stratosopheric and mesospheric flows

Marked changes in static stability at the stratopause and mesopause, and strong mean-flow curvature, may give rise to further isolated regions of negative $\bar{q}_y$ in the stratosphere and mesosphere. In this case radiative dissipation and the lack of a rigid boundary to confine the perturbation give rise to lower growth rates than found in the troposphere, and any perturbations which may arise through instability probably play an insignificant role compared with their tropospheric counterparts. References to stratospheric and mesospher calculations may be found in Simmons (1977b).

Bounds on phase speed and growth rate

Bounds on the phase speed and growth rate of eigensolutions of the problem represented by equations (2.3) - (2.7) have been determined by Pedlosky (1964a). These are summarized here. $\bar{U}\min$ denotes the minimum value of $\bar{u}$, and $\bar{U}\max$ the maximum value.

The phase speed, Re(c), is bounded in the following way:

$$\bar{U}\min - \frac{\beta}{2(k^2+\pi^2/Y^2)} \leqslant \mathrm{Re}(c) \leqslant \bar{U}\max. \qquad (2.22)$$

Thus an unstable normal mode can move no faster than the maximum zonal-mean velocity. Its phase speed may be less than the minimum zonal-mean velocity by an amount which depends on the planetary vorticity gradient, β, and the scale of the motion. Such a phase speed has indeed been found in some examples (e.g. Garcia & Norscini 1970), although growth rates in such cases are found to be small.

An inequality linking the real and imaginary parts of c is

$$\left(\tfrac{1}{2}(\bar{U}\max - \bar{U}\min)\right)^2 + \tfrac{1}{2}\beta(\bar{U}\max - \bar{U}\min) \,/\, (k^2+\pi^2/Y^2)$$

$$\geqslant (\mathrm{Re}(c) - \tfrac{1}{2}(\bar{U}\max + \bar{U}\min))^2 + (\mathrm{Im}(c))^2 \qquad (2.23)$$

and this yields the following inequality for growth rate:

$$kc_i \leqslant k\left\{\left(\tfrac{1}{2}(\bar{U}\max - \bar{U}\min)\right)^2 + \tfrac{1}{2}\beta(\bar{U}\max - \bar{U}\min)/(k^2+\pi^2/Y^2)\right\}^{\frac{1}{2}} \qquad (2.24)$$

where $c_i = \mathrm{Im}(c)$. This shows the growth rate generally to decrease as the zonal wavelength becomes large (i.e. as $k \to 0$).

Pedlosky obtained two further bounds on the growth rate. The first is

$$kc_i \leq \tfrac{1}{2} \left(\frac{\text{Max}\{\frac{f_o^2}{N^2} (\frac{\partial \bar{u}}{\partial z})^2 + (\frac{\partial \bar{u}}{\partial y})^2\}}{1 + \pi^2/k^2Y^2} \right)^{\frac{1}{2}} \qquad (2.25)$$

and the second, which holds only if surface zonal winds are zero or uniform in y (and equal at z = 0 and z = H if the upper boundary condition is w = 0 at z = H), is

$$kc_i \leq \left(\frac{\text{Max}\{\bar{u}\bar{q}_y\}}{1 + \pi^2/k^2Y^2} \right)^{\frac{1}{2}} \qquad (2.26)$$

In the special case of infinite meridional scale ($\pi/Y = 0$) and pure baroclinic instability ($\frac{\partial \bar{u}}{\partial y} = 0$), (2.25) gives

$$kc_i \leq .5 \frac{f_o}{N} \text{Max}(\frac{\partial \bar{u}}{\partial z}),$$

a result obtained from energy considerations by Eady (1949).

For comparison, the explicit solution for the Eady model discussed in the following lecture gives

$$\text{Max}(kc_i) = .31 \frac{f_o}{N} \frac{\partial \bar{u}}{\partial z}$$

Inequality (2.24) shows that the large growth rates which can occur for large f_o or small N must occur for short zonal wavelengths (i.e. for large k).

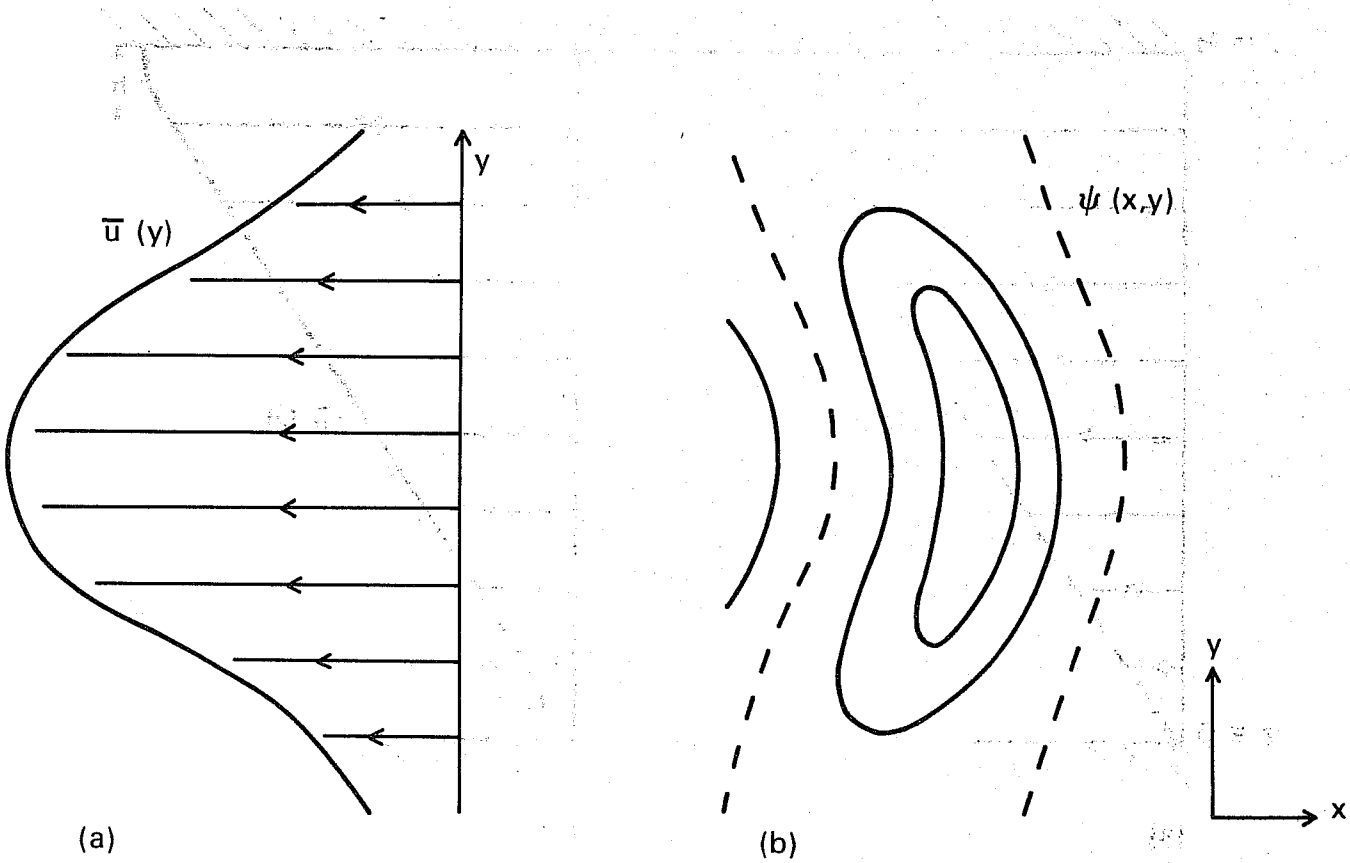

Fig. 2.1 Sketch showing (a) a barotropically unstable easterly jet and (b) the structure of a developing disturbance

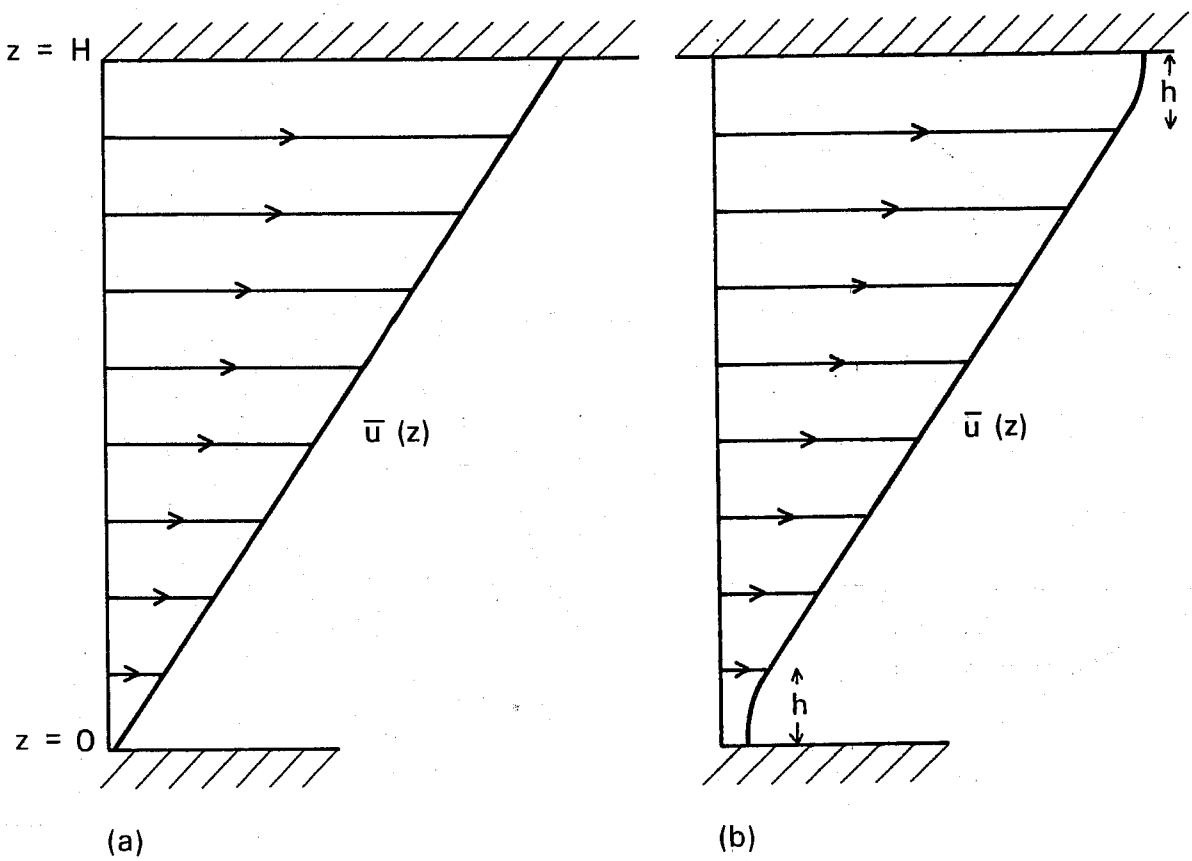

Fig. 2.2 a) A flow with uniform shear in $0 < z < H$

b) A flow with uniform shear in $h < z < H-h$, and no shear at $z = 0$ and $z = H$

3. THE EADY MODEL

The analysis performed in the previous section shows that baroclinic instability may exist. The first two models that showed that the instability actually occurred were due to Charney (1947) and Eady (1949). The Eady model is simpler and is amenable to analytic solution and so we shall concentrate on it in this section. Many of the features of the solutions carry over to much more complicated situations.

We use the Boussinesq form of the quasi-geostrophic equations with $\beta = 0$ and consider a fluid bounded above and below by 2 rigid horizontal planes distance H apart, and having N^2 = const. and a uniform shear $\bar{u}_z = U/H$. This corresponds to a uniform poleward potential temperature gradient $\bar{\theta}_y = - \theta_\infty fU/(gH)$. To simplify the analysis we shall choose a coordinate system moving with the fluid at the mid-level and shift the origin of z also to this level. The basic zonal flow is now $\bar{u} = Uz/H$. The situation is summarised in Fig. 3.1.

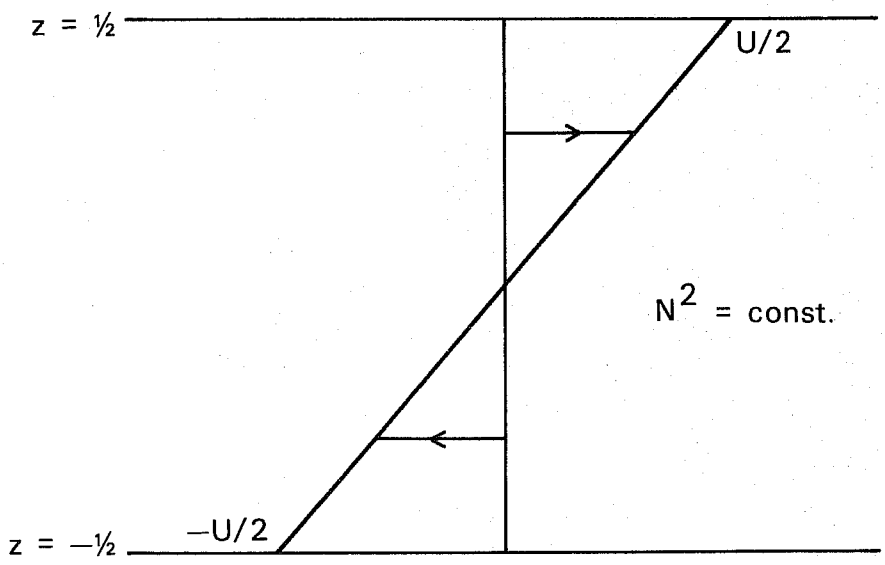

Fig. 3.1 The basic flow for the Eady wave analysis

For this model $\bar{q}_y \equiv 0$ and the perturbation problem (2.1) reduces to

$$\left(\frac{\partial}{\partial t} + \frac{Uz}{H}\frac{\partial}{\partial x}\right) q' = 0 \qquad (3.1)$$

where $$q' = \frac{\partial^2 \psi'}{\partial x^2} + \frac{\partial^2 \psi'}{\partial y^2} + \frac{f^2}{N^2}\frac{\partial^2 \psi'}{\partial z^2} \qquad (3.2)$$

and on $z = \pm H/2$, $w = 0$ or

$$\left(\frac{\partial}{\partial t} + \frac{Uz}{H}\frac{\partial}{\partial x}\right)\frac{\partial \psi'}{\partial z} - \frac{U}{H}\frac{\partial \psi'}{\partial x} = 0 \qquad (3.3)$$

We introduce non-dimensional variables

$$z = H\tilde{z} \quad , \quad x = L_R\tilde{x} \quad , \quad y = L_R\tilde{y} \quad , \quad t = \frac{L_R}{U}\tilde{t} \quad . \quad (L_R = NH/f_0) \qquad (3.4)$$

Suppressing the tildes, the perturbation problem (3.1)-(3.3) becomes

$$\left(\frac{\partial}{\partial t} + z\frac{\partial}{\partial x}\right) q' = 0 \quad , \qquad (3.5)$$

where $$q' = \frac{\partial^2 \psi'}{\partial x^2} + \frac{\partial^2 \psi'}{\partial y^2} + \frac{\partial^2 \psi'}{\partial z^2} \quad , \qquad (3.6)$$

with $$\left(\frac{\partial}{\partial t} + z\frac{\partial}{\partial x}\right)\frac{\partial \psi'}{\partial z} - \frac{\partial \psi'}{\partial x} = 0 \quad \text{on } z = \pm \tfrac{1}{2} \quad . \qquad (3.7)$$

The simplest way of satisfying (3.5) is to make q identically zero for all time. Suppose we look for a solution independent of y of the form

$$\psi' = (a \cosh kz \cos kx + b \sinh kz \sin kx)e^{\sigma t} \qquad (3.8)$$

Since this gives $q' \equiv 0$, the interior equation (3.5) is satisfied identically. Note that we are looking for exponential growth or decay. We must now check that it is possible to satisfy the boundary conditions (3.7) and see what they imply about the growth rate.

Substituting (3.8) into (3.7) gives

$$\sigma k(a\ sh\ c + b\ ch\ s) + zk^2(-a\ sh\ s + b\ ch\ c) - k(-a\ ch\ s + b\ sh\ c) = 0 \text{ on } z = \pm \tfrac{1}{2},$$

where ch, sh, c, s stand for cosh kz, sinh kz, cos kx, sin kx respectively. The coefficients of c and s must separately be zero on both $z = \pm \frac{1}{2}$.

$$\left.\begin{array}{ll} \underline{c} & \sigma a\ sh + b\ kz\ ch - b\ sh = 0 \\ \underline{s} & \sigma b\ ch - a\ kz\ sh + a\ ch = 0 \end{array}\right\} \text{ on } z = \pm \tfrac{1}{2} \quad . \tag{3.9}$$

Note that the coefficient of c is an odd function of z and that of s is an even function of z. Therefore if (3.9) is satisfied at $z = + \frac{1}{2}$ it is automatically satisfied at $z = - \frac{1}{2}$. Thus we require

$$\sigma a\ sh\ k/2 + b\ k/2\ ch\ k/2 - b\ sh\ k/2 = 0 \quad , \tag{3.10}$$

$$\sigma b\ ch\ k/2 - a\ k/2\ sh\ k/2 + a\ ch\ k/2 = 0 \quad . \tag{3.11}$$

Dividing (3.10) and (3.11) by b sh k/2 and a ch k/2 respectively gives

$$\sigma \frac{a}{b} = \coth \frac{k}{2} \left[\tanh \frac{k}{2} - \frac{k}{2}\right] \tag{3.12}$$

$$\sigma \frac{b}{a} = \tanh \frac{k}{2} \left[\frac{k}{2} - \coth \frac{k}{2}\right] \quad . \tag{3.13}$$

These are the conditions that a solution of the form (3.8) is possible. Multiplying them gives an equation for the square of the growth rate:

$$\sigma^2 = \left[\frac{k}{2} - \tanh \frac{k}{2}\right]\left[\coth \frac{k}{2} - \frac{k}{2}\right] \quad . \tag{3.14}$$

Reference to Fig. 3.2 shows that the right hand side is positive for $0 < k < 2.3994$. Thus for wavelengths in this range there are modes that grow exponentially (and also modes

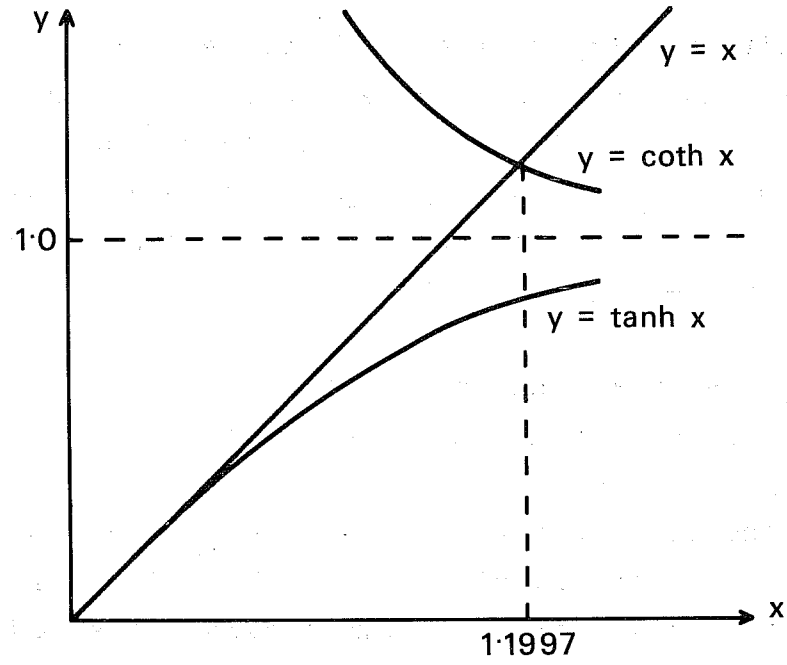

Fig. 3.2 Graphs of y = x, y = coth x and y = tanh x

that decay exponentially). The growth rate curve is sketched in Fig. 3.3

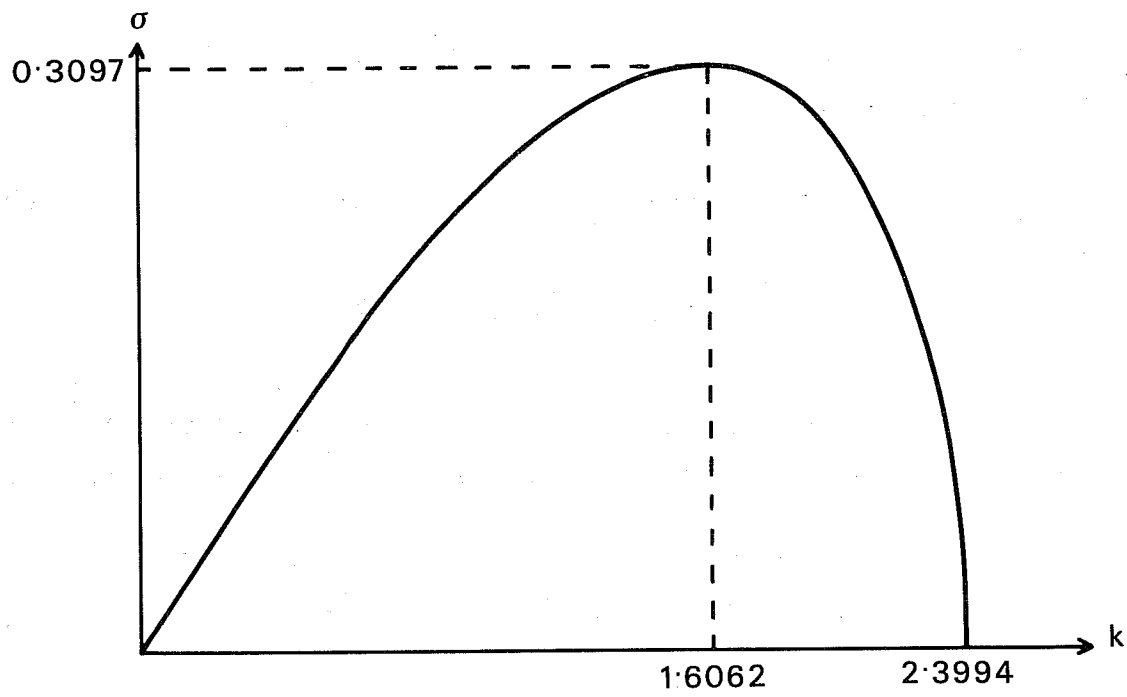

Fig. 3.3 The growth rate curve for two-dimensional Eady modes

There is a short wave cut off at k = 2.3994 and the growth rate maximum is σ = .3097 at k = 1.6062. Taking $N \sim 10^{-2}$ s^{-1}, $f_0 \sim 10^{-4}$ s^{-1}, $H \sim 10^4$ m, $U \sim 30$ m s^{-1} ($L_R = 10^6$ m) there is

growth for wavelengths longer than about 2500 km, with a maximum at about 4000 km wavelength where the e-folding time $T_e = \frac{1}{\sigma} \sim 1.1$ days. Note that the waves are stationary in the coordinate system used. This implies that they move at the speed of the fluid at the mid-level. Such a level is often referred to as the steering level.

The speed is typically 15 m s^{-1}. All these numbers are in good agreement with the observed behaviour of mobile, developing, mid-latitude lows and highs.

To see the structure of the modes, we divide (3.12) by (3.13) and take the square root to give

$$\frac{a}{b} = \pm \left\{ \frac{\frac{k}{2} - \tanh \frac{k}{2}}{\coth \frac{k}{2} - \frac{k}{2}} \right\}^{\frac{1}{2}} \coth \frac{k}{2} \quad . \tag{3.15}$$

From (3.12) $\sigma a/b$ is always negative so that the growing modes correspond to the negative sign in (3.15). The structure of the most unstable mode is typical of the fast growing Eady modes and so for definiteness we concentrate on it. The phases of pressure (streamfunction), temperature and vertical velocity for the most unstable mode are sketched in Fig. 3.4.

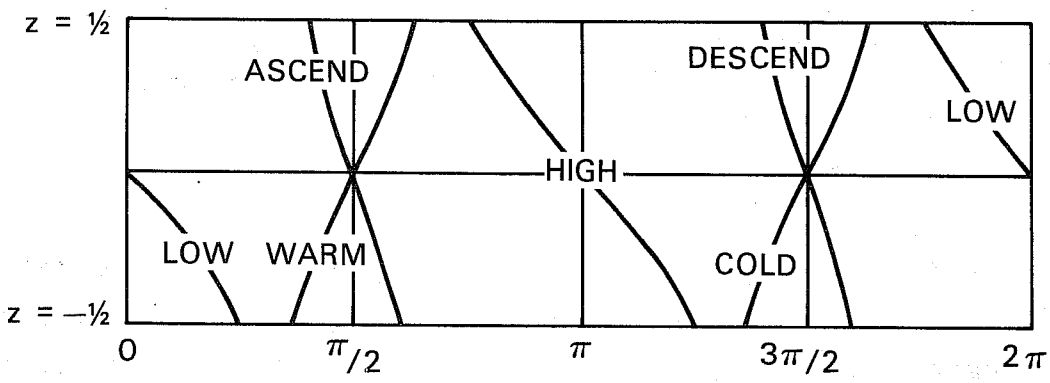

Fig. 3.4 The phases of pressure (ψ), temperature and vertical velocity perturbations for the most unstable two-dimensional Eady mode. One wavelength is shown. For definiteness a has been taken as negative and b positive

The pressure wave tilts westwards with height. The vertical velocity wave tilts rather less westward, but the thermal wave tilts eastwards with height. Ahead of the low, warm air moves polewards and upwards. Behind the low the cold air moves equatorwards and downwards. This is consistent with the energetic description in section 2. In fact any solution of the form (3.8) has northward heat flux $\propto \frac{\partial \psi}{\partial x} \frac{\partial \psi}{\partial z} = -\frac{1}{2} abe^{2\sigma t}$ independent of height.

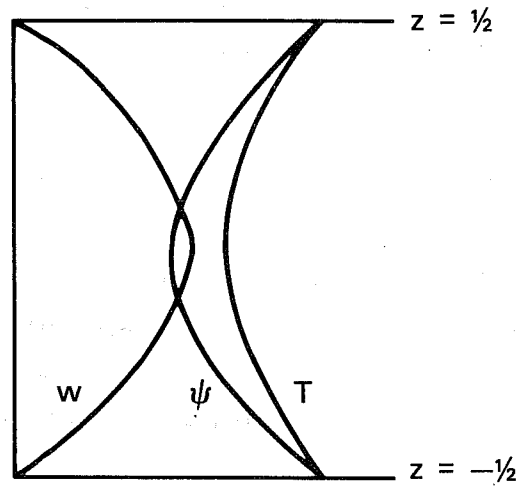

Fig. 3.5 Amplitudes of pressure (ψ), temperature (T) and vertical velocity (w) waves as a function of height for the most unstable two-dimensional Eady mode

The amplitudes of pressure, temperature and vertical velocity as a function of height are shown in Fig. 3.5. The pressure and temperature perturbations are largest on the boundaries, but the vertical velocity is largest at the mid-level. We note that the vertical velocity shown is consistent with the omega equation (1.34)-(1.36) which for the Eady problem becomes

$$N^2 \nabla_h^2 w + f_0^2 \frac{\partial^2 w}{\partial z^2} = 2f_0 \frac{U}{H} \frac{\partial^3 \psi}{\partial x^3} \quad . \qquad (3.16)$$

Considering the lid as representing the tropopause, the structure of the most unstable mode is in good qualitative agreement with that observed.

The decaying modes, corresponding to the positive sign in (3.15) have a similar structure except that the tilts in the vertical are reversed. The pressure wave tilts eastward and the temperature wave tilts westward with height.

The most general y-independent form for the solution of $q' \equiv 0$ would have included in (3.8) terms like $c \sinh kz \cos kx + d \cosh kz \sin kx$. However, the problem for (c,d) separates from and is entirely equivalent to that for (a,b).

If y independence is included by modifying (3.8) to

$$\psi' = \sin \ell y (a \cosh Kz \cos kx + b \sinh Kz \sin kx) e^{\sigma t} \qquad (3.17)$$

where $K^2 = k^2 + \ell^2$, then $q' \equiv 0$ and the boundary conditions now give instead of (3.12) and (3.13)

$$\sigma \frac{a}{b} = \frac{k}{K} \coth \frac{K}{2} \left(\tanh \frac{K}{2} - \frac{K}{2} \right) \qquad (3.18)$$

$$\sigma \frac{b}{a} = \frac{k}{K} \tanh \frac{K}{2} \left(\frac{K}{2} - \coth \frac{K}{2} \right) . \qquad (3.19)$$

For fixed ℓ, the growth rate curve is shifted towards longer wavelengths and the maximum value of growth rate is reduced. For very long total wavelengths, the asymptotic growth rate is unaltered: $\sigma \sim k/\sqrt{12}$.

In terms of the general theory in the previous section we note that the Eady model gives pure baroclinic instability. The modes tilt in the vertical but not in the horizontal. The interior potential vorticity gradient is zero and the instability is possible only because of the temperature gradients (or equivalently the vertical shear in the zonal wind) having the same sign at the upper and lower boundaries. The instability is thus associated with the boundaries and pressure and temperature perturbations are largest there.

Finally, we note that the two-dimensional (y independent) Eady wave is a solution of the nonlinear quasi-geostrophic equations. The zero potential vorticity always satisfies the interior equation and the boundary advection of potential temperature:

$$\left[\frac{\partial}{\partial t} + (\bar{u} + u') \frac{\partial}{\partial x} + v' \frac{\partial}{\partial y}\right]\left(\bar{\theta}(y) + \theta'\right) = 0$$

always simplifies to the linear equation because u' and θ' are independent of y. Quasi-geostrophic theory predicts unbounded growth of the two-dimensional Eady mode, drawing its energy from the uniform equatorward temperature gradient which is infinite in extent.

4. ADDITIONAL LINEAR INSTABILITY THEORY

In this lecture, we present some additional computations and general theory relating to linearly-growing waves. We also discuss the changes to the zonal-mean state that are induced by these waves. This serves as an introduction to the fully non-linear behaviour to be described in Lecture 6.

The inclusion of β and mean density variations

In models of baroclinic instability more complex than that posed by Eady (1949) it is generally necessary to use numerical techniques to solve the complete eigenvalue problem. One such model is that considered originally by Green (1960) in which the β-effect and compressibility are added to the Eady model. Accurate numerical solutions for this case are discussed in this section.

The dotted curves in Fig. 4.1 show growth rate and phase speed as functions of wavenumber for the Eady problem while the solid curves represent corresponding results when the β-effect is added. Here $f_o = 1.03 \times 10^{-4}\ S^{-1}$, $\beta = 1.6 \times 10^{-11}\ S^{-1}$, $N = 10^{-2}\ S^{-1}$, $H = 10^4$m and $Y = 5 \times 10^6$m. The vertical shear is 3 $(ms^{-1})km^{-1}$.

Inclusion of the β-effect has little effect on the growth rate of the most unstable wave, but gives rise to a slowing of its eastward movement by some 4 ms^{-1}, a value close to the $4\frac{1}{2}$ ms^{-1} westward phase movement of a pure Rossby wave with similar length scale. The β-effect also has a pronounced effect on the stability of shorter and longer wavelengths.

For short zonal wavelengths, there is a destabilization which can be related to the distribution of potential vorticity gradients. As in the Eady problem, there is negative $\tilde{q}_y$ at the lower boundary, but with β included, there is also positive $\tilde{q}_y$ throughout the interior of the fluid. Thus however short the wavelength of a disturbance concentrated at the lower boundary, it can be influenced by the change in sign of $\tilde{q}_y$. Asymptotic solutions in the limit as $k \to \infty$ (as derived by McIntyre (1972) for a related problem) reveal a growth rate that is directly proportional to the value of $\tilde{q}_y$ in the interior of the fluid to leading order in k^{-1}.

The β-effect also gives rise to a marked stabilization for low wavenumbers with very weak growth rates for zonal wavelengths longer than about 9000 km. For the latter wavelengths there also exists a neutral mode which behaves as a barotropic Rossby wave in the limit of vanishing wavenumber. Analysis of such long wavelength behaviour has been given by Burger (1962) and Miles (1964) in the content of the instability problem with $H = \infty$ first studied by Charney (1947).

Also shown in Fig. 4.1 are growth rates and phase speeds when a mean density variation with

$$\left(-\frac{1}{\rho_o}\frac{d}{dz}\rho_o\right)^{-1} = 7.315 \text{ km}$$

is included as well as β. A further slowing of phase speeds and short-wave destabilization are evident. These can be linked with an increased interior potential vorticity gradient, which is given in this case by

$$\tilde{q}_y = \beta + \frac{f_o^2 \Lambda}{N^2 \rho_o}\left(-\frac{d\rho_o}{dz}\right),$$

and has the value $6\text{x}10^{-11}\text{s}^{-1}$ for the parameter values noted previously.

The structure of the most unstable normal mode with β and the mean density variation included is shown in Fig. 4.2. In comparison with the Eady model, we note similar overall phase tilts, although the meridional velocity tilts more at low levels, and less at upper levels. The three fields shown are again particularly well correlated at the steering level, which is much lower in this case. The low-level vertical motion is thus better correlated with the temperature field. The amplitude of the temperature wave is significantly larger at lower levels while, conversely, the vertical velocity is somewhat biased towards upper levels. The poleward eddy heat flux (Fig. 4.3) is a maximum at the lower surface. Held (1978) has discussed its dependency on mean-state parameters.

The tendency for the phase of v', w' and θ' to be coincident at the steering level may be seen directly from the perturbation thermodynamic equation. For a normal mode, this gives

$$kIm(c)\theta' + (\bar{u} - Re(c)) \frac{\partial \theta'}{\partial x} + v' \frac{\partial \bar{\theta}}{\partial y} + \frac{N^2 \theta_o}{g} w' = 0$$

Since $\frac{\partial \theta'}{\partial x}$ is 90^o out of phase with θ', <u>if</u> v', θ' and w' are in phase anywhere, this <u>must</u> occur where $\bar{u} - Re(c) = 0$, i.e. at the steering level.

<u>Mean-flow and static stability variations</u>

Modification of the baroclinic instability model to include an upper-level jet maximum and stratospheric increase in static stability is found to give rise to little significant change in the solutions discussed above, although growth rates are slightly smaller, and perturbation velocities larger in the upper troposphere. The eddy heat flux is generally found to be poleward in the lower stratosphere, and thus countergradient. A net upward eddy energy flux is thus

required across the tropopause both to give wave growth in the stratosphere and to compensate for the conversion from eddy to zonal potential energy associated with the counter-gradient heat flux. This accounts for the reduction in growth rate noted above.

A low-level increase in vertical wind shear or decrease in static stability is found to increase the maximum growth rate, which occurs at a shorter wavelength. Examples of stability calculations demonstrating this include those by Eady (1949) and, more recently, by Staley and Gall (1977), while Mansfield (1974) has discussed the application of baroclinic instability theory for a shallow layer of fluid to explain the development of polar lows in cold air outbreaks.

Meridional variations of the basic state

There have been a number of studies of how meridional variation of the mean zonal flow and spherical geometry influence the baroclinic instability problem. Early numerical studies of the influence of zonal-mean shear include those by Eliasen (1961), Pedlosky (1964b) and Brown (1969), while analytical approaches include those of Stone (1969), McIntyre (1970), Simmons (1974) and Gent (1974, 1975). Recent numerical studies (all of which use spherical geometry) include those by Hollingsworth (1975), Moura and Stone (1976), Gall (1976a), Warn (1976), Simmons and Hoskins (1976, 1977) and Frederiksen (1978). Some of these utilized the primitive equations; detailed comparisons by Simmons and Hoskins (1976) showed quasi-geostrophic normal-mode solutions to be generally similar to those of the primitive equations, although such small differences as did occur were often consistent from case to case.

The results of these studies generally show that growth rates, phase speeds and the structure of each mode near the latitude of maximum disturbance are much as found in β-plane models without meridional shear. Meridional shear and spherical geometry influence mainly the meridional scale of a disturbance, the location of its maximum and its horizontal phase tilts.

For a symmetrical jet flow on a β-plane, the disturbance maximum is located at the jet axis for the most unstable mode, and the disturbance generally has a meridional scale given by the geometric mean of its zonal scale and the meridional scale of the jet. Inclusion of spherical geometry gives generally a small poleward shift to the latitude of maximum disturbance, a result which has been interpreted as due both to the larger Coriolis parameter closer to the pole and to the larger angular velocity slightly poleward of the jet maximum.

The eddy momentum flux

For the pure baroclinic instability problem

$$\psi' = \mathrm{Re}\left\{ \phi(z) \sin \frac{m\pi y}{Y} e^{ik(x - ct)} \right\}, \qquad (4.1)$$

where m is an integer.

Such a solution has no phase tilt in the horizontal, and thus no associated eddy momentum flux, $\overline{u'v'}$. This is evidently a major deficiency of the classical theory since observations indicate the flux to play an important role in the momentum balance of the general circulation.

Some general remarks may be made concerning the eddy momentum flux. The imaginary part of (2.17) gives

$$\frac{\partial}{\partial z}\left\{\frac{\rho_o f^2}{N^2}\,\mathrm{Im}\left(\phi^*\frac{\partial\phi}{\partial z}\right)\right\} + \frac{\partial}{\partial y}\left\{\rho_o\,\mathrm{Im}\left(\phi^*\frac{\partial\phi}{\partial y}\right)\right\} = -\,\mathrm{Im}(c)\frac{\rho_o\bar{q}_y|\phi|^2}{|\bar{u}-c|^2},$$

and using (2.14), (2.15) and (2.16), this may be re-written

$$\frac{\partial}{\partial z}\left(\frac{gf_o}{\theta_o N^2}\rho_o\,\overline{v'\theta'}\right) - \rho_o\frac{\partial}{\partial y}\left(\overline{u'v'}\right) = -\tfrac{1}{2}k\,\mathrm{Im}(c)\,\frac{\rho_o\bar{q}_y|\phi|^2}{|\bar{u}-c|^2}\,e^{2k\,\mathrm{Im}(c)t}$$

The right-hand side of (4.2) may be written more generally as $\overline{v'q'}$, and in this form the equation is not restricted to normal-mode disturbances. It has been used by Green (1970) as the basis of a parameterization of the momentum transfer by large-scale eddies. Here we use the form (4.2) to gain insight into the pattern of the eddy momentum flux associated with growing waves.

Consider first purely barotropic motion. Equation (4.2) then becomes

$$\frac{\partial}{\partial y}\left(\overline{u'v'}\right) = \tfrac{1}{2}k\,\mathrm{Im}(c)\bar{q}_y\,\frac{|\phi|^2}{|\bar{u}-c|^2}\,e^{2k\,\mathrm{Im}(c)t}\,, \qquad (4.3)$$

showing the sign of the gradient of the eddy momentum flux to be determined by the sign of the mean potential vorticity gradient, $\beta - d^2\bar{u}/dy^2$ in this case (Kuo 1951). The eddy momentum flux is a maximum or minimum at the latitudes where $\bar{q}_y$ vanishes. For the easterly jet illustrated in Fig. 4.4a, the distribution of $\bar{q}_y$ is sketched in Fig. 4.4b, and the pattern of eddy momentum flux for an unstable wave is shown in Fig. 4.4c.

A generalization of (4.2) for baroclinic motion has been discussed by Held (1975). Integrating Equation (4.2) from z = 0 to z = H, and using the generalized potential vorticity gradient (2.21), we obtain

$$\frac{\partial}{\partial y}\int_0^H \rho_o \overline{u'v'}\, dz = \tfrac{1}{2}k\,\mathrm{Im}(c)\int_0^H \frac{\rho_o \tilde{q}_y |\phi|^2}{|\bar{u}-c|^2} e^{2k\,\mathrm{Im}(c)t}\, dz \qquad (4.4)$$

For each latitude y we may refer to the fluid as being <u>locally</u> stable if $\tilde{q}_y$ is one-signed at that latitude, i.e. if a baroclinic stability analysis applied for latitudinally uniform flow using the flow parameters appropriate to the latitude in question would yield stability. If $\tilde{q}_y$ is positive at all heights, (4.4) shows that

$$\frac{\partial}{\partial y}\int_0^H \rho_o \overline{u'v'}\, dz > 0$$

Thus, if a baroclinically-unstable region is bounded latitudinally by regions in which $\tilde{q}_y$ is positive at all heights, there will be a net eddy transfer of westerly momentum into the region of local instability.

In the earth's troposphere, there is generally a region of marked local baroclinic instability in middle latitudes but at most a weaker baroclinic instability elsewhere, particularly in the tropics where the Coriolis parameter is small. As suggested by the above results, there is a general convergence of the eddy momentum flux in middle latitudes. Some examples of this flux obtained from baroclinic instability calculations with meridional shear and spherical geometry reported by Simmons and Hoskins (1977) are given in Fig. 4.5. The flux has maxima at the ground and at the tropopause. There is a tendency for a bias towards poleward fluxes, although this is not as marked as in atmospheric observations. The influence of spherical geometry on such fluxes has been discussed by Hollingsworth et al (1976).

The mean meridional circulation and zonal-mean changes

Equations for the evolution of the zonal-mean zonal flow, $\bar{u}$, and potential temperature, $\bar{\theta}$, are given in the quasi-geostrophic approximation by

$$\frac{\partial \bar{u}}{\partial t} = f_o \bar{v} - \frac{\partial}{\partial y} (\overline{u'v'}) \tag{4.5}$$

and

$$\frac{\partial \bar{\theta}}{\partial t} = - \frac{\partial}{\partial y} (\overline{v'\theta'}) - \frac{N^2 \theta_o}{g} \bar{w} \tag{4.6}$$

where $\bar{v}$ must be calculated to higher than geostrophic accuracy owing to its multiplication by a Coriolis parameter large compared with the inverse of the time scale of zonal-flow changes (assumption 1.9).

Equations (4.5) and (4.6) are completed by the zonal-mean continuity equation :

$$\frac{\partial \bar{v}}{\partial y} + \frac{1}{\rho_o} \frac{\partial}{\partial z} (\rho_o \bar{w}) = 0 \tag{4.7}$$

and the thermal wind equation

$$\frac{g}{\theta_o} \frac{\partial \bar{\theta}}{\partial y} = - f_o \frac{\partial \bar{u}}{\partial z} \tag{4.8}$$

which may be obtained from (1.16), (1.17) and (1.21).

The circulation in the height-latitude plane defined by $(\bar{v},\bar{w})$ is known as the (Eulerian) mean meridional circulation. In the quasi-geostrophic approximation it maintains thermal wind balance when eddy fluxes of heat and momentum, and more generally diabatic and frictional effects, tend to destroy this balance. It is determined by using (4.7) to introduce

a streamfunction Ψ

$$\bar{v} = \frac{1}{\rho_o} \frac{\partial}{\partial z} (\rho_o \Psi) \qquad \bar{w} = - \frac{\partial \Psi}{\partial y}$$

and (4.8) to eliminate time-derivatives in (4.5) and (4.6):

$$f_o^2 \frac{\partial}{\partial z} \left(\frac{1}{\rho_o} \frac{\partial}{\partial z} (\rho_o \Psi)\right) + N^2 \frac{\partial^2 \Psi}{\partial y^2} = f_o \frac{\partial^2}{\partial y \partial z}(\overline{u'v'}) + \frac{g}{\theta_o} \frac{\partial^2}{\partial y^2}(\overline{v'\theta'}) \tag{4.9}$$

This is a zonally-averaged form of the omega equation (1.34).

For a solution of form (4.1) to the pure baroclinic instability problem, neglecting the exponential growth factor,

$$\overline{v'\theta'} = F(z)\sin^2 \pi y/Y, \text{ and } \overline{u'v'} = 0$$

for some function F(z). Equation (4.9) becomes

$$f_o^2 \frac{\partial}{\partial z}\left(\frac{1}{\rho_o} \frac{\partial}{\partial z} (\rho_o \Psi)\right) + N^2 \frac{\partial^2 \Psi}{\partial y^2} = \frac{2\pi^2 g F(z)}{Y^2 \theta_o} \cos \frac{2\pi y}{Y} \tag{4.10}$$

with

$$\Psi(0,z) = \Psi(Y,z) = \Psi(Y,0) = \Psi(Y,H) = 0 \ .$$

The general solution to (4.10) may readily be written down, but we indicate the form of the solution for the simpler case of the Eady model, for which $F(z)/\theta_o$ is independent of height. In this case

$$f_o^2 \frac{\partial^2 \Psi}{\partial z^2} + N^2 \frac{\partial^2 \Psi}{\partial y^2} = \frac{2\pi^2}{Y^2} F_o \cos \frac{2\pi y}{Y} \tag{4.11}$$

where F_o is constant.

The solution is

$$\Psi = G(z)\cos\frac{2\pi y}{Y} + \sum_{n=1}^{\infty} a_n \sin\frac{n\pi z}{H}\left\{e^{\frac{nf_o\pi y}{NH}} + e^{\frac{nf_o\pi(Y-y)}{NH}}\right\} \quad (4.12)$$

where

$$G(z) = -\frac{F_o}{2N^2}\left\{1 - \left(\sinh\frac{2\pi Nz}{f_o Y} + \sinh\frac{2\pi N(H-z)}{f_o Y}\right)/\sinh\frac{2\pi NH}{f_o Y}\right\}$$

and

$$\tfrac{1}{2}\, a_n\left(1+e^{f_o\pi Y/NH}\right) = -\int_o^H G(z)\sin\frac{n\pi z}{H}\, dz$$

The first term on the right-hand side of (4.12) is a particular integral of (4.11) with a positive value for $\frac{Y}{4} < y < \frac{3Y}{4}$, and negative values for $0 < y < \frac{Y}{4}$ and $\frac{3Y}{4} < y < Y$. The second term is the complementary function satisfying

$$f_o^2 \frac{\partial^2\Psi}{\partial z^2} + N^2 \frac{\partial^2\Psi}{\partial y^2} = 0$$

which yields the correct boundary conditions on $y = 0$ and $y = Y$.

The solution for the most unstable Eady mode is illustrated in Fig. (4.6a) . As first noted by Phillips (1954) the tendency of the eddy heat flux to heat the region $\frac{Y}{2} < y < Y$ and cool the region $0 < y < \frac{Y}{2}$ results in a 3-cell mean meridional circulation with maximum rising and sinking motion close to $y = \frac{3Y}{4}$ and $y = \frac{Y}{4}$, the latitudes of maximum heating and cooling. The cooling and heating associated with this mean upward and downward motion partially compensates for the changes due to the eddy heat flux in the interior of the fluid, but can have no such effect at the boundaries, where changes are largest. In the absence of an eddy momentum flux the zonal-mean zonal

flow changes only due to the Coriolis force associated with the mean meridional motion. At the lower surface westerlies are formed for $\frac{Y}{4} \lesssim y \lesssim \frac{3Y}{4}$, with easterlies elsewhere. Zonal wind changes of similar strength and opposite sign occur at the upper boundary.

Fig. 4.6b shows the mean meridional circulation for the most unstable mode when the β-effect and mean density variation are included. The eddy heat flux (Fig. 4.3) is now significantly larger at lower levels, giving a largest change in zonal-mean temperature at the lower surface. The associated mean meridional circulation however, shows little concentration in lower layers, and zonal-flow changes at the upper surface are only some 20% weaker than at low levels.

These results for upper levels are changed markedly in calculations which include meridional variations of the mean state. It is generally found that the eddy transfer of westerly momentum in towards the jet maximum almost exactly cancels the effect of the Coriolis force due to the mean meridional motion. An example of the resulting change in the zonal-mean zonal flow (again taken from Simmons and Hoskins 1977) is shown in Fig. 4.7. At low levels the eddy momentum flux reinforces the mean meridional circulation in forming the pattern of westerlies and easterlies. The associated change in the zonal-mean temperature is an order of magnitude larger at the surface than at the tropopause. Detailed examples and discussion may be found in Simmons and Hoskins (1976, 1977).

Vertical eddy heat transfer

We conclude this lecture with some remarks on vertical eddy heat transfer. Equation (4.6) shows that in the quasi-geostrophic approximation the zonal-mean temperature changes only due to a horizontal eddy heat flux and to mean vertical motion. The vertical velocity scaling (1.19) is such that the convergence of the vertical eddy heat flux, $\frac{\partial}{\partial z}(\overline{w'\theta'})$ is formally negligible. A consequence of this is that the area-mean temperature, and thus the mean static stability, does not change in time.

Quasi-geostrophic theory does yield an estimate of the vertical eddy heat flux, and Fig. (4.2) shows vertical velocity and temperature to be better correlated at the height when the product of their amplitudes is a maximum than are horizontal velocity and temperature. This results in the vertical eddy heat flux playing a more significant role than scaling alone suggests, as illustrated by Simmons and Hoskins (1976) in a strict comparison of zonal-mean changes in the primitive-equation and quasi-geostrophic systems.

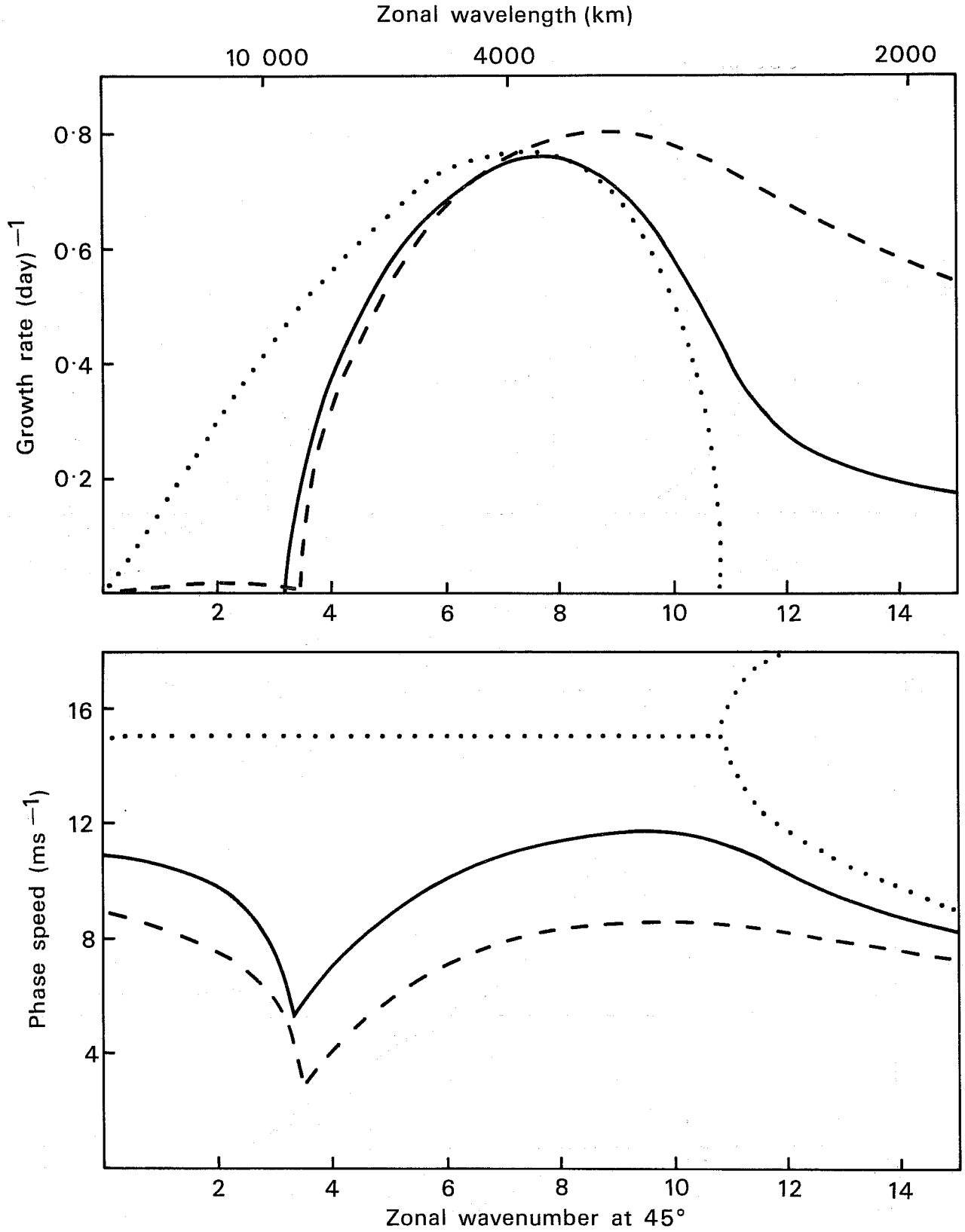

Fig. 4.1 Growth rates and phase speeds as functions of zonal wavenumber for the Eady model (dotted), with β included (solid), and with β and compressibility included (dashed).

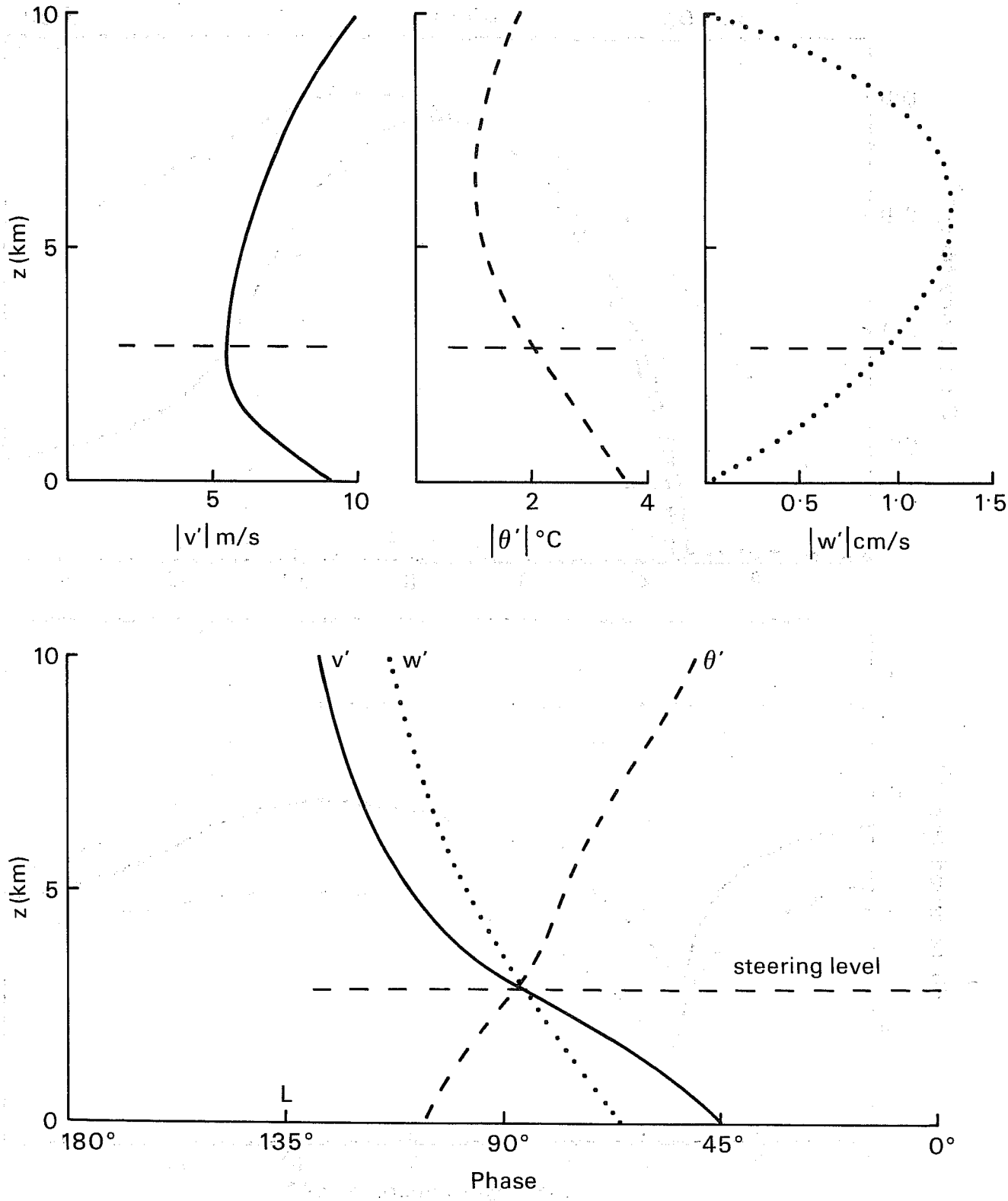

Fig. 4.2 Aspects of the vertical structure of the most unstable mode shown in Fig. 4.1 for the case with the β-effect and compressibility included. The amplitude of the wave is chosen such that the maximum velocity perturbation is 10 ms^{-1}. L denotes the position of the surface low. Consistent with approximation (1.11) θ_o has been assigned a uniform value of 250 K.

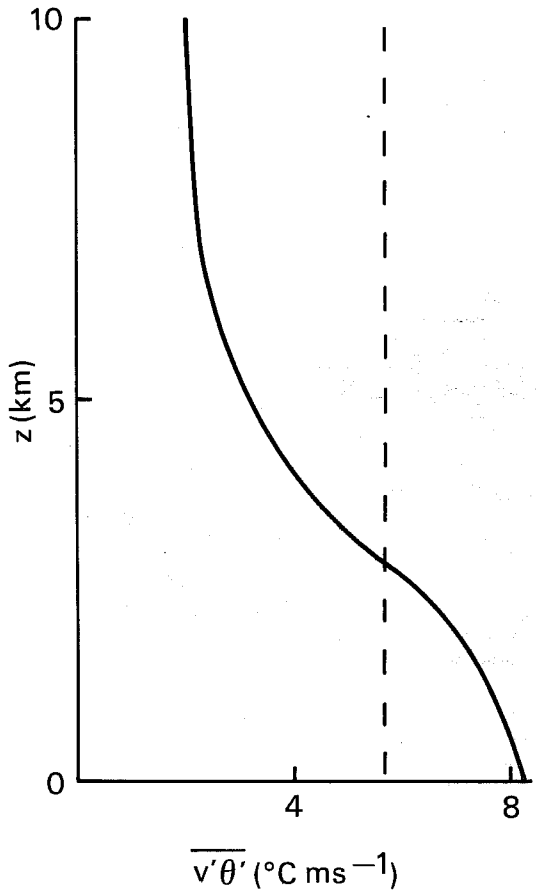

Fig. 4.3 The variation with height of the poleward eddy heat flux for the most unstable Eady mode (dashed) and for the most unstable mode with β and compressibility included (solid). The normalization is as in Fig.4.2.

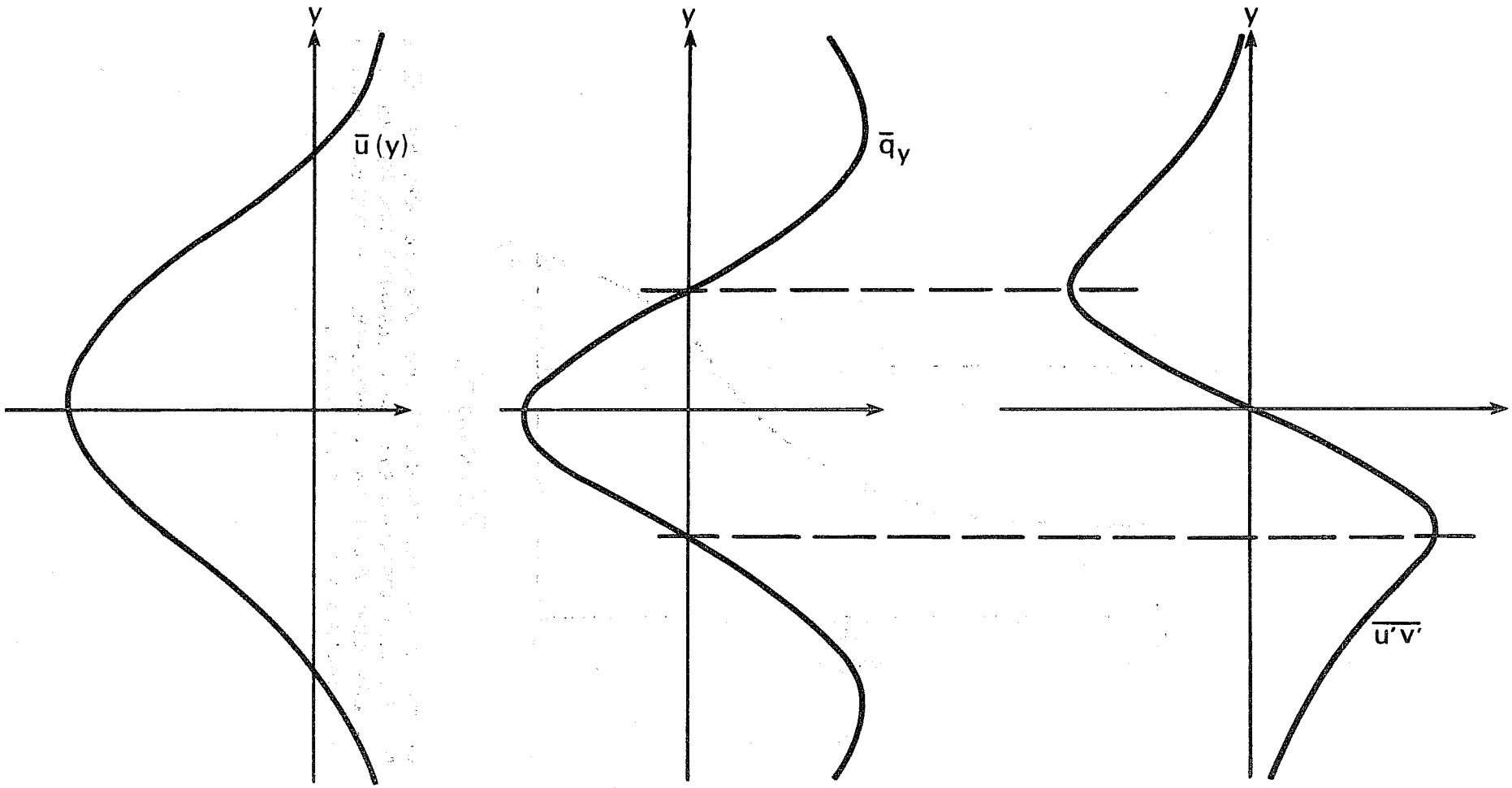

Fig. 4.4 Characteristic distributions of zonal flow, $\bar{u}(y)$, mean vorticity gradient, q_y, and eddy momentum flux, $\overline{u'v'}$, for barotropic instability.

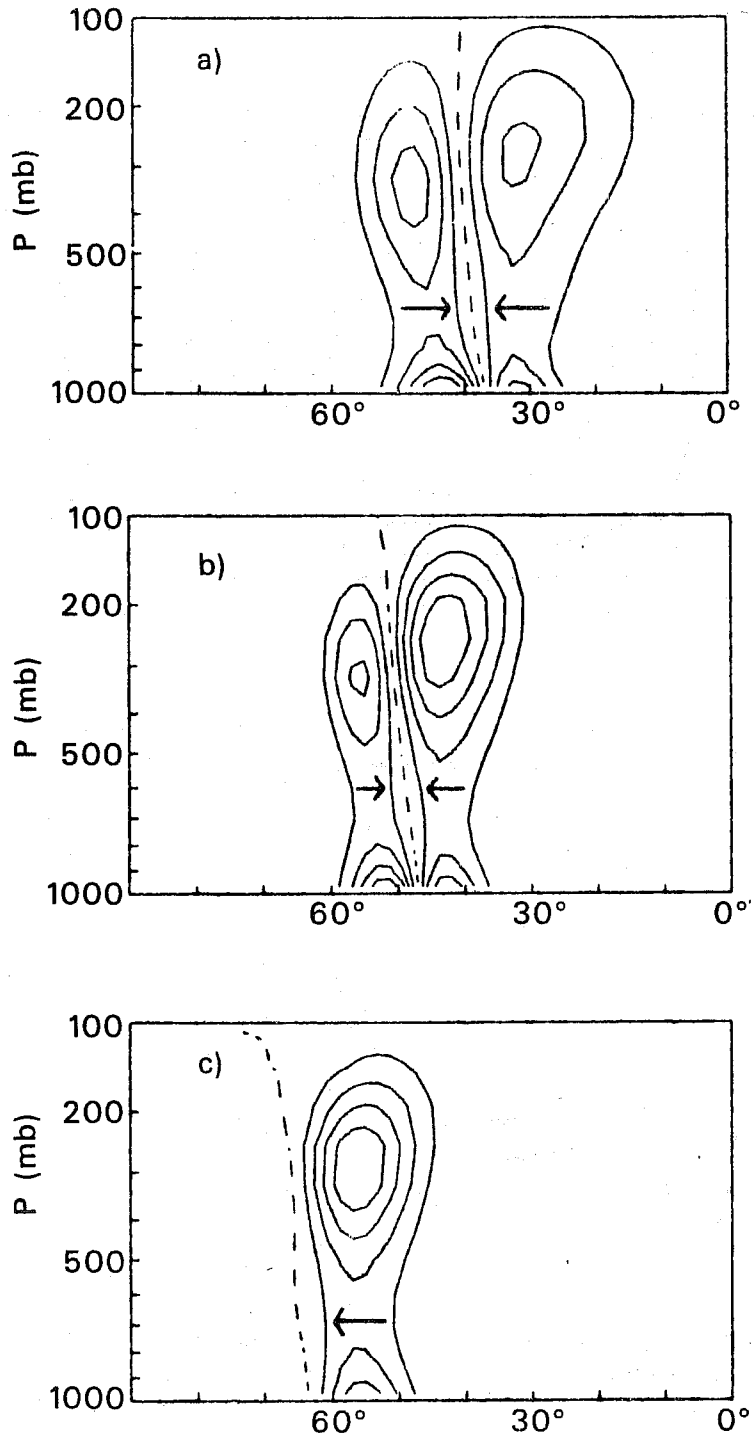

Fig. 4.5 Meridional (pressure/latitude) cross-sections showing typical results of computations of poleward eddy momentum fluxes associated with baroclinic instabilities of jet-like flows in a spherical geometry. Jet maxima are at 30^{o}, 45^{o} and 55^{o} latitude for cases a), b), and c) respectively.

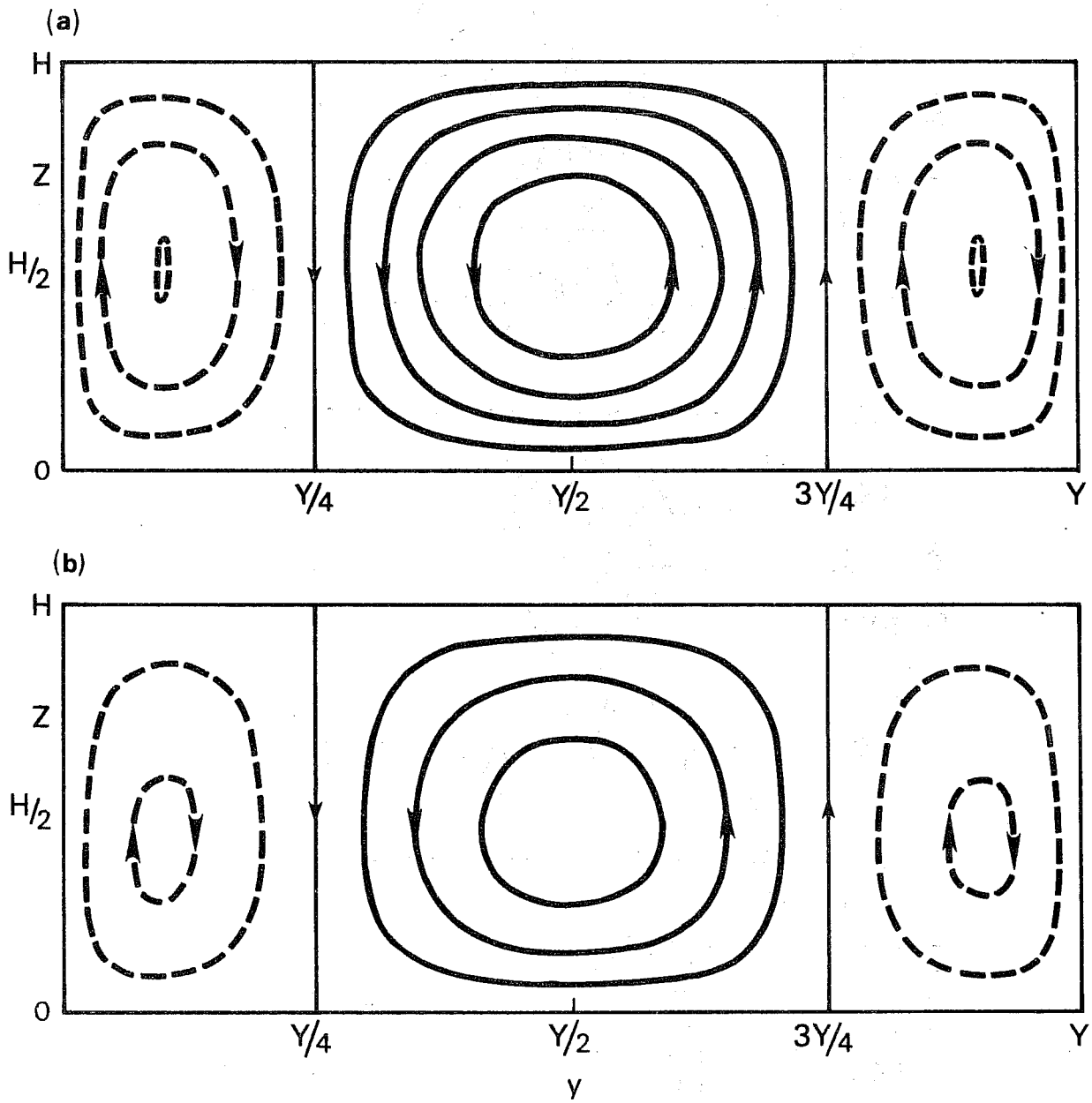

Fig. 4.6 Meridional cross-sections showing the mean-meridional circulation induced by a) and the most unstable Eady mode, and b) the most unstable mode with β and compressibility included.

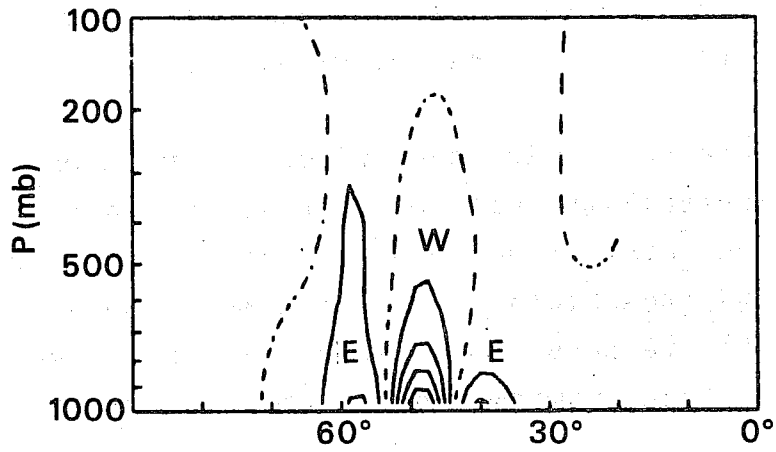

Fig. 4.7 The net rate of change of zonal-mean zonal velocity resulting from a baroclinic instability. The corresponding poleward momentum flux is shown in Fig. 4.5. The zero contour is dashed and W and E denote respectively westerly and easterly accelerations.

5. THE INITIAL-VALUE PROBLEM FOR BAROCLINIC INSTABILITY

In the preceding lectures we have adopted a normal-mode approach, seeking solutions for disturbances to a zonal flow which grow exponentially, move uniformly, and possess a purely sinusoidal dependence on longitude. We have thus considered the growth of a wave in the presence of a sequence of identical waves both upstream and downstream. Attention has been concentrated on the mode whose wavelength gives rise to the maximum growth rate.

In this lecture we examine the initial-value problem for baroclinic instability, with particular emphasis on the case for which normal-mode stability was first examined by Eady (1949) (see Lecture 3). The discussion will be focussed on the response to an initially-localized perturbation. We thus examine dispersion in an unstable fluid.

The initial-value problem for the Eady model was first considered by Pedlosky (1964c). Subsequent analyses using two-layer models have been published by Thacker (1976) and Merkine (1977), while a more general investigation has been reported by Simmons and Hoskins (1979). This lecture is based largely on the latter paper, to which reference should be made for further detail.

The observational motivation for the examination given here is that local growth of a particular large-scale system is commonly followed between one and three days later and some 55^{o} to 90^{o} downstream by either the development of a new system or the amplification of a pre-existing wave (see, for example. Petterssen 1956). This has been interpreted in terms of the dispersion of stable Rossby waves (Rossby, 1945; Yeh, 1949) but it is clear that baroclinic processes must also be important in

general (Krishnamurti et al., 1977).

The linearized initial value problem for the Eady model

We consider small amplitude perturbations to the basic state considered by Eady, one of uniform vertical shear, $\bar{u} = \Lambda z$, with uniform mean density and static stability, and no β-effect. Writing the perturbation stream function in the form

$$Re\{\phi(z,t)\ \sin(\pi y/Y)e^{ikx}\} \tag{5.1}$$

and scaling z by H and t by $\Lambda(f_o/N)(1 + \pi^2/Y^2k^2)^{-\frac{1}{2}}$ the linearized potential vorticity equation (2.1) becomes

$$(\frac{\partial}{\partial t} + i\alpha z)\ (\frac{\partial^2\phi}{\partial z^2} - \alpha^2\phi) = 0 \tag{5.2}$$

with boundary conditions

$$\frac{\partial^2\phi}{\partial t\partial z} + i\alpha\frac{\partial\phi}{\partial z} - i\alpha\phi = 0 \quad \text{at } z = 1 \tag{5.3}$$

and $$\frac{\partial^2\phi}{\partial t\partial z} - i\alpha\phi = 0 \qquad \text{at } z = 0 \tag{5.4}$$

where
$$\alpha = (NH/f_o)\ (k^2 + \pi^2/Y^2)^{\frac{1}{2}}$$

Examination of the solution to the problem represented by (5.2), (5.3) and (5.4) has been made by Pedlosky (1964c) using Laplace transformation. Pedlosky showed that this solution could be written as terms of normal-mode form plus a residual. The latter comprised a contribution which was O(1) as $t \to \infty$ for wavelengths shorter than the short-wave cut-off to normal-mode instability, while for longer wavelengths the residual decayed at large time. Thus if an initial perturbation is represented by a Fourier expansion of terms of form (5.1) the solution is eventually dominated by the most unstable mode.

An explicit solution to the initial-value problem was discussed by Simmons and Hoskins (1979). (5.2) was integrated with respect to time to give

$$\frac{\partial^2\phi}{\partial z^2} - \alpha^2\phi = \left[\frac{\partial^2\phi}{\partial z^2} - \alpha^2\phi\right]_{t=o} e^{-i\alpha zt} \qquad (5.5)$$

and in the special case of an initial perturbation with amplitude independent of height, and equal to unity, the right-hand side of 5.5 became simply $-\alpha^2 \exp(-i\alpha zt)$. Then

$$\phi(z,t) = \frac{e^{-i\alpha zt}}{(1+t^2)} + A(t)\cosh\alpha z + B(t)\sinh\alpha z \qquad (5.6)$$

with A(t) and B(t) determined by the boundary conditions (5.3) and (5.4). Explicit expressions for A and B have been given by Simmons and Hoskins.

As a particular example we take the initial perturbation to be independent of height, with a relative vorticity which varies longitudinally as

$$\cos^2\frac{\pi x}{L}\exp(-x^2/d^2) \quad , \; -\frac{L}{2} < x < \frac{L}{2}$$

Assuming periodic boundary conditions at $x = -\frac{L}{2}$ and $\frac{L}{2}$, solutions of the form 5.6 are determined for $k = 2n\pi/L$, $n = 1, 2, 3 \ldots$, and combined numerically to give an initial perturbation of form 5.7. Parameter values are $\Lambda = 3(\text{m s}^{-1})\text{km}^{-1}$, H = 10 km, $f_o = 10^{-4}$ s^{-1}, $N = 10^{-2}$ s^{-1}, Y = 5000 km, L = 30,000 km and d = 1000 km.

Height/longitude cross sections showing the initial relative vorticity perturbation and that after 2, 4 and 6 days are presented in Fig. 5.1. Immediate consequences of the symmetry of the basic state are that the initial disturbance moves at the mid-level with the flow speed at that level, and also that the upper-level downstream development is identical to the low-level development upstream of the

initial disturbance. The latter can be seen to develop soon the westward tilt with height which characterizes a growing baroclinic wave, and thereafter a succession of troughs and ridges develop upstream and downstream. New disturbances appear first with a small horizontal length scale which expands towards that of the most unstable normal mode. Fig. 5.1 shows the low-level disturbances to form regularly close to one fixed longitude in this case of zero surface flow, while downstream disturbances first appear at a position on the upper surface which moves with a speed indistinguishable from that of the basic flow at this surface.

	DAY					
	4	5	6	7	8	9
Amplitude of	.05	.26	.82	2.2	5.8	14.6
upper maximum	(.06)	(.23)	(.75)	(2.2)	(5.8)	(14.6)
Zonal extent (km)	1400	1300	1400	1500	1600	1700
Phase speed (m s^{-1})	17	18	18	17	16	16
Growth rate (day^{-1})	2.2	1.4	1.1	1.0	0.9	0.9
$\frac{\text{Upper-level amplitude}}{\text{Surface amplitude}}$	-	-	13.7	7.2	5.3	4.3

TABLE 5.1 The variation in time of several properties of the positive vorticity region which at day 4 is the latest downstream system. Zonal extent, phase speed and growth rate are estimated at the upper surface.

Further detail is given in Table 5.1 for the latest downstream disturbance shown in the plot of the vorticity at day 4. For comparison, the most unstable normal mode has a half wavelength of 2100 km, equal surface and upper maxima in relative vorticity, a phase speed of 15 ms^{-1} and a growth rate of .74 day^{-1}. Thus from the Table it is seen that the growth rate of the new upper-level disturbance is significantly more rapid

than that of the most unstable normal mode, while its phase speed is only slightly faster. The vertical variation of amplitude only slowly approaches normal-mode form, although phase tilts appear from Fig. 5.1 to be set up more quickly. It should in addition be noted that downstream development at the lower surface also occurs substantially faster than a normal-mode calculation based on the local amplitude of the incipient surface perturbation would suggest. Examination of maps of surface pressure shows this commonly to be the case in reality, and it is clear that very rapid initial growth rates, such as found by Buzzi and Tibaldi (1978) in a case study of lee cyclogenesis, do not imply that baroclinic instability is not a causative factor.

The bracketed figures for upper-level amplitude in Table (5.1) are obtained from the part of the solution that is given by exponentially-growing normal modes, and the agreement with unbracketed figures clearly illustrates the results of Pedlosky's analysis.

Interpretation

a. Omega equation

A diagnosis of the initial-value problem for the Eady model may readily be made using the formulation of the quasi-geostrophic "ω-equation" described by Hoskins et al. (1978), and introduced in the first lecture. We consider the development in time of the vertical component of relative vorticity, ξ. It satisfies the prognostic equation

$$\left(\frac{\partial}{\partial t} + \bar{u}\,\frac{\partial}{\partial x}\right)\xi = f_o\,\frac{\partial w}{\partial z} \qquad (5.8)$$

with the vertical velocity w determined diagnostically by solution of the equation.

$$f_o^2 \frac{\partial^2 w}{\partial z^2} + N^2 \nabla_h^2 w = 2 f_o \frac{d\bar{u}}{dz} \frac{\partial \xi}{\partial x} \qquad (5.9)$$

Since the left-hand side of 5.9 is of the form of a three-dimensional Laplacian operator acting on w, to a first approximation the sign of w will be opposite to the sign of the right-hand side. Thus when westerly winds increase with height in the northern hemisphere ($f_o\ d\bar{u}/dz > 0$) we anticipate ascent in a region in which the relative vorticity decreases with increasing longitude ($\partial\xi/\partial x < 0$), and descent in the reverse case. As vertical velocity vanishes at the upper and lower boundaries a region of ascent will, through the "stretching" term on the right-hand side of (5.8), give a tendency for a reduction in vorticity at upper levels, and an increase at lower levels. Vorticity will also change as a result of advection by the basic zonal-mean flow, but for a vorticity distribution of limited spatial extent, the solution of (5.9) will generally give a vertical velocity distribution of broader extent than the vorticity gradient, and thus the stretching term dominates at the fringe of the disturbance.

The development illustrated in Fig. 5.1 may be analysed in terms of these ideas. The initial isolated source of positive vorticity gives ascent downstream of the vorticity maximum, and descent upstream (Fig. 5.2a). The resultant stretching term at the upper boundary is generally larger than the advection term (measured relative to the mean flow) and thus at the upper level there is a tendency to generate negative vorticity downstream of the initial maximum, and positive vorticity upstream. Since the reverse occurs at the lower surface, the region of positive vorticity acquires a westward tilt with height, and regions of negative vorticity form downstream at the upper surface and upstream

at the lower surface (Fig. 5.2b). Areas of downstream descent and upstream ascent are associated with these regions of negative vorticity, and the consequent stretching and shrinking yields the vorticity distribution sketched in Fig. 5.2c). It should also be noted that the pattern of vertical velocity shown in Fig. 5.2b) tends to lead to the reinforcement of the initial vorticity maximum.

Computations of the stretching and advection terms for this case, and further discussion, are given by Simmons and Hoskins (1979).

b. The normal-mode approach

We have already noted that the solution at large time is dominated by a sum of exponentially-growing modes, and as modes with different wavenumbers have different growth rates it is clear that an initially-isolated disturbance will spread as a series of developing troughs and ridges. Asymptotic theory may be used to determine some of the characteristics of this spreading.

We examine solutions of the form

$$\psi(x,z,t) = \int_{-\infty}^{\infty} a(k)\ \phi_k(z) e^{ik(x-c(k))t} dk \qquad (5.10)$$

in the limit as $t \to \infty$. Here $c(k)$ is the complex phase speed determined by the normal-mode instability problem for wavenumber k, and $\phi_k(z)$ is the corresponding vertical structure function. $a(k)$ is determined by the form of the initial perturbation.

The asymptotic theory for expressions of the form 5.10 has been extensively developed in plasma physics (see, e.g., Bers (1975)), and limited applications to baroclinic instability in two-level models have been made by

Thacker (1976) and Merkine (1977). We consider the solution at a point x which moves downstream with velocity U. Then

$$\psi = \int_{-\infty}^{\infty} a(k)\ \phi_k(z) e^{-i\Omega(k)t} dk \qquad (5.11)$$

where $\Omega(k) = k(c(k) - U)$. The rate of spreading of the disturbance is given by the velocities U which are limiting values beyond which (5.11) yields decay as $t \to \infty$

The asymptotic theory requires $a(k), \phi_k(z)$ and $c(k)$ to be sufficiently well behaved functions of k for the contour of integration in (5.11) to be deformed off the real-k axis. This deformation is performed in the direction which diminishes $\mathrm{Im}(\Omega(k))$ for all k, and continues until one of two possibilities occurs. The first of these is that a contour is reached with $\mathrm{Im}(\Omega(k)) \leqslant 0$ for all k, in which case ψ does not grow as $t \to \infty$, and the solution is seen as stable by an observer watching a point moving with the particular velocity U. The second possibility is that one encounters a saddle point, at $k = k_s$ say, where $\partial\Omega/\partial k = 0$, and $\mathrm{Im}(\Omega(k_s)) > 0$. In this case, as discussed by Bers, instability occurs locally and the solution as $t \to \infty$ is proportional to

$$a(k_s)\ \phi_{k_s}(z)\ t^{-\frac{1}{2}}\ e^{-i\Omega(k_s)t}$$

This gives a local wavelength $2\pi / \mathrm{Re}(k_s)$, a local growth rate $\mathrm{Im}(\Omega(k_s))$, and a local phase speed $\mathrm{Re}(\Omega(k_s))/\mathrm{Re}(k_s) + U$.

For the Eady problem a dimensionless form of Ω is

$$\Omega(k) = k(\tfrac{1}{2} - U) \pm \sqrt{(\tfrac{\alpha}{2} - \coth\tfrac{\alpha}{2})(\tfrac{\alpha}{2} - \tanh\tfrac{\alpha}{2})} \qquad (5.12)$$

where k is scaled by f_o/NH, U by ΛH, and $\alpha = \sqrt{k^2+\pi^2N^2H^2/f_o^2Y^2}$
In the special case of infinite meridional scale, $\alpha = k$, a solution of analytical form may be found for the fringe of the instability.

Replacing α by k, (5.12) gives

$$\frac{\partial\Omega}{\partial k} = \frac{1}{2} - U \pm \frac{1}{4}\left(X + \frac{1}{X}\right) \qquad (5.13)$$

where

$$X = \tanh^2\frac{k}{2}\sqrt{\left(\frac{k}{2} - \coth\frac{k}{2}\right)\left(\frac{k}{2} - \tanh\frac{k}{2}\right)}\ .$$

Taking the positive root, a saddle point $(\partial\Omega/\partial k = 0)$ occurs for

$$X = -(1 - 2U) \pm 2\sqrt{U^2 - U}$$

When U = 1, the dimensionless speed of the basic flow at the upper surface, $\partial\Omega/\partial k \to 0$ as $k \to \infty$, and analytical solutions may be obtained for values of U close to 1.

We set $U = 1 - \varepsilon$, where $0 < \varepsilon \ll 1$. The saddle point then occurs for

$$X = 1 \pm 2i\varepsilon^{\frac{1}{2}} + O(\varepsilon).$$

and this gives

$$k_s = -\ell n(\varepsilon^{\frac{1}{2}}) - \ell n(\tfrac{1}{2}) \pm i\frac{\pi}{2} + O(\varepsilon^{\frac{1}{2}})$$

The positive root gives a saddle point with positive $Im(\Omega)$, and thus demonstrates the existence of local instability with a short zonal wavelength of order $-2\pi/\ell n(\varepsilon^{\frac{1}{2}})$, a local growth rate of order $\varepsilon\pi/2$, and a phase speed of order $1 + 1/\ell n(\varepsilon^{\frac{1}{2}})$. A similar approach reveals local

stability for negative ε.

The above analysis thus indicates that the downstream fringe of the disturbance will move with the speed of the basic zonal flow at the upper surface. Although further analysis shows that the time at which the asymptotic solution becomes formally valid increases without bound as $\varepsilon \to 0$ this result is in good agreement with the behaviour of the complete solution as examined after as short a time as one day. By symmetry, or by analysis of the negative root of (5.13) as $k \to -\infty$, the asymptotic theory predicts that each new low-level disturbance will develop at the same location if the zonal flow is zero at the surface.

Repetition of the analysis for $U = 1 - \varepsilon$ when the perturbation has finite meridional scale Y reveals stability to leading order in ε, with $k_s \sim (NH\pi/f_o Y)^{\frac{2}{3}} \varepsilon^{-\frac{1}{3}}$. However, a numerical determination of saddle points for Y = 5000 km, the case considered in Fig. 5.1, indicates that instability occurs for $U \leqslant .996$, and local wavelengths, phase speeds and growth rates, which are shown in Fig. 5.3, differ little from the case of infinite Y. As found for the complete solution discussed previously, new disturbances rapidly attain a phase speed little more than of unstable normal modes. Wavelengths are initially about half that of the most unstable normal mode, and subsequently increase gradually. The local growth rate increases with increasing distance from the fringe.

It is important not to confuse the "local growth rate" discussed above with the growth rate estimated for a particular disturbance, which we have seen can well exceed normal-mode values. The local growth rate for a point moving with velocity U is a measure of the rate of increase of amplitude <u>at that point.</u> However, phase speed

is less than U if $\frac{1}{2} < U < 1$, and individual disturbances will thus be moving towards lower U, and thus towards a region of higher local growth rate. The growth rate estimated for a particular disturbance may thus significantly exceed the local growth rate.

Further linear quasi-geostrophic solutions

Further linear quasi-geostrophic solutions have been discussed by Simmons and Hoskins (1979), and we summarize these here. Considering first the Eady basic state we note that for infinite meridional scale the time scale of the development is simply inversely proportional to the vertical shear of the mean flow, and this holds to good approximation for meridional scales of the order of several thousand km. Changing the Coriolis parameter or static stability does not significantly alter the rate of spreading, but changes the local wavelength and growth rate. Asymptotic theory predicts that the rate of spreading, and local wavelength, phase speed and growth rate, are generally independent of the form of the initial perturbation; some comparisons are given in Fig. 5.4.

Fig. 5.5a) illustrates the vorticity at day 6 for a parabolic flow profile with the same velocity difference between upper and lower surfaces as in Fig.5.1 but with shear concentrated near $z = 0$. The rate of spreading of the instability is much as before, but the downstream development is of longer wavelength and deeper vertical extent. Fig. 5.5b) shows the change to the case shown in Fig. 5.1 that results from inclusion of compressibility with a density scale height of 7 km. There is a small reduction in the rate at which the instability spreads downstream.

Fig. 5.6 shows how the solutions for day 6 presented in Figs. 5.1 and 5.5b) are modified by including the β -effect. Here $\beta = 1.6 \times 10^{-11} s^{-1}$. The fringes of unstable regions are masked by small-amplitude longer-wavelength components of Rossby-wave type, but detailed examination shows the upstream fringe again to be located close to a fixed position. Fig. 5.6 re-emphasizes the slowing of the downstream fringe which results from the variation of density with height, and the β -effect itself causes some further slowing. Downstream disturbances are generally of longer wavelength and deeper extent than found for the Eady basic state, while upstream disturbances are somewhat shorter and shallower.

Non-linear primitive-equation results

Simmons and Hoskins (1979) also presented results from some non-linear integrations using a hemispheric primitive-equation model. Fig. 5.7 illustrates one initial distribution of surface pressure, together with the resulting distributions at days 5, 8 and 11. New disturbances form downstream with a length scale that corresponds closely to that of zonal wavenumber 6, and the downstream fringe moves at about $35\text{-}40^{o}$ longitude/day, this corresponding to a velocity of 33-37 m s^{-1} at the latitude of the jet maximum, where the initial flow speed is 47 m s^{-1}. We again note the formation of smaller-scale upstream disturbances at a position close to that of the initial perturbation.

Most of the upper-level wave activity is associated with the developing downstream disturbances, and these reach larger amplitude than found either for earlier disturbances or for normal-mode initial conditions (see Lecture 6). Downstream development occurs first in the upper troposphere, and upper-level maxima occur earlier than surface

maxima in later systems.

In the linearized problems considered earlier in the lecture the wavelength of a particular disturbance eventually approaches that of the most unstable mode. In this and other non-linear examples wave growth ceases before normal-mode form is established, with downstream length scales some 30% longer than that of the most unstable mode, and some significant differences in structure. Further discussion has been given by Simmons and Hoskins.

Predictability

The possibility that the major trigger of baroclinic instability is provided not by random small-amplitude perturbations, but by large-amplitude disturbances some distance from the region in which a new disturbance develops, is evidence for the longer-term predictability of large-scale atmospheric motion. Conversely, models designed for weather prediction are prone to errors in phase speed, and might be thought to be weak at simulating events involving dispersion which typically depends on the variation of phase speed and growth rate with wavenumber. The examples considered in this paper indicate, however, that the overall development is not especially sensitive to details of the model employed, particularly as regards the spreading of the instability, and it is thus difficult to draw any specific conclusions regarding predictability from these studies.

Hollingsworth et al. (1979) have recently examined the numerical simulation of observed cases of downstream propagation. The mainly dynamical nature of the phenomenon was confirmed by the similarity of results obtained using two quite different physical parameterizations. Both successful and unsuccessful simulations were noted, and

it appeared that forecast success depended strongly on the initial data. In a successful case the phenomenon was predictable nine days ahead. Hollingsworth et al. also noted the necessity to maintain correctly the location of the quasi-stationary troughs for a successful forecast of downstream propagation.

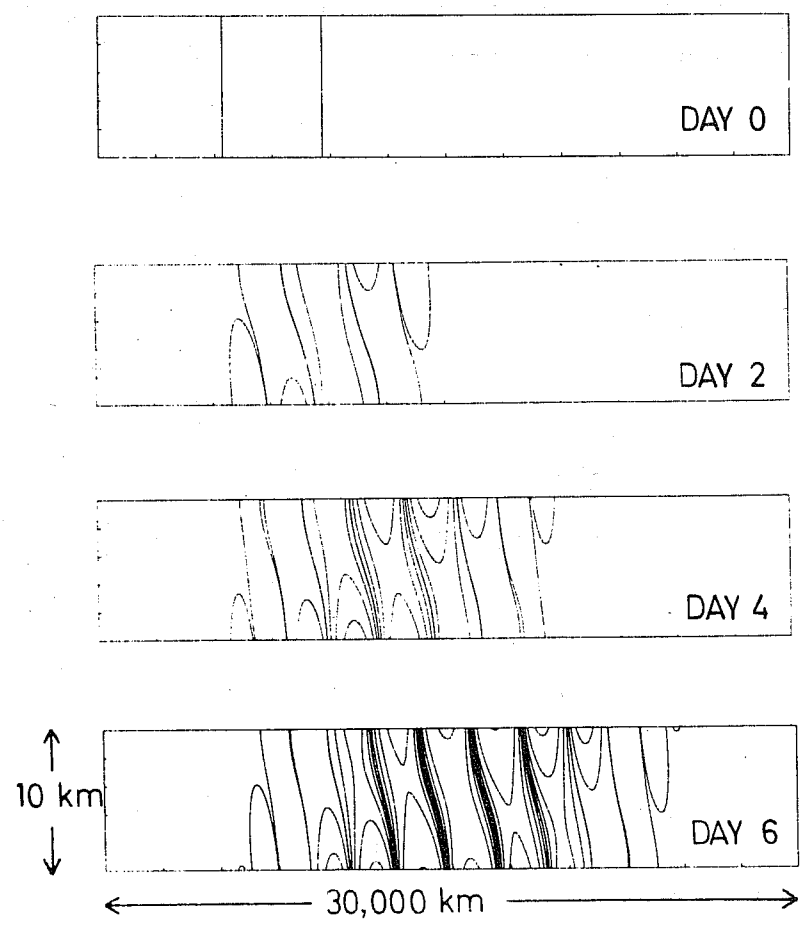

Fig. 5.1 Height/longitude sections showing the relative vorticity at days 0, 2, 4 and 6 for the Eady basic state. Contours are drawn for values ±.01, ±1, ±2.5, ±5, ±10 and ±25. The zero contour is not drawn in order to avoid the illustration of small-scale variability of negligible amplitude.

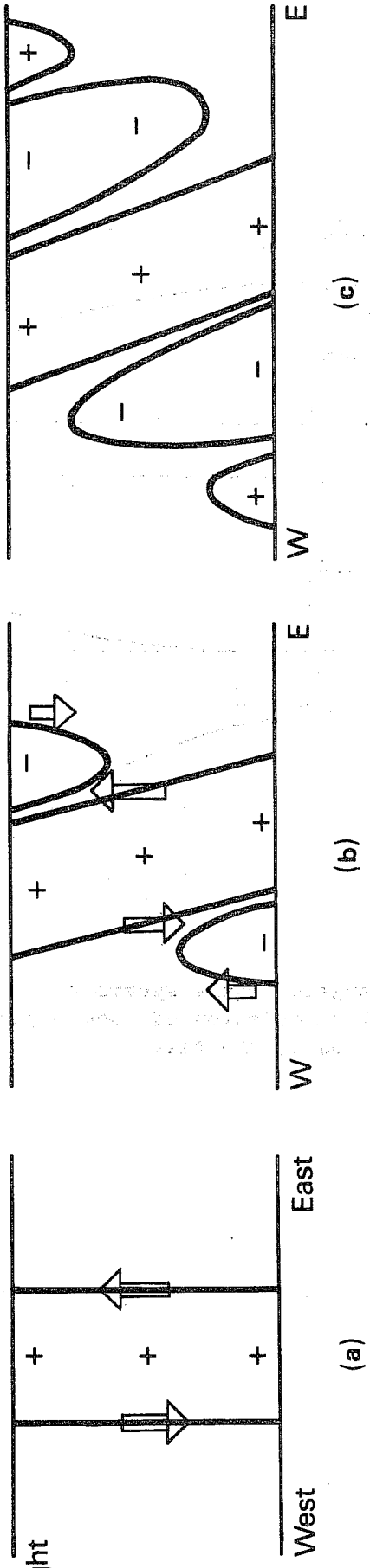

Fig. 5.2 Height/longitude sections showing schematic pictures of perturbation relative vorticities (denoted by + and -) and vertical motion (denoted by arrows) for

a) an isolated initial distribution of vorticity,

b),c) the distributions at later times.

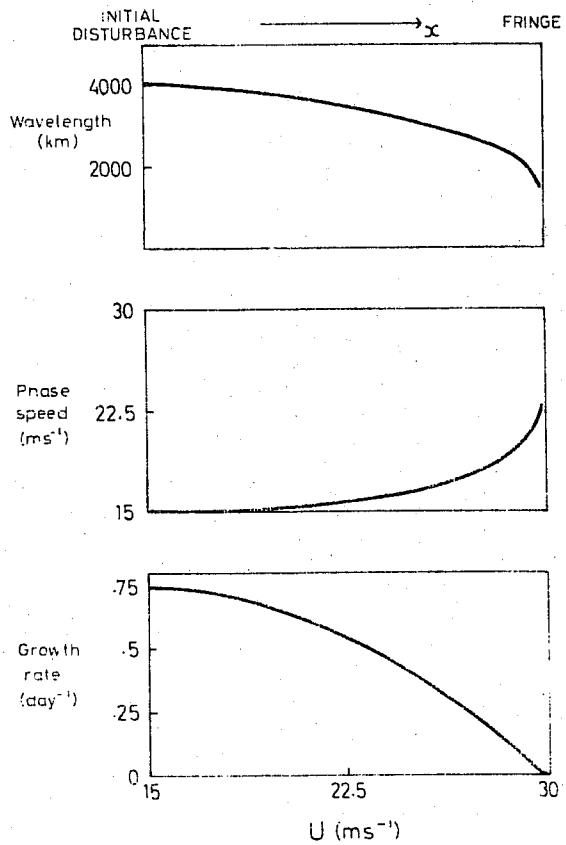

Fig. 5.3 Local wavelengths, phase speeds and growth rates determined by numerical calculation of saddle points for the Eady basic state specified in the text.

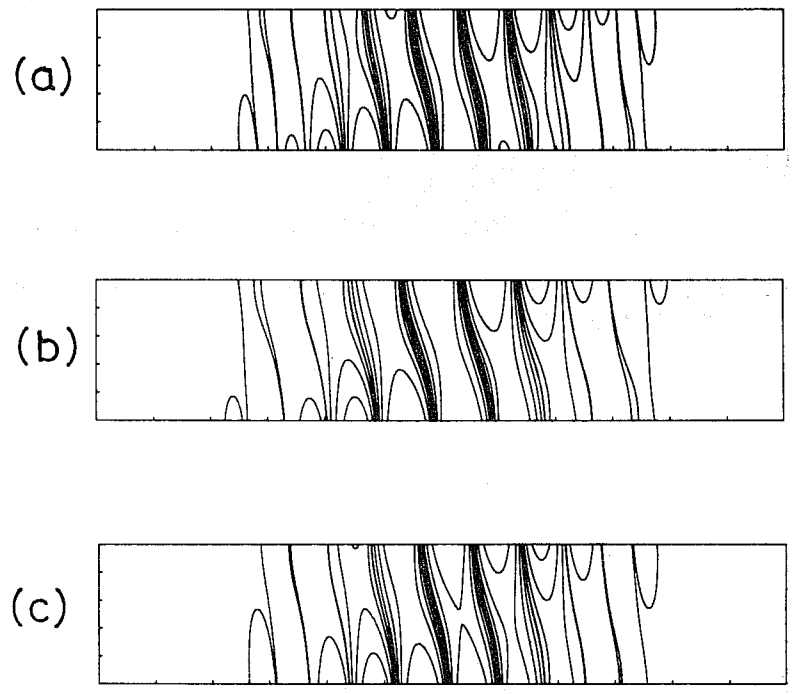

Fig. 5.4 Height/longitude sections showing vorticities at day 6 for three different initial perturbations. Details are as for Fig. 5.1. For Cases a) and b) the initial longitudinal scale of the perturbation differs from that in Fig. 5.1 while for case c) the initial perturbation is concentrated at upper levels.

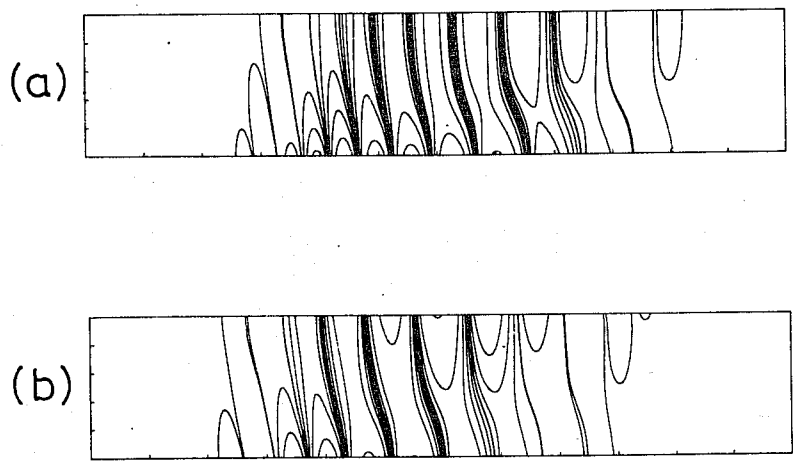

Fig. 5.5 Vorticities at day 6 for (a) a parabolic velocity profile and (b) a calculation including a decrease in mean density with height.

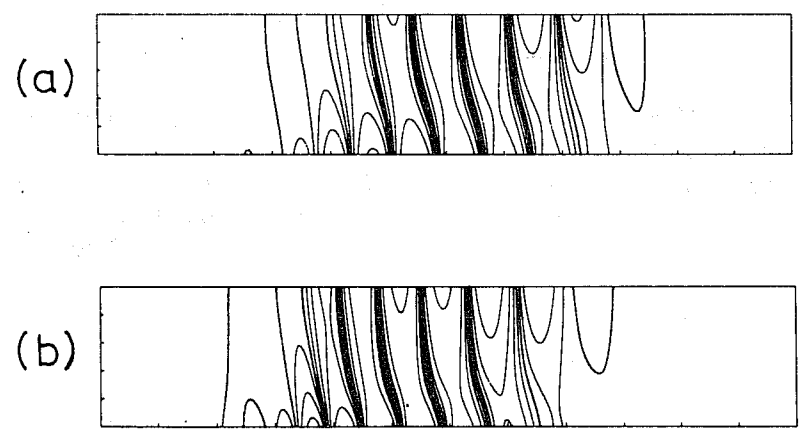

Fig. 5.6 Vorticities at day 6 for two calculations including the β-effect. In this case the zero contour is drawn (with a heavier line) in place of the contours ±.01.

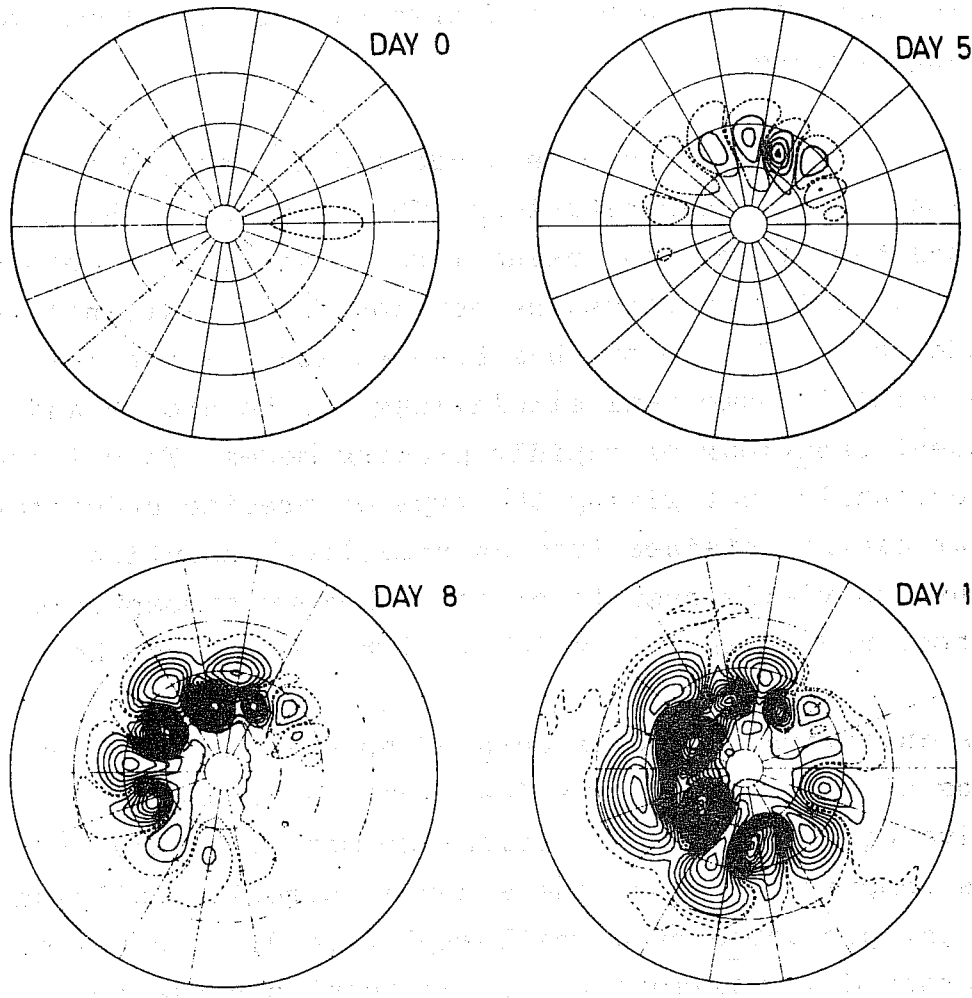

Fig. 5.7 North polar stereographic plot showing surface pressure at days 0, 5, 8 and 11. Solid contours are drawn at intervals of 4 mb for values 4 mb, 8 mb ....., while the dashed contours are for values $\pm\frac{1}{2}$ mb. Background lines of latitude and longitude are drawn at intervals of 20^{o}.

6. THE LIFE CYCLES OF NON-LINEAR BAROCLINIC WAVES

In this lecture we examine the non-linear development of baroclinic waves, concentrating our attention on the behaviour of the larger scales of motion. The formation, on a smaller scale, of atmospheric fronts will be the topic of following lectures.

Two types of approach have been adopted in the study of large-scale non-linear behaviour. The first (e.g. Pedlosky 1972) has been to examine using largely analytical methods how non-linearity modifies the development of marginally-unstable modes. The second has been to investigate relatively complete numerical simulations of the growth and subsequent behaviour of rapidly-growing modes. This latter approach, whilst not giving the type of precise understanding that can be obtained from an analytical solution, nevertheless yields results of more obvious atmospheric relevance, and it is this which will be considered here.

We thus investigate some aspects of non-linear behaviour by means of a series of numerical integrations of the primitive equations with spherical geometry. Initial conditions comprise in each case a zonal, baroclinically-unstable jet perturbed by a small-amplitude disturbance of predetermined normal-mode form. The results presented largely summarize the study published by Simmons and Hoskins (1978), which confirmed a number of results concerning the non-linear modification of wave growth obtained earlier by Simons (1972) and Gall (1976 b), and which also provided evidence concerning the behaviour of the large-scale fields once baroclinic growth has ceased.

The numerical model

The numerical model used to obtain the results presented here was the spectral model described in detail by Hoskins

and Simmons (1975). For these calculations a triangular truncation at total wavenumber 42 and 14 unequally-spaced levels in the vertical were used. The model included no parameterization of physical processes other than a bi-harmonic internal horizontal diffusion. Further details are given in Simmons and Hoskins (1978).

Initial Conditions

Each integration had as initial conditions a zonal jet perturbed by a small-amplitude disturbance of normal-mode form. For a given zonal wavenumber this mode was predetermined by applying the initial-value technique used by Brown (1969) to a linearized, adiabatic version of the numerical model. When used as initial conditions for a non-linear integration each mode was scaled to give a surface pressure wave of amplitude 1 mb.

The zonal flows chosen for study were those whose linear stability was examined by Simmons and Hoskins (1977). All have a maximum at 200 mb, and will be referred to by their horizontal structures, which comprise jets of relatively broad meridional scale centered at 30^{o} and 55^{o} latitude, a jet centered at 45^{o}, and a second 30^{o} jet of smaller meridional scale. These flows were not intended to model in detail any specific observed or climatological profile, and should be regarded as particular examples from a range of possible atmospheric flows. Since the qualitative nature of solutions varies little from flow to flow, we concentrate on results for the 45^{o} jet. Most discussions will refer to initial perturbations with zonal wavenumber 6.

Some synoptic features

The surface pressure and low-level temperature after seven days of integration are illustrated in Fig. 6.1 for the

wavenumber 6 disturbance to the 45° jet. By this time the surface low has deepened to an amplitude of about 32 mb and moved some 8° poleward to a position 12° north of the jet maximum. There is a larger area of weaker high pressure to the south. The temperature wave shows a pronounced distortion, with the strongest gradients located in positions typical of occluded and cold fronts, and the region of relatively warm air has diminished as the wave develops. These and other fields are in close agreement with the usual synoptic picture of an occluding mid-latitude disturbance. Little further intensification occurs at the surface beyond this time.

The streamfunction at an upper tropospheric level is illustrated in Fig.6.2 for day 8 and the five following days. The sequence shows the disturbance continuing to grow up to a time between day 9 and day 10, during which there is a gradual enhancement of the southwest to northeast tilt to the south of the disturbance maximum and a reduction of the opposite tilt to the north. In the absence of vertical coupling such a pattern would imply a barotropic strengthening of the jet and decrease in wave amplitude. Just such a process is observed to occur rapidly beyond day 10. During this time the tilt of the wave is from southwest to northeast at almost all latitudes and the corresponding eddy momentum flux is almost entirely poleward.

A similar sequence occurs at other upper tropospheric and lower stratospheric levels. Such pronounced tilts are not evident in patterns of low-level streamfunction, but here too there is a significant loss of eddy energy between days 10 and 12 and an enhancement of the easterly-westerly-easterly distribution of surface zonalmean wind forced by the wave in its growing phase.

Energetics

The growth and decay indicated by the synoptic features described above are illustrated in Fig. 6.3 which shows the variation in time of eddy energy for initial wavenumber 6 disturbances to three zonal flows. In each case growth of the disturbance is followed by a period during which it decays at much the same rate as that at which it grew. It is clear that well-defined life cycles exist.

An example of the variation with time of the various energy conversions is given in Fig. 6.4 for the wavenumber 6 disturbance to the 45^{o} jet. Up to day 8 baroclinic processes evidently dominate, with conversions from zonal to eddy available potential energy and from the latter to eddy kinetic energy. As these conversions decrease in magnitude the barotropic conversion from eddy to zonal kinetic energy becomes dominant, reaching a maximum value at day 11 when the baroclinic conversions have decreased almost to zero. Although at each day the internal dissipation is weak compared with the major conversions, its overall effect is significant, the net loss of zonal available potential energy being slightly more than twice the gain of zonal kinetic energy. A similar cycle is found in other cases.

A feature of the nonlinear growth of many disturbances is the development of amplitudes that are substantially larger at upper levels than close to the surface. This is illustrated in Fig. 6.5 which shows the distribution with latitude and height of the eddy kinetic energy density at days 0 and 10, and the distribution averaged over the 10 day period from day 4 to day 14. At day 10 the eddy kinetic energy is a maximum, and the contribution from about this time dominates the average over the life cycle, as is the case for many other fields.

Factors determining the cessation of wave growth

Results for a variety of flows reveal substantial variations in the maximum attained levels of eddy energy. Maximum values are reached a few days after the time the meridional temperature gradient first reverses somewhere at the surface, and at a time when the low level static stability has been significantly increased. Determination of the most unstable normal mode for the zonal-mean state at this time indicates that a marked change of structure would be required to achieve further (but much weaker) baroclinic growth. What appears to happen in the examples presented here is that barotropic processes bring about a decay of amplitude, and further zonal-mean changes, before such an adjustment can be completed. As growth ceases there remains a considerable amount of zonal available potential energy. Thus the indication is that growth is limited largely by a local stabilization of the flow, rather than by the overall amount of available energy.

We have already noted a tendency for some growth at upper levels after it has ceased at the surface, this giving relatively larger upper-level amplitudes than found for normal modes. In diagnosing this, it is found that vertical energy transfer plays a relatively small role in the separate kinetic energy budgets of the upper and lower troposphere. Larger upper level amplitudes may thus be viewed as resulting from a larger upper level conversion of eddy avalable potential energy to eddy kinetic energy. This in turn may be linked with the tendency inherent in normal-mode results for zonal-mean changes to be concentrated at the surface, thus leaving an upper level structure initially more suitable for further baroclinic growth than that at lower levels. This lasts only for a limited period of time,and upper-level growth ceases as barotropic effects become dominant.

Barotropic effects may also exert an influence on eddy energy levels earlier in the life cycle. A marked example of this is given in Fig. 6.6, which shows the two conversion terms involving eddy kinetic energy for two integrations using wavenumber 6 initial conditions. Both have a virtually identical zonal-mean temperature field (which is close to that associated with the 45^{o}jet) but in case W55 there is an approximately barotropic flow component with a 10 ms^{-1} westerly surface maximum at latitude 55^{o} and a latitudinal width of 30^{o} superimposed on the balanced jet with zero surface flow, while for E55 the barotropic component is of similar form, but easterly. Normal-mode growth rates for the two cases differ little, and the development is similar to day 5. Between day 5 and day 7, however, the barotropic conversion for case E55 changes markedly from normal-mode form, and instead of inhibiting growth it enhances it. The resulting maximum eddy kinetic energies differ by a factor of more than 5.

Although the above case is extreme in that particularly strong surface easterly flow is set up near 55^{o} in the absence of surface friction, it nevertheless appears that such barotropic effects may be of some quantitative importance in reality. Certainly the level of energy reached by a growing baroclinic wave appears to be determined rather subtly.

Eddy fluxes and mean meridional circulations

Meridional cross sections showing (normalized) poleward eddy heat fluxes averaged over the life cycles of various disturbances with initial zonal wavenumber 6 are presented in Fig. 6.7. In comparison with linear calculations (e.g. Fig. 4.3, solid curve) upper tropospheric fluxes are significantly larger relative to surface values, and now exhibit the observed secondary upper tropospheric maximum

(Oort and Rasmusson, 1971; Newell et al., 1974). Fluxes are also of broader meridional scale, particularly at low levels.

The corresponding patterns of poleward eddy momentum fluxes are illustrated in Fig. 6.8, and exhibit much less variation from flow to flow than is the case for linear modes (Fig. 4.5). Increases in upper level amplitude and changes in tilt as the waves mature and decay are reflected in momentum fluxes which in all cases are concentrated in the upper troposphere, with predominant poleward maxima located at latitudes close to those of the initial jet maxima. Such results are in good agreement with observed net transient eddy fluxes (Oort and Rasmusson, 1971; Newell et al., 1972).

The magnitudes of eddy momentum fluxes measured relative to heat fluxes are much larger than in linear solutions, and these also are in better agreement with observations.

The corresponding mean meridional circulations differ from those induced by the normal modes in that there is an increase in the relative strength of the cell equatorward of the jet maximum, and a reduction in the polar cell. We have already seen that in the quasi-geostrophic approximation the mean circulation is determined by eddy heat and momentum fluxes and acts to maintain thermal-wind balance. The change noted here is consistent with the enhanced upper-level poleward momentum flux discussed previously.

Zonal-mean changes

The different regimes of baroclinic growth and barotropic decay are clearly illustrated in Fig. 6.9, which shows the strength of the maximum upper level zonal-mean flow as a function of time for the 45^{o} jet. A feature of normal-mode

solutions that has been noted is a relatively small induced upper level change to the zonally averaged state, and this result appears from Fig. 6.9 to continue to hold up to about the time of maximum disturbance energy, day 9, although by this time some change in shape of the upper level jet has occurred, the maximum being located some 5^{o} nearer the pole.

Rapid production of a stronger jet of smaller meridional extent takes place over the next three days as the wave decays, and this is followed by a slow decrease in the strength of the jet. During the latter there is a weak transfer of zonal to eddy kinetic energy, and the internal dissipation of zonal kinetic energy is of the same order.

Zonal-mean temperature changes over the life cycles of disturbances are largest at the surface, where there is a marked reduction in the mid-latitude temperature gradient, although sharper gradients are formed to north and south. There is remarkably little overall change in the middle and upper troposphere, and an enhanced (reversed) lower-stratospheric temperature gradient in association with the stronger upper troposphere jet.

Shorter zonal wavelength perturbations

Shorter zonal wavelength normal modes generally have amplitudes more concentrated at the surface than longer wavelength modes, and differences in structure revealed by linear theory are found to be enhanced by non-linear effects. In the absence of any representation of moist processes these shorter waves do not exhibit a pronounced upper level growth around the time growth ceases at the surface, and although linear growth rates may be larger than for longer wavelength modes, maximum energy levels are generally significantly smaller. In addition the

horizontal structure of short wavelength disturbances remains similar to normal-mode form, Simmons and Hoskins (1978) showing a predominantly equatorward eddy momentum flux for the wavenumber 9 initial perturbation to the 45° jet.

Eady (1949) pointed out that the low effective static stability associated with moist air may result in the rapid development of shorter wavelength features, and the influence of moisture has been the subject of a number of more recent stability studies. For example, Tokioka (1973) showed that inclusion of a parameterized convective heating caused a decrease in the most unstable wavelength and an increase in growth rate. Non-linear integrations by Gall (1976c) showed wavenumber 15 to have a much more pronounced growth and much larger upper level amplitudes when moist processes were included. The longer waves nevertheless reached significantly larger energy levels, as in the dry experiments noted above.

The large differences in the non-linear behaviour of long and short waves may pose difficulty for eddy-flux parameterizations of the type used in climate models. In particular it appears necessary in a parameterization to specify the spectral distribution of eddy fluxes. Knowledge of the linear growth rate spectrum may be of help in this respect, but it is not clear that this is sufficient.

The barotropic decay process

A detailed discussion of the barotropic decay process noted for longer-wavelength disturbances has also been given by Simmons and Hoskins (1978). It was shown both experimentally and theoretically that as baroclinic growth ceases, the motion becomes to good qualitative accuracy as described by the barotropic vorticity equation, as indeed has been long recognized synoptically (Charney et al.

1950). However, the vorticity actually changes at about half the rate which would occur in a purely barotropic fluid (see Fig. 6.10) because of an adjustment (through vertical motion) of the temperature field to maintain thermal wind balance.

Further barotropic integrations clarified the reasons for the pronounced wave tilts and decay of eddy energy. As in essence recognized synoptically by Namias and Clapp (1944), marked latitudinal variations in the mean flow and length scale of the quasi-barotropic wave gave rise to different phase movements at different latitudes. In particular, the change in the zonal-mean vorticity gradient was shown to be of crucial importance for the establishment of predominantly poleward momentum fluxes. Reference should be made to the paper by Simmons and Hoskins for further detail.

Some numerical aspects

a) Horizontal resolution

A number of integrations have been performed using different horizontal resolutions for the case of the 45^{o} jet with wavenumber 6 initial conditions. Use of triangular truncation at wavenumber 63 (T63) gave results very similar to those using T42, but some marked differences were found using lower resolutions.

The lower-resolution integrations comprised runs with triangular truncation at wavenumber 21 and rhomboidal truncation at zonal wavenumber 16, together with a zonally truncated version retaining only zonal-mean and wavenumber 6 components, meridional resolution being as in T42. The resulting variation in eddy energy shown in Fig. 6.11 indicates close agreement up to day 7. Maximum energies reached at day 9 are 20% lower in all three lower resol-

ution integrations, agreement being apparently fortuitous as there are larger but cancelling differences in energy conversions at day 8.

Results beyond day 9 show more substantial differences. The rhomboidal integration captures the relatively rapid decay in wave amplitude found in higher resolution results, but the other two show little initial decay and generally less loss of eddy energy, with averaged poleward momentum fluxes that are only about half that obtained using higher resolutions. The rhomboidal resolution used here represents the hemispheric meridional structure of zonal wavenumber 12 by eight nonzero modes, just three more than in the lower resolution triangular truncation, but these additional modes appear to give rise to a much more accurate representation of the decay. Care should be taken in interpreting this as evidence favouring rhomboidal truncation for general use, since for relatively low resolution the appropriate choice of truncation appears to be quite dependent on the particular nature of the problem under investigation (Simmons and Hoskins, 1975).

b) Internal diffusion

Some form of internal dissipation is necessary in numerical experiments designed to simulate the full life cycles of baroclinic waves in order to prevent the attempted formation of fronts on scales that cannot be resolved, but the ideal form of dissipation is far from clear. To obtain some indication of the sensitivity of results presented in this lecture to dissipation, several experiments have been performed. For the wavenumber 6 disturbance to the 45^{o} jet these comprised halving the diffusion coefficient everywhere, reducing it above $\sigma=0.5$ to a quarter of its standard value, and doubling it everywhere as applied to vorticity and divergence but halving

it as applied to temperature. Resulting changes were small, amounting to at most 10% for the averaged eddy heat and momentum fluxes, and up to 20% for the more subtle net change to the upper level zonal-mean flow. Such differences are insignificant in the present context in view of marked quantitative differences from flow to flow and qualitative differences between wavenumbers 6 and 9.

Recent analytical studies of the interaction between waves and the zonal-mean state (Andrews and McIntyre, 1976,1978; Boyd, 1976) have generalized earlier work and reemphasized the crucial importance of transience and dissipation in bringing about zonal-mean changes. With this in mind it should be noted that our finding that net changes are not particularly sensitive to the formulation of the internal dissipation does not imply that dissipation itself is unimportant. We have already noted that over the life cycle of the wavenumber 6 disturbance to the 45° jet the net dissipation accounts for about as much of the loss of zonal available potential energy as does the gain in zonal kinetic energy. In the corresponding experiments with different forms of diffusion, compensating changes in the amplitudes of smaller scales result in net dissipations which differ by less than 25%. The lack of sensitivity to the precise formulation suggests the possibility that the dissipation is mainly determined by the large-scale motion. This is consistent with theoretical work presented in the following lectures that envisages frontogenesis as being a direct result of the large-scale flow in a growing baroclinic eddy.

Concluding Remarks

It is evident from the examples presented in this lecture that nonlinearity can significantly modify several results of linear stability theory. Finite-amplitude disturbances exhibit more baroclinic growth at upper than lower levels,

and a subsequent quasi-barotropic behaviour. Related changes in structure are of particular significance in that the largest eddy fluxes occur close to the time of maximum eddy energy, when deviations from linear theory are marked. One result is that net eddy fluxes of both heat and momentum have upper level amplitudes substantially larger relative to surface values than given by linear stability analyses, and agreement with observation is improved.

Barotropic processes become important as the disturbance occludes, although the three-dimensional nature of the motion is such that the response of the vorticity field is about half that which would occur in a barotropic fluid. Eddy momentum fluxes become stronger relative to heat fluxes, and predominantly poleward for the longer wavelength disturbances which dominate at upper levels. These changes are also such as to bring results into closer agreement with observation. In the present examples we find a barotropic decay of wave energy at a rate similar to that of baroclinic growth.

We have noted a number of factors which influence the level of energy reached by a developing wave, but this level has been found to be quite variable from case to case, and difficult to estimate in advance of numerical integration. Barotropic processes depend on the second derivative with respect to latitude of the zonal-mean zonal flow, and the decay is inadequately represented in lower resolution models. Errors in the intensity and dissipation of mid-latitude systems can be a problem in numerical models designed for forecasting or general circulation studies, and diagnosis of the causes of any such errors is unlikely to be straightforward.

The differences in behaviour noted here between longer and

shorter wavelength disturbances is consistent with the classical synoptic distinction between "long waves" (with zonal wavenumbers 3-7) which typically dominate the upper level flow and shorter, shallower "cyclone waves," several of which may develop in succession superimposed on a relatively stationary long-wave pattern(see e.g., Palmen and Newton, 1969). Although the shorter waves are responsible for much of the day-to-day variability of surface weather in middle latitudes, their individual influence on the upper flow is weak. Studies of the longer waves (e.g., Cressman, 1948) have noted their tendency to remain almost stationary for several days, but emphasis has also often been placed on their growth, distortion or decay (such as illustrated in this lecture) since a change in long-wave pattern may bring about a basic change in weather type, and thus may be of importance for extended range forecasting.

Such synoptic considerations lead us to stress in conclusion, that we have examined some nonlinear aspects of baroclinic waves in what is still, in comparison with the atmosphere, a very simple situation. In particular, the barotropic decay of a wave takes place with identical disturbances and jets both upstream and downstream. Examination of either sequences of 300 mb charts or past synoptic studies (e.g., Newton et al., 1951) does indeed reveal events resembling those illustrated in Fig. 6.2, but a variety of other behaviour may also be observed. Thus the barotropic decay discussed here, and associated effects on eddy fluxes and the zonal-mean state, should be regarded not as general properties of mature atmospheric systems, but rather as properties of one particular type of atmospheric behaviour.

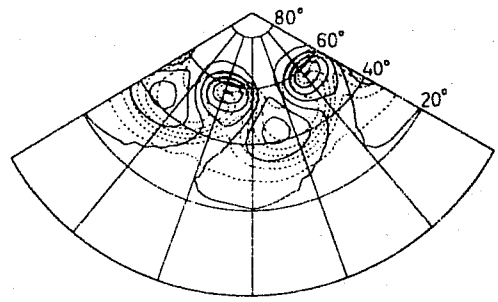

Fig. 6.1 North polar stereographic plot showing surface pressure (solid contours) and low-level temperature (broken contours) after seven days of integration for the wavenumber 6 perturbation to the 45° jet. Contours are drawn at intervals of 8 mb and 4°C using linear interpolation between values on the computational grid comprising 32 "Gaussian" latitudes and 32 regularly spaced points per 90° longitude. Background lines of latitude and longitude are drawn at intervals of 20°.

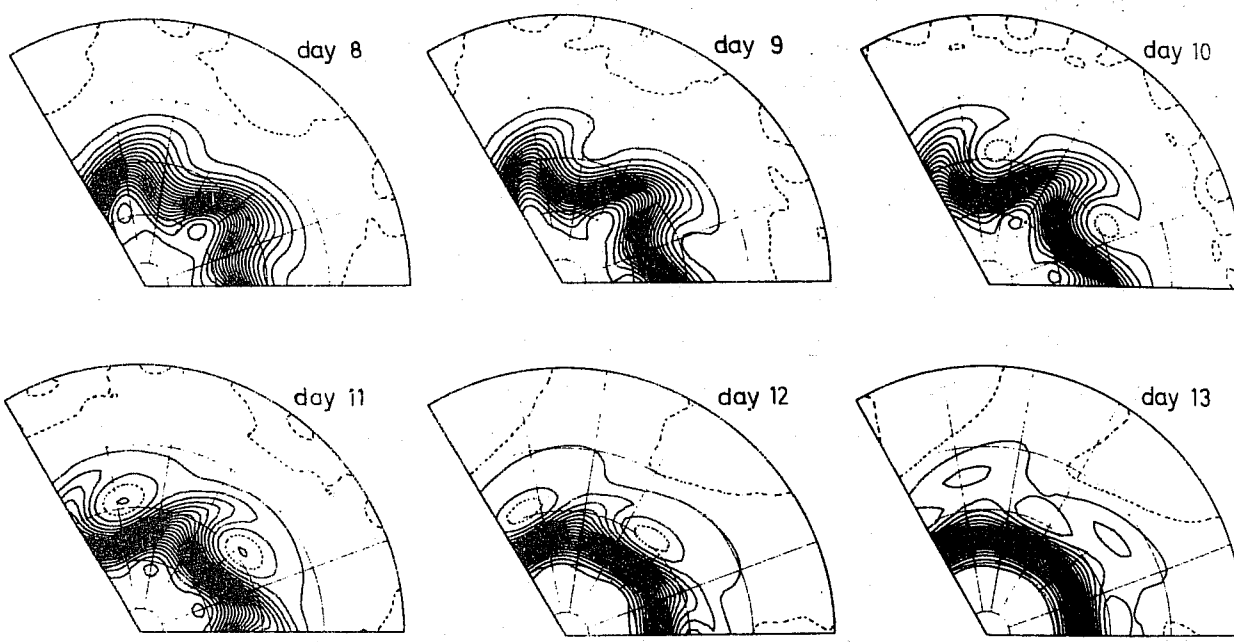

Fig. 6.2 Streamfunction at an upper tropospheric level at daily intervals from day 8 to day 13 for the wavenumber 6 perturbation to the 45° jet. The zero contour is dashed to avoid emphasis of insignificant small-amplitude variability close to the equator, and the contour interval is $1.5 \times 10^{-3}\ a^2\Omega$, where a is the radius of earth and Ω its angular velocity.

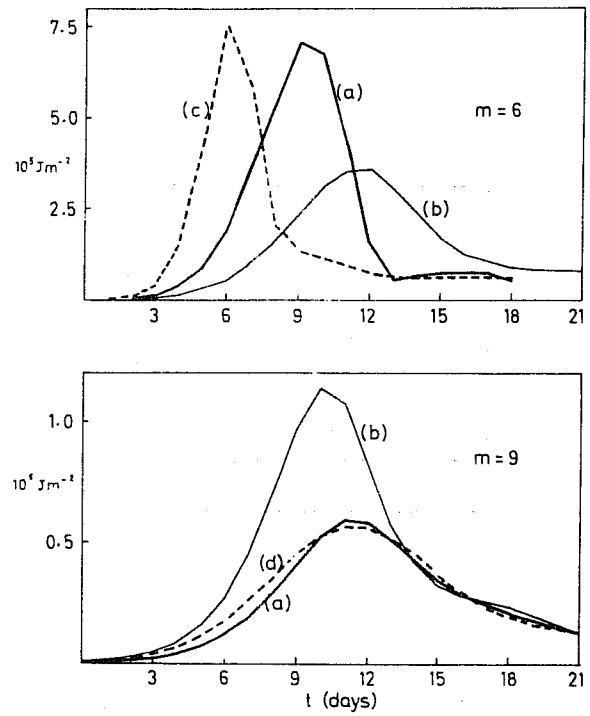

Fig. 6.3 Variation with time of the sum of eddy kinetic and eddy available potential energy for wavenumber 6 disturbances to (a) the 45° jet, (b) the broad 30° jet, and (c) the 55° jet.

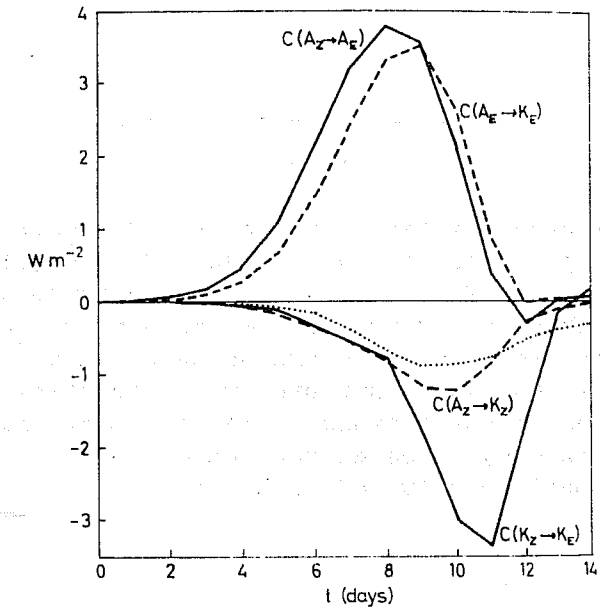

Fig. 6.4 Variation with time of various energy conversions and the net rate of energy dissipation (dotted curve) for the wavenumber 6 disturbance to the 45° jet. A_z and K_e are the zonal and eddy available potential energies, and K_z and K_e the corresponding kinetic energies. Positive values of $C(A_z \rightarrow A_e)$ imply a transfer from A_z to A_e, and negative values imply a reversed transfer.

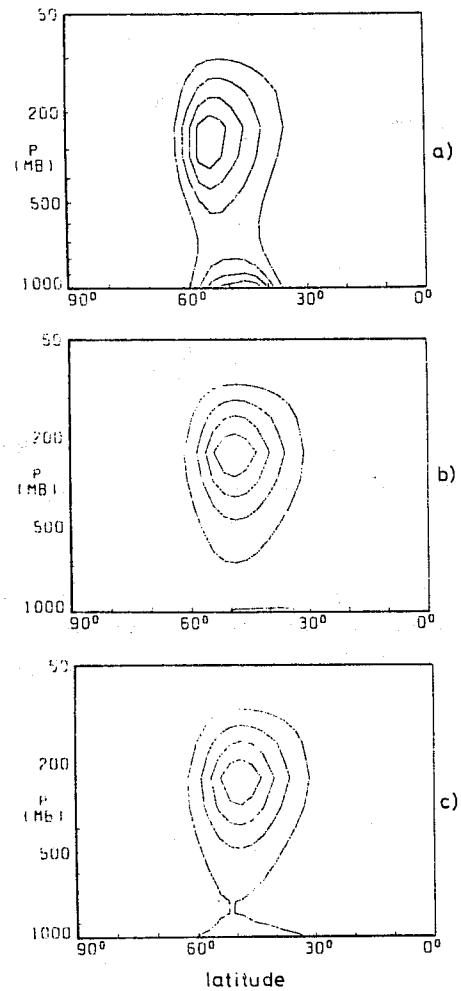

Fig. 6.5 Meridional cross sections of eddy kinetic energy density $[\frac{1}{2}(u'^2+ v'^2)]$ at (a) day 0, (b) day 10, and (c) averaged from day 4 to day 14, for the wavenumber 6 disturbance to the 45° jet. For this and subsequent sections values are linearly interpolated to pressure coordinates using a mean surface pressure of 1000 mb. Contours are drawn using linear interpolation between values defined on the computational grid, and results are normalized by choosing the contour interval to be one fifth the maximum value of each field.

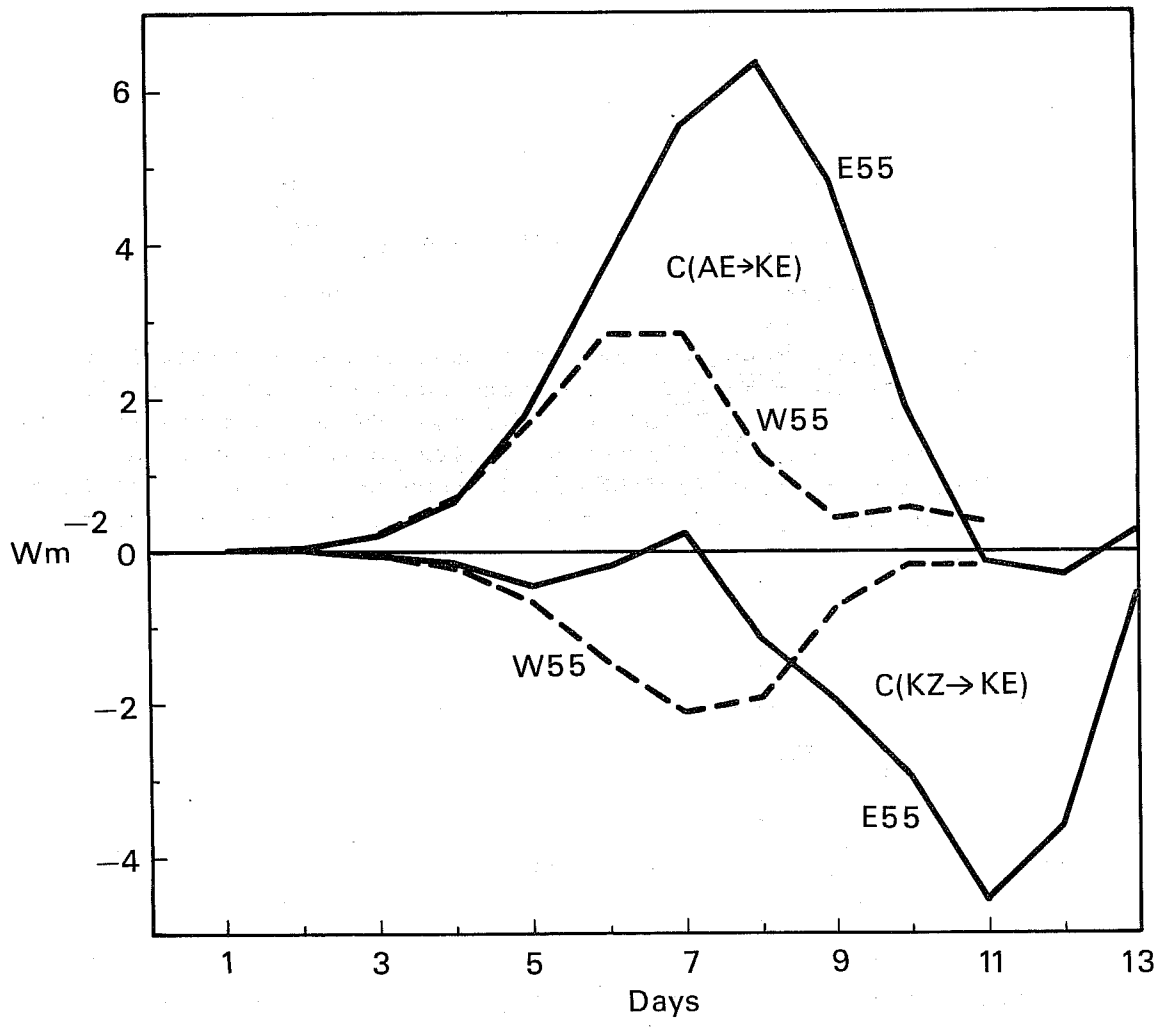

Fig. 6.6 Variation with time of the conversion from eddy available to eddy kinetic energy, and from zonal to eddy kinetic energy for two cases discussed in the text.

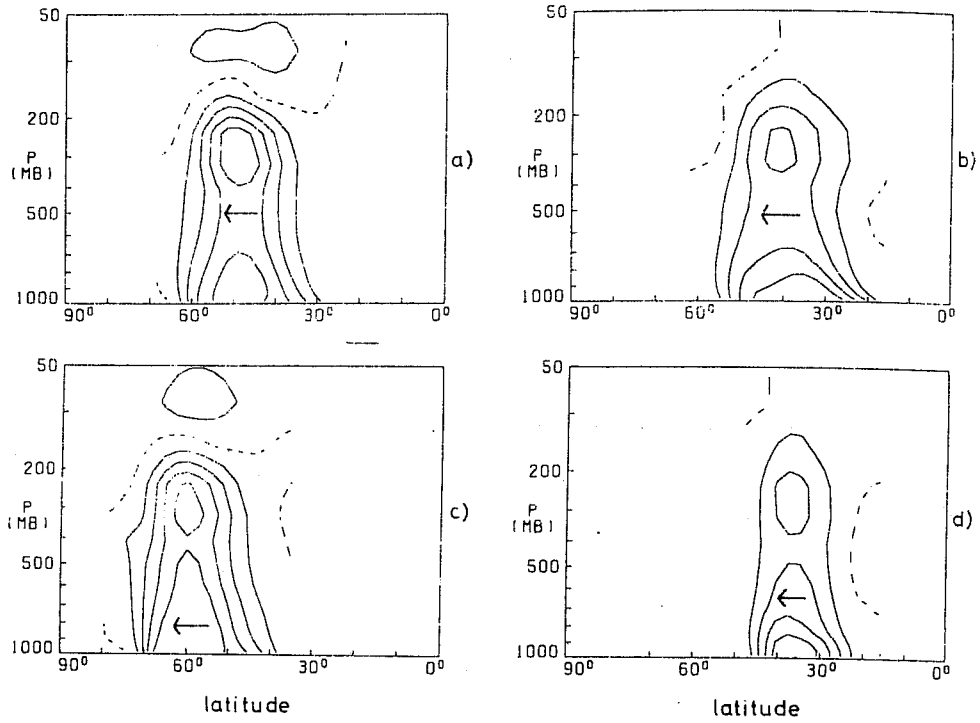

Fig. 6.7 Meridional cross sections of time-averaged horizontal eddy heat fluxes $\overline{v'T'}$ for wavenumber 6 disturbances to (a) the 45° jet, (b) the broad 30° jet, (c) the 55° jet and (d) the narrow 30° jet. The direction of each flux is indicated by an arrow. The zero contour is dashed and drawn only at those latitudes where the amplitude at some level exceeds one-tenth of the contour interval.

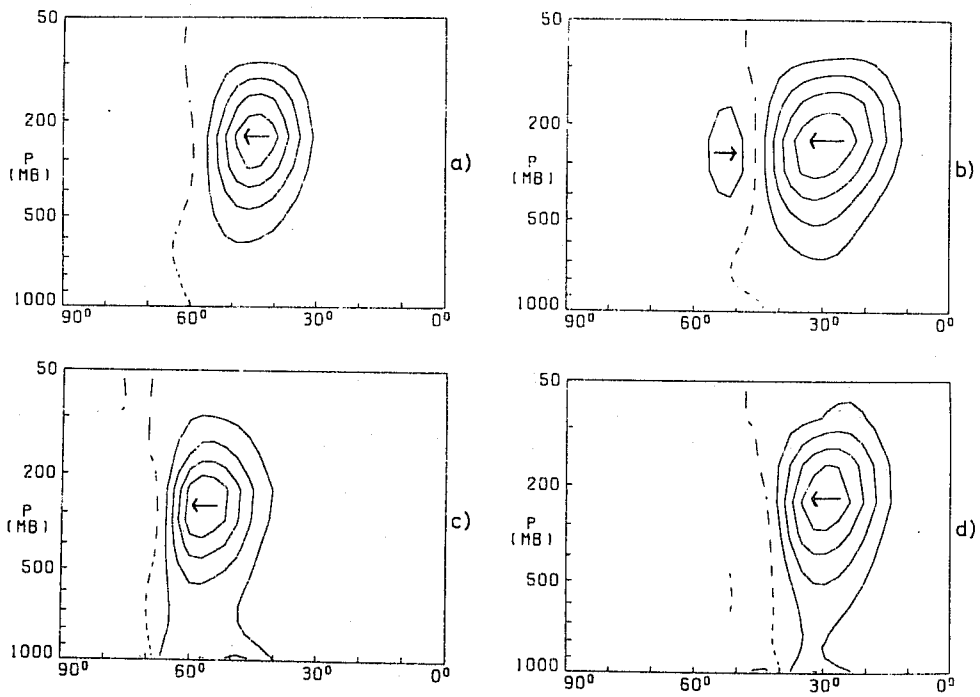

Fig. 6.8 Meridional cross sections of horizontal eddy momentum fluxes $\overline{u'v'}$ for the same cases as in Fig. 6.7.

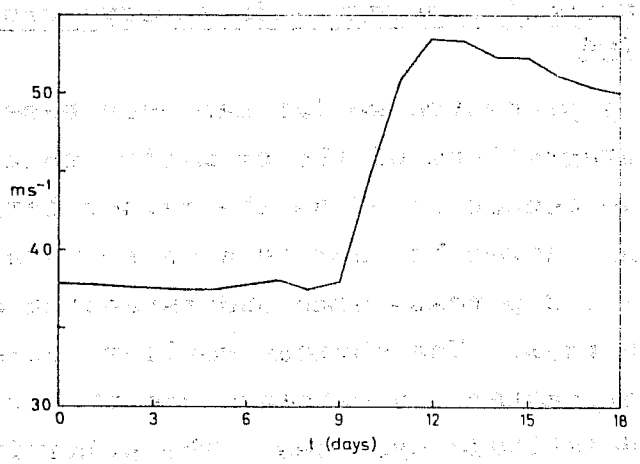

Fig. 6.9 Variation with time of the maximum zonal-mean velocity in the case of the wavenumber 6 disturbance to the 45° jet.

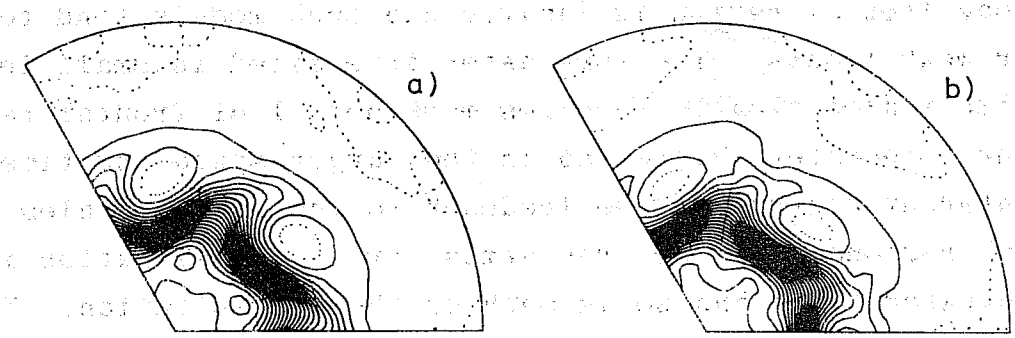

Fig. 6.10 Streamfunction after (a) 12 h and (b) 1 day from an integration of the barotropic vorticity equation which used as initial conditions the field at day 10 shown in Fig. 6.2.

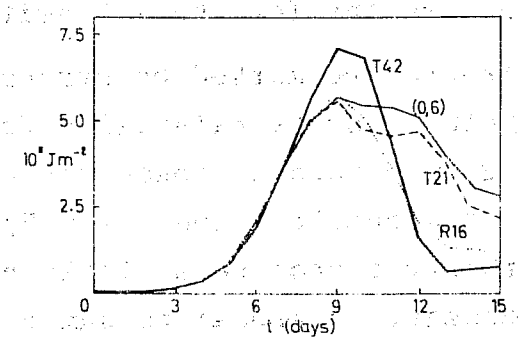

Fig. 6.11 Variation with time of the net eddy energy for the wavenumber 6 disturbance to the 45° jet integrated using triangular truncation at total wavenumber 42 (T42), triangular truncation at wavenumber 21 (T21), rhomboidal truncation at zonal wavenumber 16 (R16) and a severe zonal truncation [(0,6)].

7. Two dimensional frontogenesis theory: cross-frontal circulation

The theory presented so far has been based on linear models or nonlinear integrations of the primitive equations on the sphere. We have concentrated on the rather larger scale features of the baroclinic waves but now we wish to turn to some of the finer structure and perhaps some understanding of the "weather" associated with them. The obvious smaller scale features which dominate the forecaster's vocabulary are the fronts which are embedded in mid-latitude cyclones. The primitive equation integrations discussed in the previous section do exhibit the formation of frontal regions, even in the absence of physical processes such as precipitation. However in any model built to represent the largest scales of the atmosphere the resolution of a strong frontal region is limited and such models tend to have rather weak fronts. The forecaster interested in small length and time scales clearly requires more detail of frontal regions. For the forecaster interested in the larger space and time scales the interest centres on the feedback to the larger scales from frontal regions. In the free atmosphere the dissipation is concentrated there and so is much of the precipitation. Thus to both forecasters more understanding of frontal regions is a necessity.

In this section we follow the work of Sawyer (1956) and Eliassen (1959, 1962) in deriving an equation for the circulation in a frontal region. We shall see how this equation leads to understanding of the reasons for the intensity of surface fronts.

Atmospheric fronts are marked by strong gradients in velocity and temperature and by rainfall. For strong fronts a velocity-scale $V \sim 20$ m s^{-1} and a cross-frontal length-scale $\ell \sim 200$ km would be reasonable. Then $R_0 = V/f\ell \sim 1$, so that quasi-geostrophic theory cannot be strictly applied. However, it is still not necessary to appeal to numerical solutions of the full nonlinear equations.

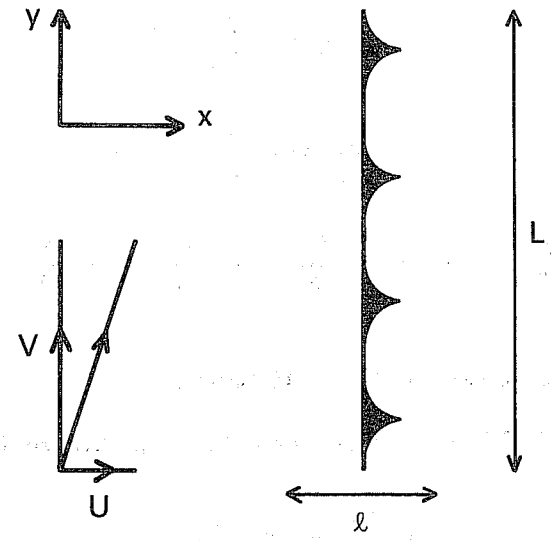

Fig. 7.1 Scales relative to a stationary front

We choose a coordinate system in which the front is stationary. As in Fig. 7.1, let ℓ, U and L,V be respectively length and velocity scales across and along the front. Observations show that V >> U. To perform a scale analysis, we assume that D/Dt $\sim$ U/ℓ. Then the ratios of the accelerations and the Coriolis forces in the x and y directions are

$$\frac{Du/Dt}{fv} = \frac{U^2/\ell}{fV} \sim \left(\frac{U}{V}\right)^2 \frac{V}{f\ell} << 1 \ , \qquad (7.1)$$

and

$$\frac{Dv/Dt}{fu} = \frac{UV/\ell}{fU} \sim \frac{V}{f\ell} \sim 1 \ . \qquad (7.2)$$

Thus we may use geostrophic balance in the cross-front direction, but not in the long-front direction: the acceleration of the long-front wind cannot be neglected.

The Boussinesq equations with the cross-front geostrophy approximation are

$$\frac{Dv}{Dt} + fu + \frac{\partial \phi}{\partial y} = 0 \ , \qquad (7.3)$$

$$\frac{D\theta}{Dt} = 0 \ , \qquad (7.4)$$

$$\nabla \cdot \underset{\sim}{u} = 0 \quad , \tag{7.5}$$

with

$$fv = \frac{\partial \phi}{\partial x} \quad , \tag{7.6}$$

$$\frac{g}{\theta_\infty} \theta = \frac{\partial \phi}{\partial z} \quad , \tag{7.7}$$

and

$$\frac{D}{Dt} = \frac{\partial}{\partial t} + u \frac{\partial}{\partial x} + v \frac{\partial}{\partial y} + w \frac{\partial}{\partial z} \quad . \tag{7.8}$$

For simplicity we take f = constant.

From (7.6) and (7.7) we have thermal wind balance

$$f \frac{\partial v}{\partial z} = \frac{g}{\theta_\infty} \frac{\partial \theta}{\partial x} \quad . \tag{7.9}$$

The role of the cross-frontal circulation is to maintain this balance when v is predicted from (7.3) and θ from (7.4).

We set

$$u = u_g + u', \; v = v_g, \; w = w' \tag{7.10}$$

where the primes indicate ageostrophic velocities, but no linearisation is implied. Using (7.8), $g/\theta_\infty \; \partial/\partial x$ of (7.4) gives

$$\begin{aligned} \frac{D}{Dt} \frac{g}{\theta_\infty} \frac{\partial \theta}{\partial x} &= - \frac{\partial u}{\partial x} \frac{g}{\theta_\infty} \frac{\partial \theta}{\partial x} - \frac{\partial v}{\partial x} \frac{g}{\theta_\infty} \frac{\partial \theta}{\partial y} - \frac{\partial w}{\partial x} \frac{g}{\theta_\infty} \frac{\partial \theta}{\partial z} \\ &= Q - \frac{\partial u'}{\partial x} \frac{g}{\theta_\infty} \frac{\partial \theta}{\partial x} - \frac{\partial w'}{\partial x} \frac{g}{\theta_\infty} \frac{\partial \theta}{\partial z} \end{aligned} \tag{7.11}$$

where the purely geostrophic contribution is

$$Q = - \frac{\partial u_g}{\partial x} \frac{g}{\theta_\infty} \frac{\partial \theta}{\partial x} - \frac{\partial v_g}{\partial x} \frac{g}{\theta_\infty} \frac{\partial \theta}{\partial y} \quad . \tag{7.12}$$

The first term in Q describes the formation of larger x-temperature gradients due to geostrophic convergence and the second term the effect of meridional shears in a basic temperature gradient. Similarly f $\partial/\partial z$ of (7.3) gives

$$\frac{D}{Dt} f \frac{\partial v}{\partial z} = - f \frac{\partial u}{\partial z} \frac{\partial v}{\partial x} - f \frac{\partial v}{\partial z} \frac{\partial v}{\partial y} - f \frac{\partial w}{\partial z} \frac{\partial v}{\partial z} - f^2 \frac{\partial u'}{\partial z}$$

$$= - Q - f \left(f + \frac{\partial v_g}{\partial x} \right) \frac{\partial u'}{\partial z} - \frac{g}{\theta_\infty} \frac{\partial \theta}{\partial x} \frac{\partial w'}{\partial z} \qquad (7.13)$$

The second line follows after a little manipulation. (7.11) and (7.13) show that the geostrophic motion acts through Q to tend to destroy thermal wind balance (7.9) by changing the two halves equally but in opposite senses. The ageostrophic circulation $(u', 0, w')$ acting through the other terms in (7.11) and (7.13) is necessary to maintain geostrophic balance.

Since the geostrophic wind is non-divergent, (7.10) in (7.5) gives

$$\frac{\partial u'}{\partial x} + \frac{\partial w'}{\partial z} = 0 \quad . \qquad (7.14)$$

Therefore we may define a cross-front streamfunction ψ such that

$$u' = \frac{\partial \psi}{\partial z} \quad , \quad w' = - \frac{\partial \psi}{\partial x} \quad . \qquad (7.15)$$

Subtracting (7.13) from (7.11) gives

$$\frac{g}{\theta_\infty} \frac{\partial \theta}{\partial z} \frac{\partial^2 \psi}{\partial x^2} - 2 \frac{g}{\theta_\infty} \frac{\partial \theta}{\partial x} \frac{\partial^2 \psi}{\partial x \partial z} + f \left(f + \frac{\partial v_g}{\partial x} \right) \frac{\partial^2 \psi}{\partial z^2} = - 2Q \qquad (7.16)$$

This is the cross-front streamfunction equation. Following Eliassen (1962) it may be turned into standard form by introducing a new variable in the x-direction:

$$X = x + v_g / f \quad . \qquad (7.17)$$

It can be shown that (7.16) then reduces to

$$\frac{\partial}{\partial X} \left(q \frac{\partial \psi}{\partial X} \right) + f^2 \frac{\partial^2 \psi}{\partial Z^2} = - \frac{2Q}{1 + \frac{1}{f} \frac{\partial v_g}{\partial x}} \qquad (7.18)$$

where

$$q = \frac{g}{f \theta_\infty} \left[\left(f + \frac{\partial v}{\partial x} \right) \frac{\partial \theta}{\partial z} - \frac{\partial v}{\partial z} \frac{\partial \theta}{\partial x} \right] \qquad (7.19)$$

is an approximation for the Ertel potential vorticity consistent with the cross-front geostrophy approximation. The equation is elliptic if q is positive which is normally true.

For a closed streamline around a region where Q is positive and the right hand side of (7.18) is negative, integration of (7.18) over the area bounded by the streamline shows that the normal derivative of ψ is negative. Thus the circulation is in the sense shown in Fig. 7.2a. Point sources give elliptical streamlines with ratio of axes $q^{\frac{1}{2}}/f$. As shown in Fig. 7.2b transformation back to x tilts the ellipses along lines X = const., and produces more intense flow in regions in which $\partial X/\partial x > 1$.

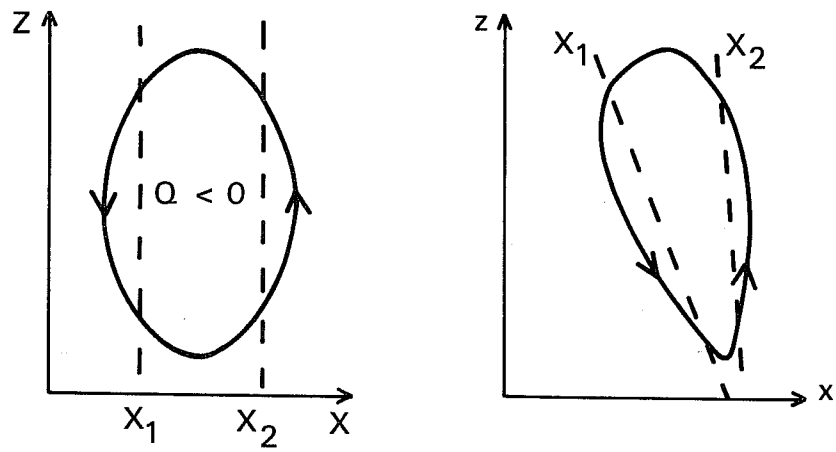

Fig. 7.2 (a) Closed streamline around a region where Q > 0, shown in transformed space.
(b) The same streamline in physical space.
Two lines X = const. are indicated

So far the coordinate transformation has been treated just as an analytical aid, but it is now worth considering it a little deeper and in particular to discover the significance of the condition $\partial X/\partial x > 1$. From (7.17), the Jacobian of the

transformation is

$$\frac{\partial X}{\partial x} = 1 + \frac{1}{f}\frac{\partial v_g}{\partial x} \qquad (7.20)$$

The cross-front geostrophic balance implies that $\partial u/\partial y$ ($\sim U/L$) should be neglected compared with $\partial v/\partial x$ ($\sim V/\ell$) in the vertical component of relative vorticity so that the vertical component of absolute vorticity is

$$\zeta = f + \partial v_g/\partial x \quad . \qquad (7.21)$$

Therefore the Jacobian of the transformation is

$$\frac{\partial X}{\partial x} = \frac{\zeta}{f} \quad . \qquad (7.22)$$

This implies that X changes rapidly compared with x in regions of large vorticity such as fronts, i.e. X acts as a stretched coordinate for regions of large vorticity. The interpretation of Fig. 7.2b is thus that there are intense gradients in cross-front circulation in regions of large positive vorticity.

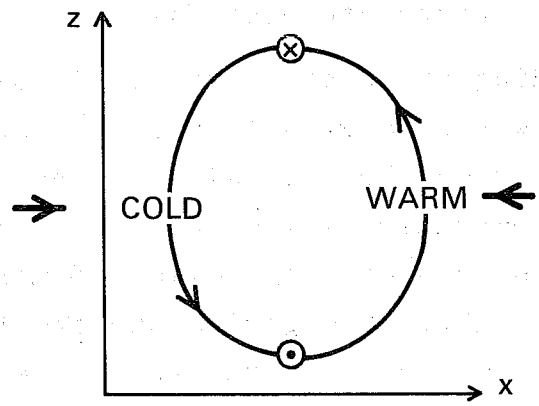

Fig. 7.3 A frontogenetic situation in which in large-scale motion is providing a region in which cold and warm air are tending to move together. ⊗ indicates flow into the paper and ⊙ out of the paper

Now consider the situation shown in Fig. 7.3. An x-temperature gradient is balanced by a vertical shear in v. The large-scale geostrophic motion is such as to tend to increase the temperature gradient either because of the horizontal convergence shown or because of horizontal shears in v in the presence of a y-temperature gradient. Thus from (7.11) and (7.12) Q is positive. We note that (7.13) shows that the geostrophic motion is tending to decrease the vertical shear in v, though this is not as obvious. To maintain thermal wind balance the cross-front circulation must be as shown, these ageostrophic motions tending to decrease $\partial\theta/\partial x$ and increase $\partial v/\partial z$. In region A, the relative vorticity is positive. The vorticity equation at the ground is

$$\frac{D\zeta}{Dt} = \zeta \frac{\partial w}{\partial z} \quad . \tag{7.23}$$

The stretching due to the ageostrophic cross-front circulation ($\partial w/\partial z$) is positive and so the vorticity increases. As the vorticity increases so the cross-front circulation gradients locally become more intense. In particular $\partial w/\partial z$ increases with ζ. Thus (7.23) predicts a nonlinear feedback leading to unbounded vorticity in a finite time. As the vorticity becomes large so does the temperature gradient.

Thus the diagnostic cross-front circulation equation can be used to explain why strong surface fronts occur. The front is predicted to occur on the warm side of the temperature contrast and to have the warm air rising above it. The ageostrophic circulation tends to slope the region of maximum positive vorticity with height, thus giving the frontal slope. Away from the surface the front can be expected to be weaker though if the tropopause acts somewhat like a lid frontogenesis can be expected also in region B. Such upper tropospheric frontogenesis is also observed.

8. Semi-geostrophic theory: two-dimensional frontogenesis

The discussion in the previous section centred on a diagnostic cross-frontal circulation equation. However the same basic cross-front geostrophy approximation and transformation of coordinates allows analytic solution of models in which the time development of two-dimensional frontal regions is described. The derivation is a specialisation of the three-dimensional semi-geostrophic theory. Here we briefly derive the semi-geostrophic equations and apply them to two-dimensional models of frontogenesis. In the next solution we shall use them to study frontogenesis in growing baroclinic waves.

The geostrophic approximation to the wind (1.4) was deduced from a small Rossby number analysis. It is however more general than this implies. It is a good approximation to the wind vector if

$$\left|\frac{D}{Dt}\,\underset{\sim}{u}_h\right| \Big/ \left|f\,\underset{\sim}{u}_h\right| \ll 1 \qquad (8.1)$$

i.e. if the magnitude and direction of the momentum of a fluid particle changes little in the time $f^{-1} \sim 3$ h. The latter restriction is equivalent to demanding that the curvature vorticity be much smaller than f. Any theory based on this approximation clearly filters out gravity-inertia waves but not frontogenesis which from the Lagrangian point of view is not a process with rapid fluctuations. All that happens in frontogenesis is that fluid particles which were initially a long way apart become neighbours.

We shall use the Boussinesq f-plane equations for the subsequent analysis. Taking the vector cross product of the momentum equation (1.42) with $\underset{\sim}{k}$ yields

$$\underset{\sim}{U}_h = \underset{\sim}{U}_g + \underset{\sim}{k} \wedge \frac{1}{f}\frac{D\underset{\sim}{U}_h}{Dt} \qquad . \qquad (8.2)$$

Using this expression for $\underset{\sim}{U}_h$ in the last term on the right hand side gives

$$\underset{\sim}{U}_h = \underset{\sim}{U}_g + \underset{\sim}{k} \wedge \frac{1}{f}\frac{D\underset{\sim}{U}_g}{Dt} - \frac{1}{f^2}\frac{D^2\underset{\sim}{U}_h}{Dt^2} \qquad . \qquad (8.3)$$

Clearly this substitution could be continued, but we now neglect the last term on the basis that symbolically $\frac{D^2}{Dt} << f^2$. This is called the geostrophic momentum approximation because the full Boussinesq equations are retained except that the momentum is approximated by its geostrophic value. The approximation was first introduced by Eliassen (1948).

Our equations are thus (1.43) - (1.45) but with (1.42) replaced by

$$\frac{D\underset{\sim}{U}_g}{Dt} + f\,\underset{\sim}{k} \wedge \underset{\sim}{U}_h + \nabla\phi = 0 \quad . \tag{8.4}$$

It should be noted that the ageostrophic motions are retained in the advection but not in the momentum. This is analogous to the hydrostatic approximation in whuch the vertical motion is also retained in the advection but not in the momentum.

Like the original Boussinesq equations, this modified set conserves potential temperature, has a full energy equation, three-dimensional vorticity equation and an Ertel potential vorticity conservation equation. The kinetic energy is only that associated with the geostrophic flow and the vorticity $\underset{\sim}{\zeta}_g$ is the full three-dimensional vorticity evaluated using geostrophic velocities plus a term that is negligible when the curvature vorticity is negligible. The Ertel potential vorticity is

$$q_g = \underset{\sim}{\zeta}_g \cdot \nabla\theta \simeq -\frac{\partial v_g}{\partial z}\frac{\partial\theta}{\partial x} + \frac{\partial u_g}{\partial z}\frac{\partial\theta}{\partial y} + \left(f + \frac{\partial v_g}{\partial x} - \frac{\partial u_g}{\partial y}\right)\frac{\partial\theta}{\partial z} \quad . \tag{8.5}$$

The inclusion of the first two terms should be noted.

Just as in the analysis of the cross-front streamfunction equation we introduce a transformation of coordinates. For the three-dimensional case we use

$$X = x + v_g/f, \quad Y = y - u_g/f, \quad Z = z, \quad T = t \quad . \tag{8.6}$$

Again the Jacobian of the coordinate transformation is

$$J = \underset{\sim}{k} \cdot \underset{\sim}{\zeta}_g / f$$

showing that they quite generally act as stretched coordinates for regions of large vorticity. The horizontal coordinates (8.6) may be referred to as geostrophic coordinates because

$$\frac{DX}{Dt} = u + \frac{1}{f}\frac{Dv_g}{Dt} = u_g \quad \text{and} \quad \frac{DY}{Dt} = v_g \quad . \tag{8.7}$$

Thus in the transformed space horizontal advection is geostrophic and the material time derivative becomes

$$\frac{D}{Dt} = D_g + w\frac{\partial}{\partial z} \quad \text{where } D_g = \frac{\partial}{\partial T} + u_g\frac{\partial}{\partial X} + v_g\frac{\partial}{\partial Y} \quad . \tag{8.8}$$

If we set

$$\Phi = \phi + \tfrac{1}{2}\left(u_g^2 + v_g^2\right) \quad , \tag{8.9}$$

it can be shown that

$$\nabla_X\Phi = \nabla_x\phi \quad , \tag{8.10}$$

so that

$$u_g = -\frac{1}{f}\frac{\partial\Phi}{\partial Y} \quad , \quad v_g = \frac{1}{f}\frac{\partial\Phi}{\partial x} \quad , \quad \theta = \frac{\theta_\infty}{g}\frac{\partial\Phi}{\partial Z} \quad . \tag{8.11}$$

Neglecting small terms in the vorticity, the non-dimensional vertical component is

$$J = 1 + \frac{1}{f}\left(\frac{\partial v_g}{\partial x} - \frac{\partial u_g}{\partial y}\right) = \left[1 - \frac{1}{f}\left(\frac{\partial v_g}{\partial X} - \frac{\partial u_g}{\partial Y}\right)\right]^{-1} \tag{8.12}$$

so that

$$J^{-1} = 1 - \frac{1}{f^2}\left(\frac{\partial^2\Phi}{\partial X^2} + \frac{\partial^2\Phi}{\partial Y^2}\right) \quad . \tag{8.13}$$

Finally it can be shown that

$$q_g = f\,J\frac{\partial\theta}{\partial Z} \quad . \tag{8.14}$$

Substituting for J from (8.13), for θ from (8.11) and rearranging,

$$\frac{1}{f^2}\left(\frac{\partial^2\Phi}{\partial X^2}+\frac{\partial^2\Phi}{\partial Y^2}\right)+\frac{f\theta_\infty}{g}\frac{1}{q_q}\frac{\partial^2\Phi}{\partial Z^2}=1 \quad . \tag{8.15}$$

We recall that q_g and θ are conserved quantities so that

$$\left(D_g+w\frac{\partial}{\partial Z}\right)q_g=0 \quad , \tag{8.16}$$

and

$$\left(D_g+w\frac{\partial}{\partial Z}\right)\frac{\partial\Phi}{\partial Z}=0 \quad . \tag{8.17}$$

If q_g is advected in the fluid using (8.16) then (8.15) is an elliptic equation for Φ and hence u_g, v_g and θ which is soluble if $\partial\Phi/\partial Z$ is determined on horizontal boundaries by (8.17) with $w \equiv 0$. Once u_g and v_g are found, the solution may be transformed back to physical space. The advection of q_g as given by (8.16) requires a knowledge of w. This could be determined by the consistency of (8.16) and (8.17). However a **diagnostic** equation for w has been derived in Hoskins and Draghici (1977). It is a generalisation of the quasi-geostrophic omega equation. In the two-dimensional case it reduces to the cross-frontal circulation equation (7.18). The equations (8.15) - (8.17) are the semi-geostrophic equations (Hoskins, 1975).

In the subsequent development we shall restrict ourselves to cases of a uniform Ertel potential vorticity fluid bounded above and below by surfaces z = constant. (8.16) is now trivial so that, setting

$$q_g=\frac{f\theta_\infty}{g}N^2 \quad , \quad \Phi'=\Phi-N^2Z^2/2 \quad , \tag{8.18}$$

the mathematical problem is to solve

$$\frac{1}{f^2}\left(\frac{\partial^2\Phi'}{\partial X^2}+\frac{\partial^2\Phi'}{\partial Y^2}\right)+\frac{1}{N^2}\frac{\partial^2\Phi'}{\partial Z^2}=0 \tag{8.19}$$

with

$$\left(\frac{\partial}{\partial T}-\frac{1}{f}\frac{\partial\Phi'}{\partial Y}\frac{\partial}{\partial X}+\frac{1}{f}\frac{\partial\Phi'}{\partial X}\frac{\partial}{\partial Y}\right)\frac{\partial\Phi'}{\partial Z}=0 \tag{8.20}$$

on horizontal boundaries.

Referring back to (1.48) we see that the problem is identical with that given by quasi-geostrophic f-plane theory for cases of uniform quasi-geostrophic potential vorticity. The crucial difference is that the solution has to be transformed back to physical space. The importance of this will become apparent below.

Guided by the quasi-geostrophic studies of Stone (1966), Williams and Plotkin (1968) and Williams (1968) we first consider a two-dimensional model in which the frontogenesis is forced by large-scale horizontal convergence, i.e. the first term in Q in (7.12). We consider a basic wind field corresponding to

$$\overline{\Phi'} = f\,\alpha\,XY \quad , \quad u_g = -\alpha X \quad , \quad v_g = \alpha Y \quad . \tag{8.21}$$

In physical space this is

$$\phi = \frac{f\alpha}{1-\frac{\alpha^2}{f^2}}\left[xy + \frac{\alpha}{2f}\,(x^2+y^2)\right] \quad , \quad u_g = -\frac{\alpha}{1-\frac{\alpha^2}{f^2}}\left(x + \frac{\alpha}{f}\,y\right) \quad ,$$

$$v_g = \frac{\alpha}{1-\frac{\alpha^2}{f^2}}\left(y + \frac{\alpha}{f}\,x\right) \quad . \tag{8.22}$$

Since we will take $\alpha/f \sim .1$, this basic flow is little different from the classical horizontal deformation field of Bergeron :

$$u_g = -\alpha x \quad , \quad v_g = \alpha y \quad . \tag{8.23}$$

If we set

$$\Phi' = \overline{\Phi'} + \tilde{\Phi} \tag{8.24}$$

in (8.19) we see that if $\tilde{\Phi}$ is initially independent of Y then it remains so. In this case the equations reduce to

$$\frac{1}{f^2}\,\frac{\partial^2\tilde{\Phi}}{\partial X^2} + \frac{1}{N^2}\,\frac{\partial^2\tilde{\Phi}}{\partial Z^2} = 0 \tag{8.25}$$

with

$$\left(\frac{\partial}{\partial T} - \alpha X\,\frac{\partial}{\partial X}\right)\frac{\partial\tilde{\Phi}}{\partial Z} = 0 \quad \text{on horizontal boundaries .} \tag{8.26}$$

(8.26) implies that if $\frac{\partial\tilde{\Phi}}{\partial Z} = \Theta(X/L_0)$ on a horizontal boundary at time $T = 0$, at any later time T its distribution on that boundary is $\Theta(X/L)$ where

$$L = L_0\,e^{-\alpha T} \quad . \tag{8.27}$$

The scale of the potential temperature distribution on boundaries decreases exponentially with time. Thus if initial boundary potential temperature distributions are specified, boundary conditions for (8.25) may be given at any subsequent time and the problem may be solved by standard methods.

For boundary potential temperature distributions of the form $\tan^{-1}(X/L)$ with 24K total temperature contrast a solution when L = 200 km is shown in Fig. 8.1. At the ground there are large gradients in velocity and temperature towards the warm side of the region. The maximum vertical component of relative vorticity is about 1.3f but the minimum is only - .36f. The maximum gradients tilt with height with a slope of order one in one hundred. For this problem it is not necessary to compute the cross-frontal circulation but for interest the figure also shows this circulation added on to the basic convergence. There is rising motion in the warm air above the surface front and descent in the colder air. The frontogenesis process is so rapid that the maximum vorticity triples for L = 150 km which for $\alpha = 10^{-5}$ s^{-1} takes 8½h. In another 5h infinite gradients are predicted.

The quasi-geostrophic solution in comparison has equal positive and negative vorticity, no tilts with height and no tendency to produce discontinuities. When the semi-geostrophic theory gives relative vorticity ζ = 1.3f, 3.9f and ∞, the quasi-geostrophic theory gives $\zeta \simeq$ .6f, .8f and 1.0f respectively. All these characteristics are associated with the ageostrophic motion implies by the coordinate transformation. This may be understood by referring to the y equation of motion which with the geostrophic momentum approximation may be written

$$\frac{Dv_g}{Dt} = - f u_{ag} = - f \frac{Dx_{ag}}{Dt} \qquad (8.28)$$

where we define x_{ag} to be the x-displacement of a particle due to ageostrophic u. Therefore if a fluid particle changes its y-velocity by Δv_g, it must suffer an ageostrophic displacement in the x-direction

$$\Delta x_{ag} = - \Delta v_g / f \quad . \qquad (8.29)$$

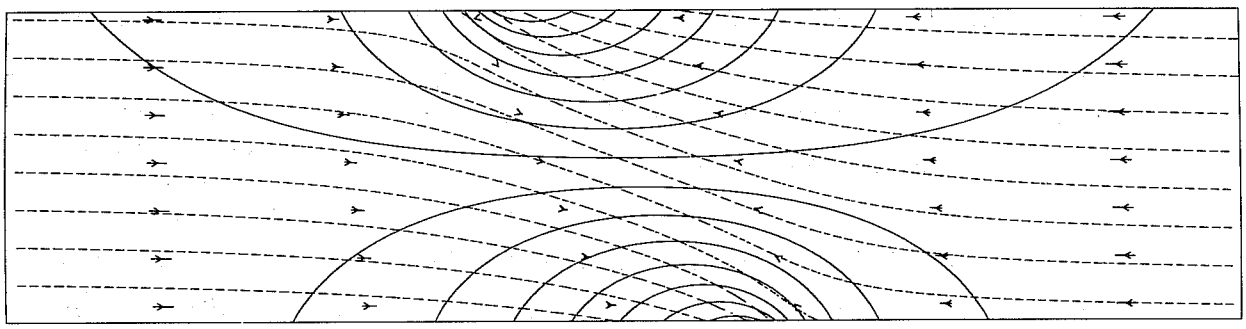

Fig. 8.1 Two-dimensional frontogenesis forced by horizontal convergence. Details in text. Dashed contours are potential temperature drawn every 4K and continous contours are long front wind v drawn every 5 ms^{-2} . The total cross-front motion is indicated by vectors.

This is precisely the displacement of the particle implied by the transformation $X \rightarrow x$.

To produce a two-dimensional frontogenesis model in which the process is forced by the second term in Q in (7.12), i.e. by meridional velocities in the presence of a temperature gradient, we again allow ourselves to be guided by quasi-geostrophic theory. The two-dimensional Eady wave discussed in section 3 was a solution of the nonlinear quasi-geostrophic equations, having uniform potential vorticity. Thus it is also a solution of the semi-geostrophic equations and the physical space solution merely requires the final coordinate transformation. Cross-sections of the solution have been given in Hoskins and Bretherton (1972) and compared with the numerical primitive equation solutions of Williams (1967). The frontogenesis is very similar to that for the convergence model though the meridional winds reach $\pm$ 50 m s^{-1} before large vorticities are formed and these vorticities are associated to some extent with temperature gradients of both sign. For a different view, a surface chart for this Eady mode is shown in Fig. 8.2. At this time, the relative vorticity maximum in the low is 2.1f. With typical numbers, infinite velocity and temperature gradients are predicted within one day.

It has been shown in Andrews and Hoskins (1978) that semi-geostrophic theory predicts for strong fronts kinetic and available potential energy spectra closely approximating a - 8/3 power law as a function of horizontal wavenumber. The energy in the smallest scales is forced directly by the largest scales. This is in direct contrast with the quasi-geostrophic turbulence arguments of Charney (1971) which predict a -3 power law. The spectrum observed in the atmosphere and in general circulation models is not inconsistent with either theory.

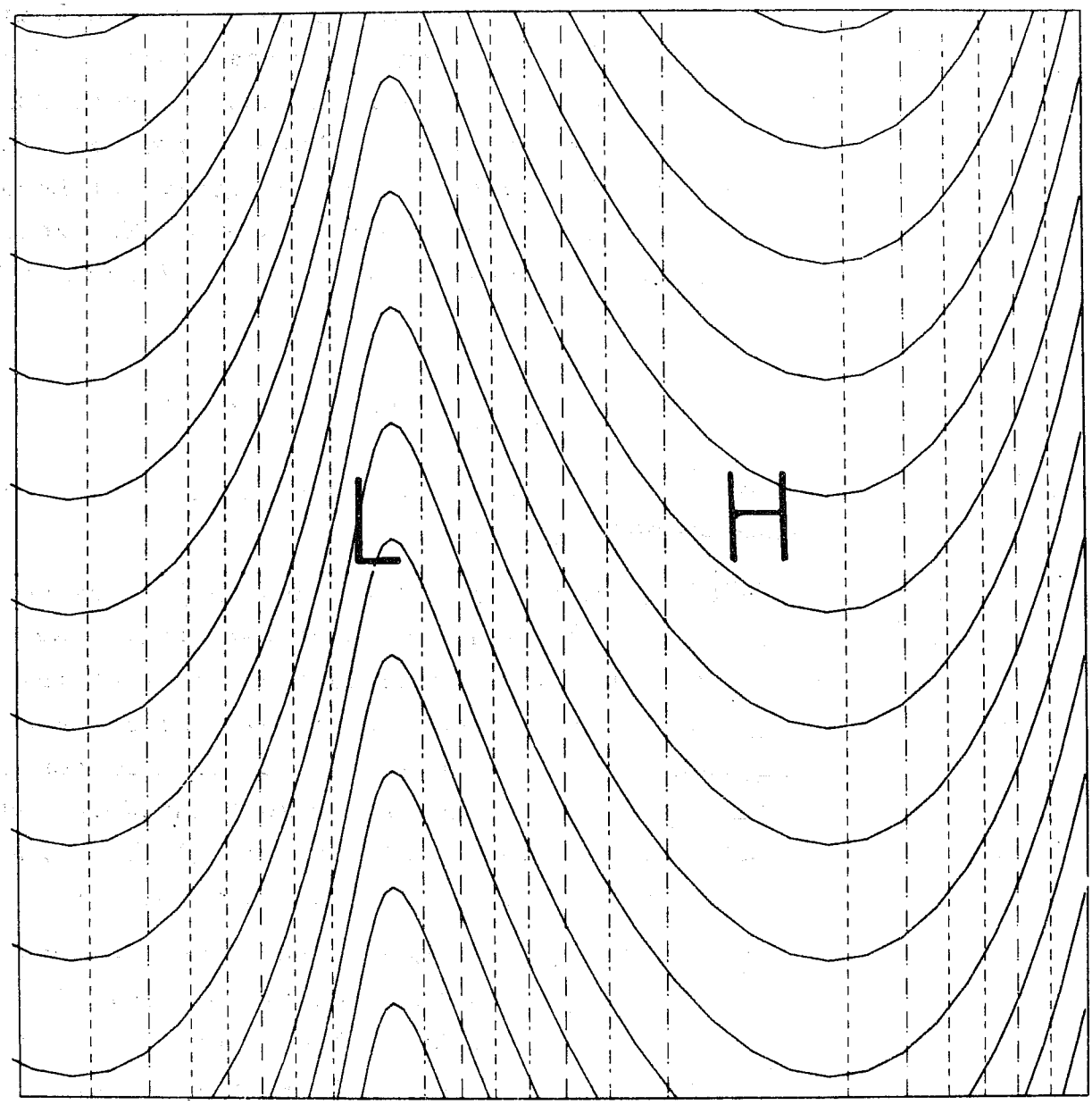

Fig. 8.2. Surface map for the nonlinear two-dimensional Eady wave. Contours of ϕ are dashed and drawn every 75m ($\sim$ 9mb) and those of θ are continuous and drawn every 6K. The domain shown is 5623 km in both horizontal directions. This is approximately $1\frac{1}{4}$ wavelengths in the zonal direction.

9. Warm and cold fronts in baroclinic waves

9.1 Simple jet flow solutions

The nonlinear two-dimensional Eady wave showed many of the characteristics of observed baroclinic waves but clearly to understand the formation of warm and cold fronts in baroclinic waves it is necessary to introduce some more complexity. The nonlinear development of Eady waves with latitudinal dependence has been investigated in Hoskins (1976). However more realistic results are obtained from consideration of the growth of baroclinic waves on zonal flows with horizontal shears. The zonal flows discussed in Hoskins and West (1979) have uniform potential vorticity and

$$\bar{u} = 0 \text{ on } Z = 0, \ \bar{u} = U - \frac{\mu}{2} U(1 + \cos \ell Y) \text{ on } Z = H . \qquad (9.1)$$

The domain is periodic in the Y direction with period $2\pi/\ell$. For $\mu = 0$ we recover the Eady flow.

The semi-geostrophic equations (8.19) and (8.20) are used first to determine the linear stability characteristics. By increasing μ from zero to unity it is found that the most unstable mode for each μ is a development from the two-dimensional Eady wave. For increasing μ, as the baroclinity becomes more concentrated near $Y = \pi/\ell$, so the amplitude of the most unstable mode becomes more biased to this region. This mode is always barotropically stable, its horizontal tilts being with the jet.

Having determined the unstable modes, these may be used as initial conditions for nonlinear integration of the semi-geostrophic equations (8.19) and (8.20). The solutions to be described here will be for the most unstable wave for that μ. The solution procedure is to set for the perturbation

$$\Phi = \sum_{-N \leq r,s \leq N} e^{i(rkX + s\ell Y)} \left(A_{r,s}(t) \cosh K_{r,s} z' + B_{r,s}(t) \sinh K_{r,s} z' \right) \qquad (9.2)$$

Then the interior equation is satisfied identically. The time tendencies of $A_{r,s}$ and $B_{r,s}$ are obtained from (8.20) using a spectral-transform technique on both boundaries. Time

integration is by means of a simple leap-frog scheme. The perturbation amplitude is determined to make $\Sigma(A_{l,s}^2 + B_{l,s}^2)$ the same for each case.

Parameter values are:

$N^2 = 1.2753.10^{-4}\ s^{-2}$, $H = 9$ km, $f = 10^{-4}\ s^{-1}$,

$U = 29.43\ m\ s^{-1}$, $g/\theta_\infty = 0.0327\ m\ s^{-2}\ K^{-1}$,

meridional wavelength $2\pi/\ell = 5623$ km,

truncation N = 21, time step 12 minutes.

The model requires 70 sec CP time per simulated day on a CDC 7600.

For $\mu = 0$, the most unstable mode has an x-wavelength of 3976 km and a doubling time of .89 days. The initial amplitude of v_g is .9 m s^{-1} and Fig. 8.2 showed the mode at day 5 when the maximum v_g was 45 m s^{-1}. For $\mu = \cdot 3$ the basic upper flow varies from 29.4 m s^{-1} in the centre to 20.6 m s^{-1} on the edges. The most unstable mode has wavelength almost exactly 4000 km and a doubling time of 1.1 days. The initial v_g amplitude is 1.5 m s^{-1}. By day $5\frac{1}{2}$ this has risen to 36 m s^{-1} and the surface pressure, temperature and relative vorticity are as shown in Fig. 9.1. The low has drifted northwards and has vorticities up to 3.8f in its centre. The high has moved southwards but has maximum negative relative vorticity only -.44f. There is a secondary maximum in positive vorticity, values up to 2.2f, and associated large horizontal temperature gradients in a cold frontal region to the south of the low. There is no warm front if one defines this to be an almost linear region with intense gradients in velocity and temperature tending to become infinite in a finite time. The kink in the zero vorticity contour ahead of the low is however interesting.

For $\mu = 1.0$, the basic flow at the lid varies from 29.4 m s^{-1} at the middle to zero at the edges. The most unstable mode has a wavelength of 4090 km and a doubling time of 1.3 days. The initial amplitude of v_g is about 1.7 m s^{-1}. By day 6 a cold front has developed and by day 6.3 (Fig. 9.2) it is intense. There are also signs of a weak warm front east of the low. The maximum northward wind is 30 m s^{-1} and the cold front contains vorticities of 5f and a temperature contrast of 4K in

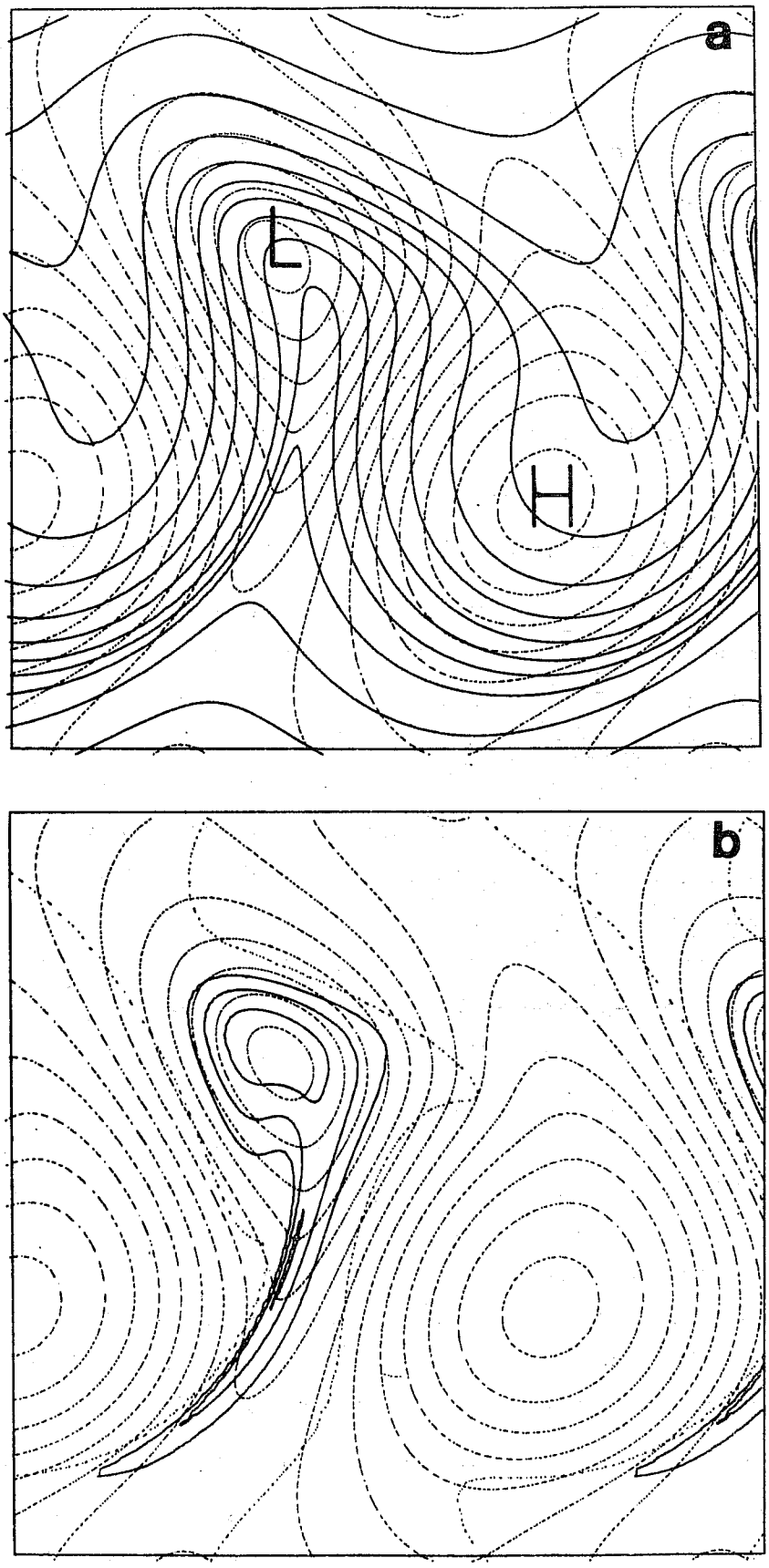

Fig. 9.1. Surface maps of (a) θ and ϕ, contours 4K and 50m ($\sim$ 6mb)
(b) relative vorticity (ξ) and ϕ
for the μ = .3 mode at day 5.5. The zero contour of ξ is dotted. Positive contours are continuous and drawn at .5f, 1f, 2f, 4f .... . Again 5623 km is shown in each horizontal direction.

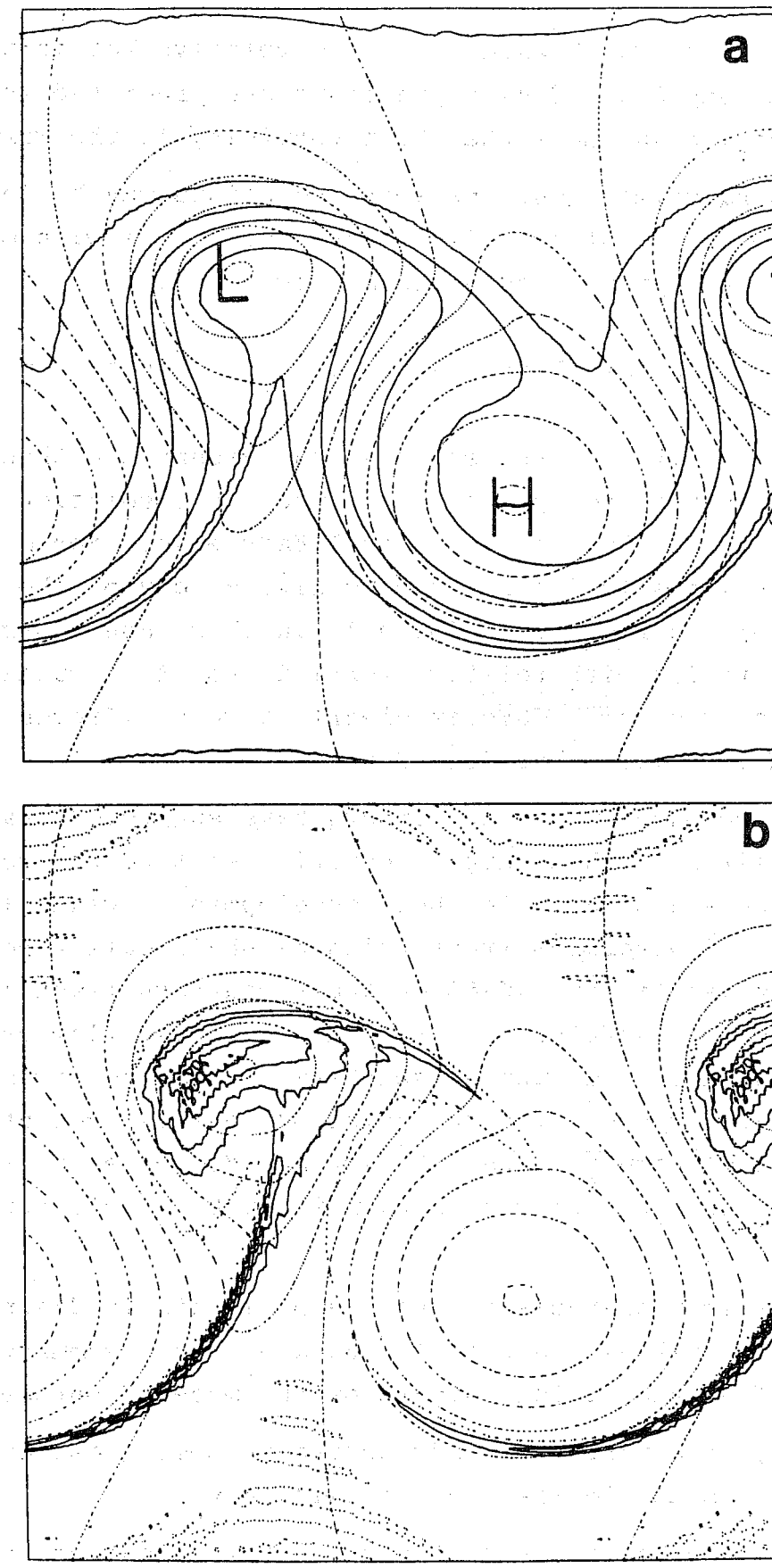

Fig. 9.2. Surface maps for the μ = 1 mode at day 6.3. Conventions as in Fig. 9.1.

40 km. In the weak warm front the relative vorticity is up to .9f. By day 6.5 infinite gradients are predicted in the cold front region and more than 1.5f vorticity in the warm front.

Using symmetries, the above solutions may be inverted to give the growth of baroclinic waves on a flow with meridional shear at the ground and uniform flow aloft:

$$\bar{u} = \frac{\mu}{2} U \cos \ell Y \text{ on } Z = 0, \quad \bar{u} = \left(1 - \frac{\mu}{2}\right) U \text{ on } Z = H. \qquad (9.3)$$

The waves tilt with the shear at the ground and thus in the opposite sense from previously. The $\mu = 0$ solution is, of course, still the two-dimensional Eady wave. For $\mu = .3$ the previous lid solution inverts to give at day $5\frac{1}{2}$ the surface maps shown in Fig. 9.3. There is in this case a strong warm frontal region with relative vorticities of 2f running south-east from the low. This is clearly a very different warm front from that exhibited in Fig. 9.2.

These experiments and others have suggested that baroclinic waves tilting with an upper westerly jet tend to produce strong cold fronts and later in their development a weak almost zonally oriented warm front which we shall call type A. Baroclinic waves tilting NW-SE on their southern flank in sympathy with positive vorticity in the surface zonal flow produce just strong warm fronts running south-east from the low and which we shall call type B. The occlusion process is present in that the area of warm air near the surface decreases in time. However the overtaking of a warm front by a cold front is not found.

The frontogenesis in these experiments is diagnosed in detail in Hoskins and West (1979) and only a summary is possible here. The crucial ingredients of the model frontogenesis are:

(1) the particle trajectories in semi-geostrophic space implied by a growing wave,

(2) the deformation fields in semi-geostrophic space produced by a growing wave,

(3) the ageostrophic motions implied by the semi-geostrophic transformation.

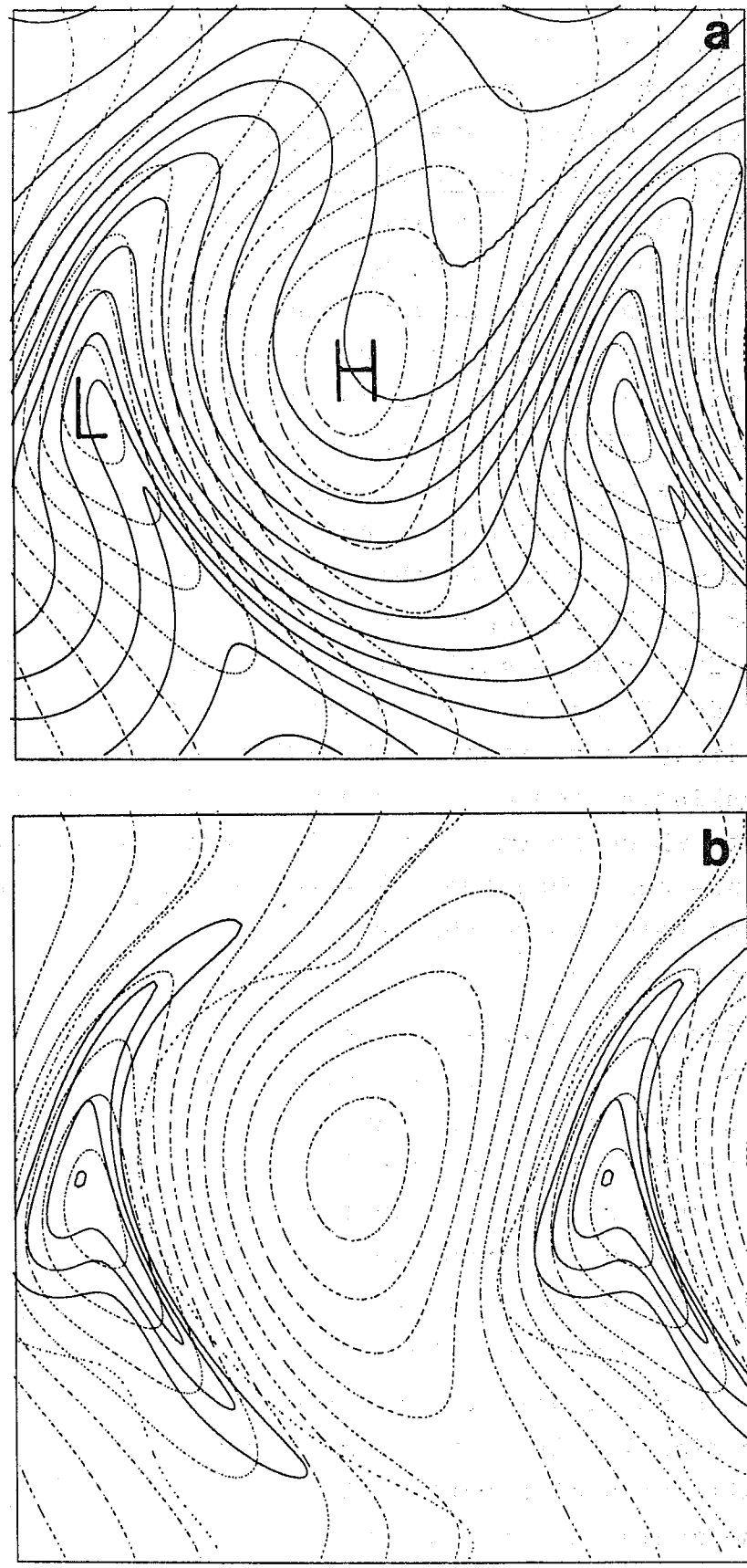

Fig. 9.3. Surface maps for the μ = .3 inverted mode at day 5.5. Conventions as in Fig. 9.1.

Fig. 9.4 shows the Z = 0 semi-geostrophic space day 6 solution for the μ = 1 flow and is equivalent to the quasi-geostrophic physical space solution. Also shown are some trajectories relative to the system from day 3 to day 6½. Initially air at the surface moves westwards relative to the growing wave at the phase speed (∿ 11½ m s^{-1}). As the wave grows, air south of the low tends to slow down and that north of the low tends to speed up. The air ahead of the low moves north and that behind it moves south. Fig. 9.5 shows the deformation field in semi-geostrophic space for this case at day 6. Its pattern is not significantly different from that given by the normal mode. As particles slow up approaching AC and then move towards BD their trajectories are correctly aligned for large temperature gradients to form in the region ABCD. The transformation implies strong frontogenesis on the warm side AB and this is the cold front. The region A′B′C′D′ is entirely symmetrical with ABCD in semi-geostrophic space but nonlinear frontogenesis occurs only on the warm side of the contrast which is this time C′D′. Here the process is slower and occurs only when the trajectories in the "warm sector" turn eastwards relative to the system. This is the formation of the warm front type A.

Deformation fields at Z = 0 for the μ = .3 inverted case at day 5.5 are shown in Fig. 9.6. This time the deformations south-east of the low are favourable for growth when the non-linear trajectories are such that air moves towards the low centre along this region and the temperature contours align with the dilatation axes there. The transformed solution contains frontogenesis on the warm side of this region and this is the warm front type B.

The crucial difference between the two cases discussed is the meridional tilt of the surface mode. It can be shown that for small tilts of a pattern the dilatation axes tilt through the same angle and this accounts for the difference between Figs. 9.4 and 9.6. The different tilt ensures that in the first case the transition region west of the warm sector exhibits frontogenesis (the cold front) while in the second it is the transition region east of the warm sector that is

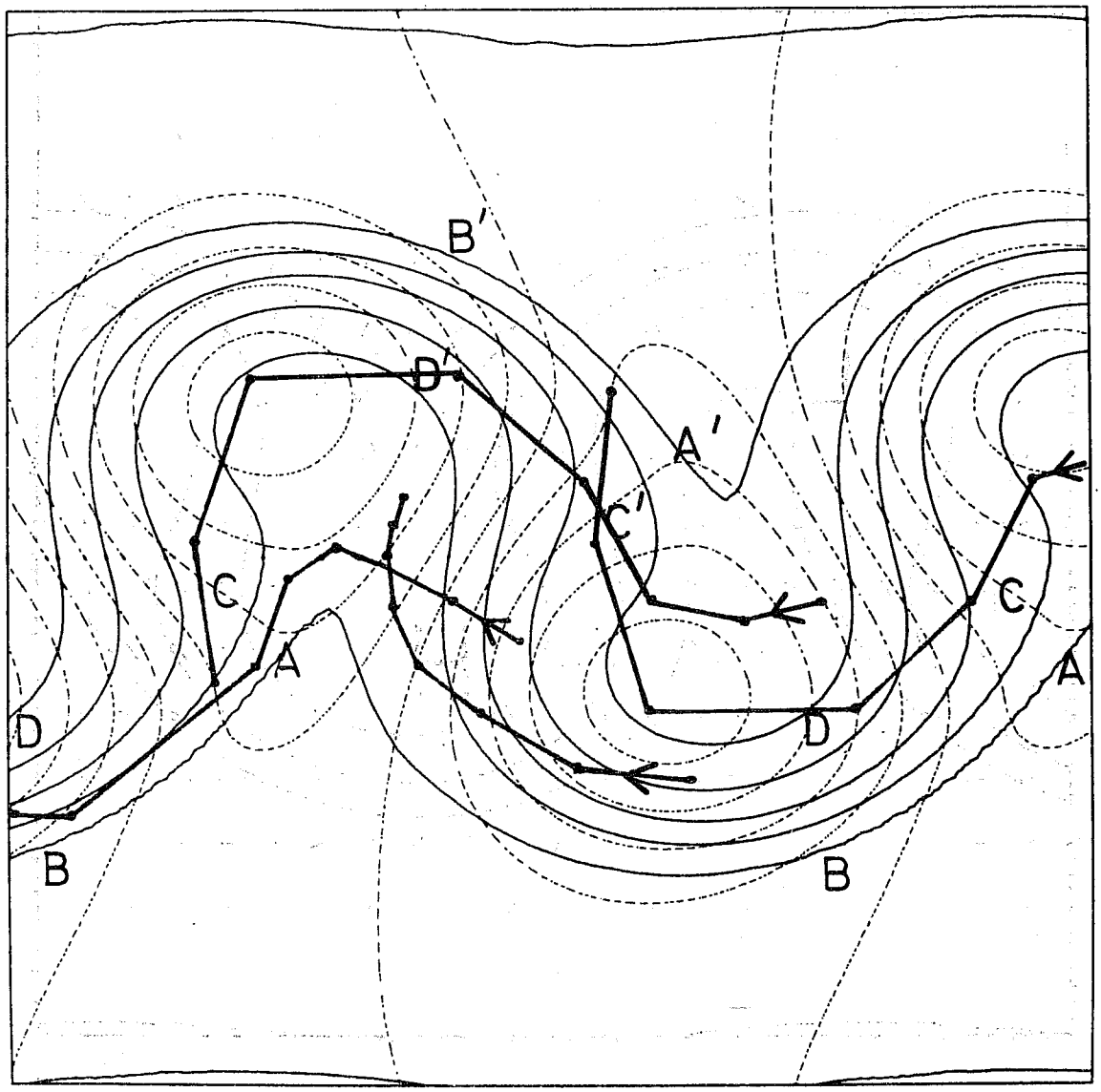

Fig. 9.4. Semi-geostrophic space Z = 0 potential temperature and height field for the μ = 1 mode at day 6. Also shown are trajectories from day 3 - day 6½ relative to the system.

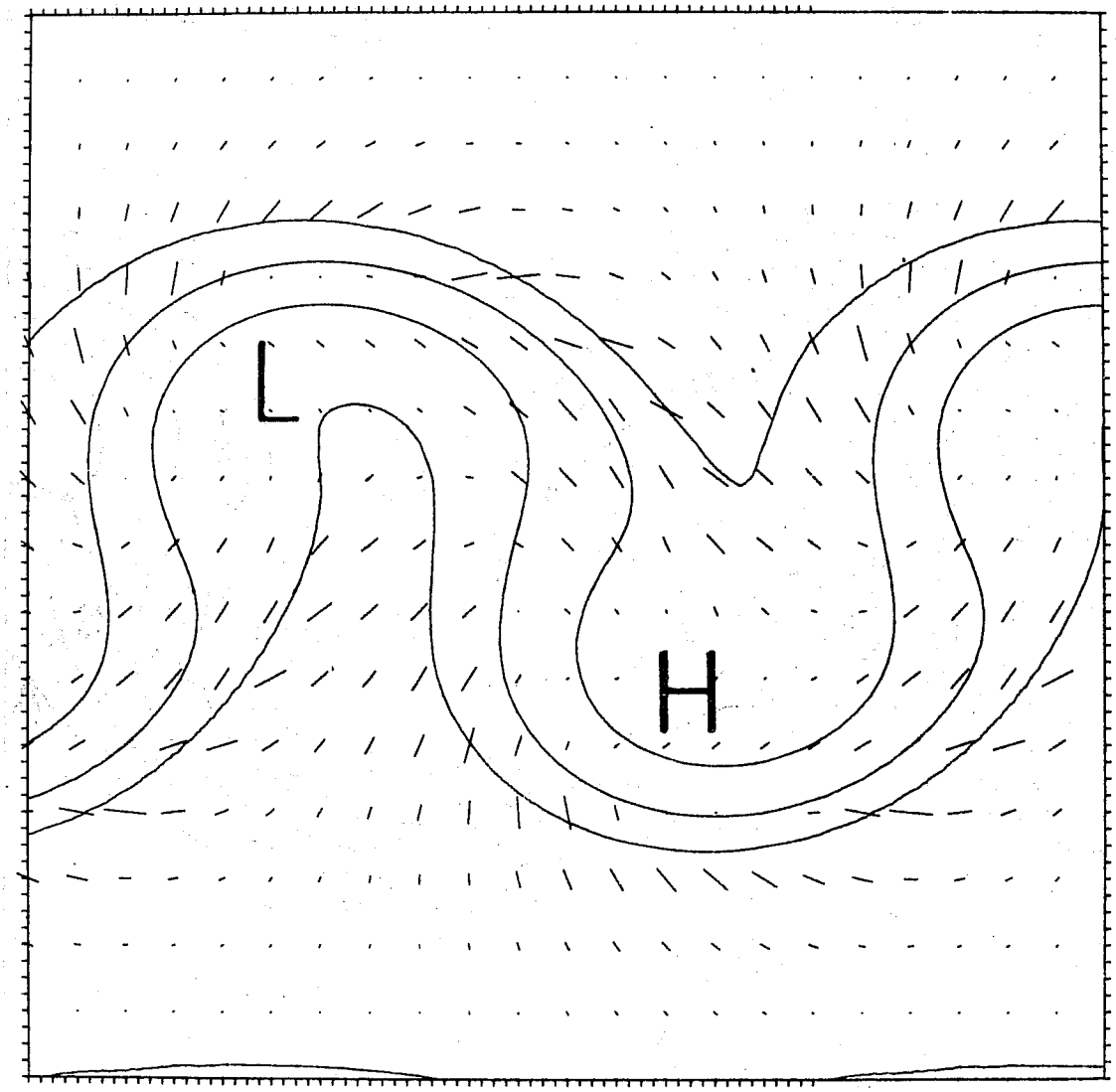

Fig. 9.5. Deformation field in semi-geostrophic space at Z = 0 for the μ = 1 mode at day 6. The dashes indicate the direction of the dilatation axis and the magnitude of the deformation. Height field extrema and some temperature contours are also shown.

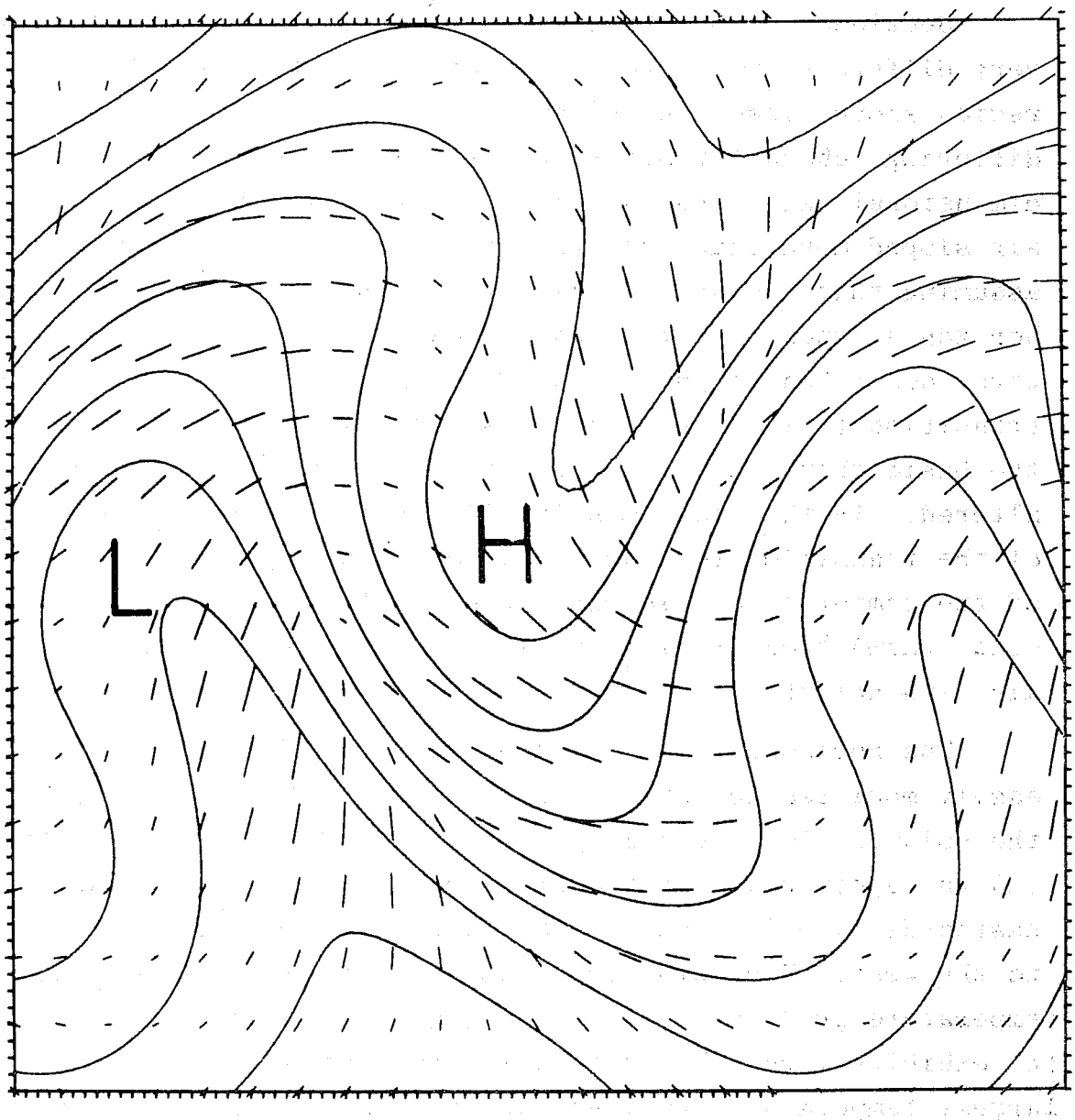

Fig. 9.6. Semi-geostrophic space deformation field at Z = 0 for the μ = .3 inverted mode at day 5.5.

enhanced (the warm front B).

9.2 Differences between cold and warm fronts

Sections across the cold front and warm front type B show very different structures. In particular the warm frontal region slopes less, in agreement with observation. These differing characteristics may be traced back to the two-dimensional Eady wave. There the transition from warm to cold air sloped more than the transition from cold to warm air, assuming that the system was moving from west to east. The horizontal shears in the zonal flows have forced the baroclinic waves described in this section to emphasise either the first transition (cold front) or the second (warm front type B) but the basic characteristics of the two transitions are not altered. In the two-dimensional Eady wave the different slopes of the transition regions are associated with the eastward tilt of the temperature wave with height. Thus in the incipient cold (warm) front region there is a tilt towards the warm (cold) air with height.

The horizontal convergence model described in section 8 is easily modified to take account of such tilts. Fig. 9.7 shows the solution for the same problem as in Fig. 8.1 except that in (a) the upper boundary temperature distribution is displaced eastwards by 500 km and in (b) it is displaced an equal amount to the west. The cold front case (a) shows large vorticity and temperature gradients in a steep region. The warm front case (b) exhibits large vorticity only near the boundaries. The largest temperature gradients occur in a region with a shallow slope.

It seems likely that many of the observed differences between cold and warm fronts may be associated with the forward tilt of the temperature wave with height, this being a necessary feature of a growing baroclinic wave.

9.3 Further studies

The basic meridional temperature fields used for the

(a)

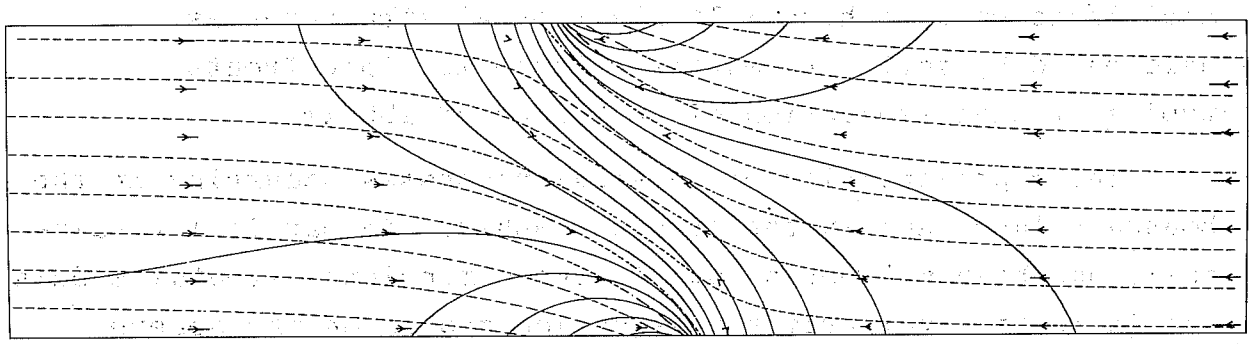

(b)

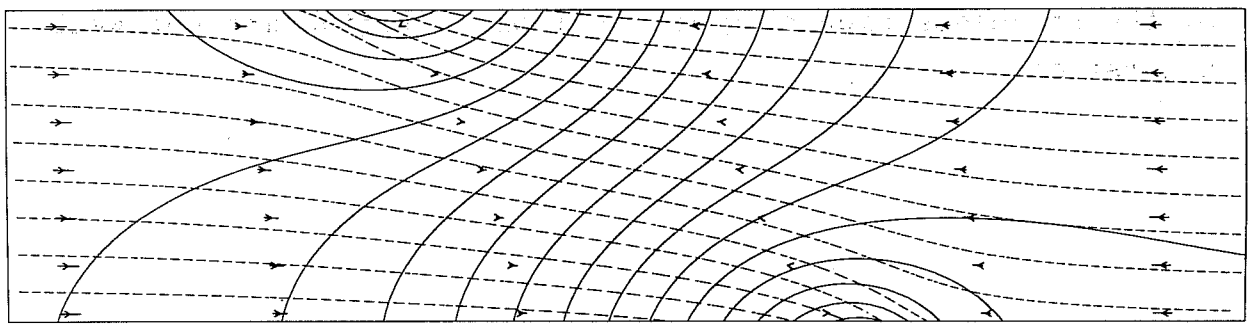

Fig. 9.7. Two-dimensional horizontal convergence model as in Fig. 8.1 but with the upper temperature wave displaced.
(a) "Cold front" - upper displacement 500 km towards warm air.
(b) "Warm front" - upper displacement 500 km towards cold air.

studies described so far have been extremely smooth. Further integrations have been performed with the uniform potential vorticity model in which irregularities have been inserted into the basic surface temperature field. With irregularities only of the order of 1K it is possible for the developing baroclinic wave to have multiple frontal structures as delineated by vorticity maxima. These multiple fronts typically have separation of the order of 150 km.

The representation of physical processes occurring in the boundary layer and in the free atmosphere, in particular rainfall, has been attempted both in two-dimensional frontal models and in multi-level primitive equation models on the sphere. The basic developments appear to change little. A growing baroclinic wave tends to produce convection along the cold front region and large-scale latent heat release ahead of and in the low pressure region. However, it is probably fair to state that the details of the feedback onto the larger scale of the processes happening in the frontal region are not well understood.

10. A mixture of theories, observations and unsolved problems

10.1 Baroclinic instability as a wave over-reflection phenomenon

Recently Lindzen and co-workers have been considering many instability phenomena in terms of the over-reflection of waves. In Lindzen et al. (1979) they propose the following picture of baroclinic instability viewed as the over-reflection of vertically-propagating gravity waves. As was suggested in section 2, the surface temperature gradient and associated low level vertical shear in the zonal wind is replaced by a layer in which $\bar{q}_y$ is large and negative. As indicated in Fig. 10.1 Rossby waves with horizontal phase speed c greater than the zonal flow speed at low levels propagate vertically in this layer. Above the layer, in region 2, $\bar{q}_y$ is now positive but $(\bar{u} - c)$ is still negative and so the vertical structure of the waves is exponential. Over-reflection from the critical layer or steering level, at which $\bar{u} = c$, can lead to a larger wave reaching the lower boundary. If the phases match then that wave reflected from the lower boundary may be in phase with the

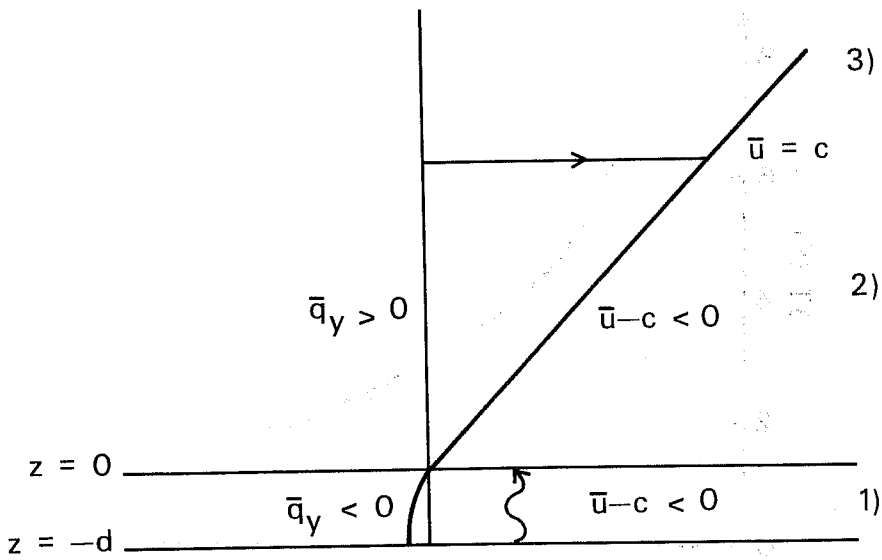

Fig. 10.1 Modification of the zonal flow and the three regions for the wave over-reflection view of baroclinic instability

original wave. Consideration of the gain in amplitude achieved in such a process and the time taken give a good first guess at the actual growth rates of baroclinic modes. The region 3 above the steering level is considered to be an "echo chamber" just passively responding to the growth below.

10.2 Critical temperature gradients

We have preferred to consider models of baroclinic instability with many levels or a continuous representation in the vertical. However the baroclinic instability of a two-level model has been studied extensively (e.g. Phillips, 1954). The stability characteristics are generally similar except that there is a critical shear

$$\left.\frac{\partial \bar{u}}{\partial z}\right|_c = \frac{\beta}{f^2} N^2 H \qquad (10.1)$$

below which instability is not possible. Stone (1978) compared the temperature gradient predicted by this criterion with the observed zonally averaged meridional gradient for the four seasons. His picture for winter is shown in Fig. 10.2.

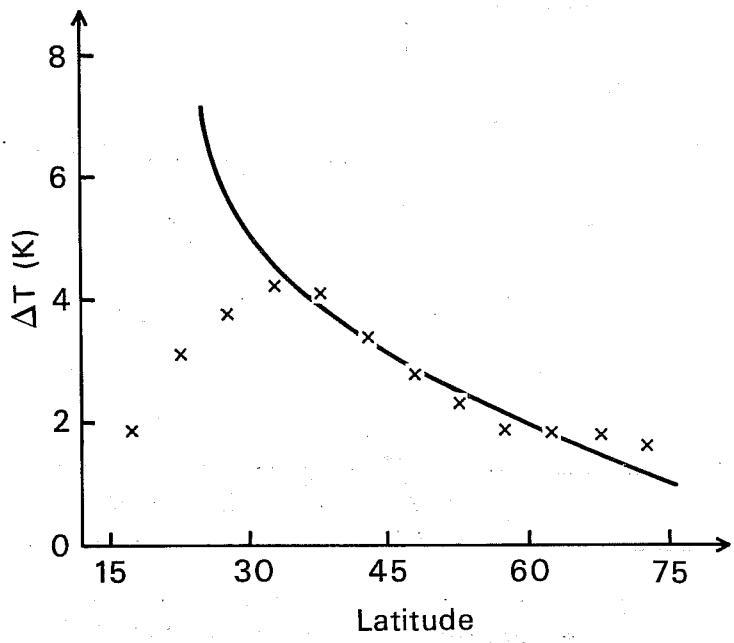

Fig. 10.2 solid curve gives the critical value as given by the 2-level model and the crosses the observed winter mean values (from Stone (1978))

The similarity of the observed shears and the critical shear is apparent in middle latitudes at all seasons. Possible reasons for this have been detailed by Held (1978). He pointed out that for shears less than $\frac{\partial \bar{u}}{\partial z}\Big|_c$ continuous or multi-level models predict instability but with a height scale

$$h = f^2 \frac{\partial \bar{u}}{\partial z} \Big/ \beta N^2 \qquad (10.2)$$

which is smaller than the scale height H which is also almost the tropospheric depth. For shears greater than $\partial \bar{u}/\partial z|_c$ the height scale is H. Scale arguments suggest that depth integrated heat transports by baroclinic eddies should be proportional to

$$N\, d^3 \left(\frac{\partial \bar{u}}{\partial z}\right)^2 \qquad (10.3)$$

where d is the height scale. For shears much less than the critical value, taking d = h as defined in 10.2 gives heat transports proportional to

$$\left(\frac{\partial \bar{u}}{\partial z}\right)^5 f^6 \Big/ \beta^3 N^5 \quad . \qquad (10.4)$$

For supercritical shears, d = H and the heat transport is proportional to

$$\left(\frac{\partial \bar{u}}{\partial z}\right)^2 NH^3 \quad . \qquad (10.5)$$

In particular, much below $\partial \bar{u}/\partial z|_c$ the heat transport is proportional to the fifth power of the shear and much above the critical value it is proportional to the square.

Therefore in an atmosphere with small meridional temperature gradients and associated vertical shears below $\partial \bar{u}/\partial z|_c$ the baroclinic eddies might be expected to be weak and shallow and thus to transport only a very small amount of heat polewards. The meridional temperature gradient may thus be expected to increase. On the other hand, in an atmosphere with supercritical meridional temperature gradients the eddies are strong and deep. Dependent on the actual diabatic heating rates, it is possible

that the temperature gradient may decrease.

Thus the similarity of the observed shears and the critical shear for a two-level model is consistent with ideas derived from linear β-plane theory. Whether non-linearity, true spherical effects and jet structure alter these ideas has yet to be tested.

10.3 Interaction of transient and steady waves

In a sequence of papers emanating from the University of Washington and NCAR, (Blackmon 1976, Blackmon et al., 1977, Lau, 1978, 1979a,b) NMC data for 9-11 winters has been used to build up a picture of the Northern Hemispheric general circulation varying in longitude as well as in latitude and pressure. Fig. 10.3 gives a summary of some of these findings. The 250mb

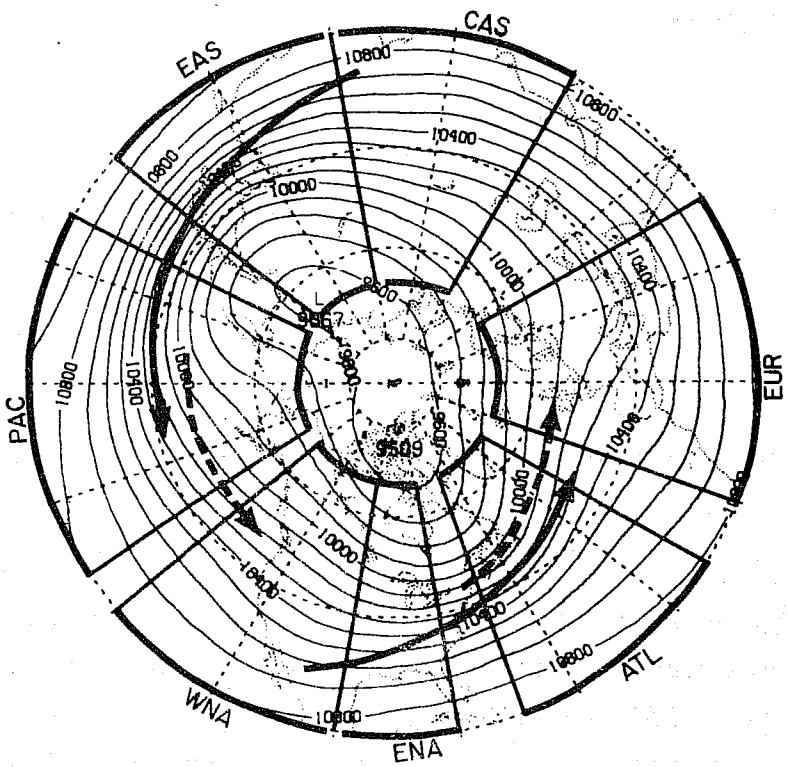

Fig. 10.3. The Northern Hemispheric winter time mean geopotential height at 250 mb plus jet streams (continuous arrows) plus transient eddy maxima (dashed arrows) (from Lau, 1978).

height field shows major troughs over east Asia and eastern N. America and a minor N. European trough. The zonal wind has

a maximum of 68 m s^{-1} off east Asia and 43 m s^{-1} over the east coast of N. America. The Pacific and Atlantic jet streams are marked in Fig. 10.3. Also marked are the regions of maximum geopotential height variability in the 2.5-6 day period. These transients appear to be a manifestation of baroclinic instability. They seem to develop downstream of the jet intensification and decay beyond the jet stream exit region.

The picture that emerges is one of mean zonal acceleration associated with upper level poleward ageostrophic velocities of 5 m s^{-1} over east Asia and 2 m s^{-1} over central N. America and then, in the Pacific and Atlantic sectors, comparable equatorward flows tending to decelerate the jets. The eddies appear to grow on this mean flow. The transports of heat and momentum by the eddies provide the feedback onto this mean flow. The transport of heat appears to act largely as a dissipation on the steady long-wave pattern. At 700 mb and 50°N, the zonal wavenumbers 2, 3 and 4 components of the horizontal eddy heat flux divergence are almost exactly in phase with the corresponding temperature wave components and give dissipation times of 7, 3 and 3 days respectively. The importance of the momentum transports $\overline{u'u'}$ and $\overline{u'v'}$ has also been stressed by Holopainen (1978). He presents evidence that suggests that vertically integrated eddy transports contribute significantly to the maintenance of the mean North Pacific and Icelandic lows.

Green (1977) has suggested that the anticyclonic vorticity of a major blocking event was also largely maintained by the transient eddies.

Thus a major new direction to the study of baroclinic instability is to view the process on a non-uniform basic flow and to discover under what conditions the eddies act to dissipate or maintain a long wave pattern. Lau (1979a) made some comparisons of the observed growth and decay in space and time of the baroclinic eddies with the life-cycle experiments described in scetion 6. However, the analogy is clearly not exact.

Frederiksen (1978, 1979) has studied the linear stability of a zonal flow plus planetary waves to perturbations of the form

$$e^{\sigma t} f(x,y) \cos[\omega t + \phi(x,y)] \quad . \qquad (10.6)$$

Each mode tends to be dominated by one zonal wavenumber and the growth rate and phase speed associated with this wavenumber is little altered by the presence of the planetary wave. The envelope of the instability f(x,y) indicates maximum amplitudes downstream of the regions where the critical shear (Eq. 10.1) is most exceeded. The non-oscillatory part of the heat and momentum transports also show maxima there.

In the U.K. Universities' Atmospheric Modelling Group nonlinear experiments on baroclinic instability on a long-wave flow have been started. These follow directly on from the previous life-cycle experiments. This time the experimental domain is hemispheric and the initial conditions contain a long wave which is the steady nonlinear solution corresponding to some prescribed forcing. Initial results indicate the interesting nature of the interaction between the long wave and the eddies but no definitive results are yet available.

References

Andrews, D.G. and Hoskins, B.J., 1978: Energy spectra predicted by semi-geostrophic theories of frontogenesis. J. Atmos. Sci., 35, 509-512.

Andrews, D.G. and McIntyre, M.E., 1976: Planetary waves in horizontal and vertical shear: The generalized Eliassen-Palm relation and the mean zonal acceleration. J. Atmos. Sci., 33, 2031-2048.

Andrews, D.G. and McIntyre, M.E., 1978: Generalized Eliassen-Palm and Charney-Drazin theorems for waves on axisymmetric flows in compressible atmospheres. J. Atmos. Sci., 35, 175-185.

Bers, A., 1975: Linear waves and instabilities. In Physique de Plasmas ed. C. De Witt and J. Peyraud, Gordon and Breach, New York.

Blackmon, M.L., 1976: A climatological spectral study of the 500 mb geopotential height of the Northern Hemisphere. J. Atmos.Sci., 33, 1607-1623.

Blackmon, M.L., Wallace J.M., Lau N.-C. and Mullen, S.L., 1977: An observational study of the Northern Hemisphere wintertime circulation. J. Atmos.Sci., 34, 1040-1053.

Blumen, W., 1968: On the stability of quasi-geostrophic flow. J. Atmos.Sci., 25, 929-931.

Boyd, J.P., 1976: The noninteraction of waves with the zonally-averaged flow on a spherical earth and the interrelationships of eddy fluxes of energy, heat and momentum. J.Atmos. Sci., 33, 2285-2291.

Bretherton, F.P., 1966: Baroclinic instability and the short wavelength cut-off in terms of potential vorticity. Quart.J.Roy.Met.Soc., 92, 335-345.

Brown, J.A., 1969: A numerical investigation of hydrodynamic instability and energy conversions in the quasi-geostrophic atmosphere. Part I. J.Atmos.Sci., 26, 352-65.

Burger, A.P., 1962: On the non-existence of critical wavelengths in a continuous baroclinic stability problem. J.Atmos.Sci., 19, 31-38.

Buzzi, A. and Tibaldi, S.,1978: Cyclogenesis in the lee of the Alps: A case study. Quart.J.Roy. Meteor.Soc., 104, 271-287.

Charney, J.G., 1947: The dynamics of long waves in a baroclinic westerly current. J.Meteor., 4, 135-162.

Charney, J.G., 1971: Geostrophic turbulence. J.Atmos. Sci., 28, 1087-1095.

Charney, J.G., Fjörtoft, R. and von Neumann, J., 1950: Numerical integration of the barotropic vorticity equation. Tellus, 2, 237-254.

Charney, J.G. and Stern, M., 1962: On the stability of internal baroclinic jets in a rotating atmosphere. J.Atmos.Sci., 19, 159-72.

Cressman, G.P., 1948: On the forecasting of long waves in the upper westerlies. J. Meteor., 5, 44-57.

Drazin, P.G. and Howard, L.N., 1966: Hydrodynamic stability of parallel flow of inviscid fluid. Advances in applied mechanics, 9, 1-89.

Eady, E.T., 1949: Long waves and cyclone waves. Tellus, 1, No. 3, 33-52.

Eliasen, E., 1961: On the interactions between the long baroclinic waves and the mean zonal flow. Tellus, 13, 40-55.

Eliassen, A., 1948: The quasi-static equations of motion. Geofys.Publikasjoner, 17, No.3.

Eliassen,A., 1959: On the formation of fronts in the atmosphere: The atmosphere and the sea in motion. New York, Rockefeller Institute Press, 277-287.
1962: On the vertical circulation in frontal zones. Geofys. Publikasjoner, 24, No. 4, 147-160.

Ertel, H., 1942: Ein neuer hydrodynamischer Wirbelsatz. Meteor.Z., 59, 277-281.

Frederiksen, J.S., 1978: Instability of planetary waves and zonal flows in two-layer models on a sphere. Q.J.Roy.Met.Soc., 104, 841-872.
1979: The effects of long planetary waves on the regions of cyclogenesis: Linear theory. J. Atmos.Sci., 36, 195-204.

Gall, R., 1976a: A comparison of linear baroclinic instability theory with the eddy statistics of a general circulation model. J.Atmos.Sci., 33, 349-373.
1976b: Structural changes of growing baroclinic waves. J.Atmos.Sci., 33, 374-390.
1976c: The effects of released latent heat in growing baroclinic waves. J.Atmos. Sci., 33, 1686-1701.

Garcia, R.V. and Norscini, R., 1970: A contribution to the baroclinic instability problem. Tellus, 22, 239-250.

Gent, P.R., 1974: Baroclinic instability of a slowly varying zonal flow. J.Atmos.Sci., 31, 1983-1994.

Gent, P.R., 1975: Baroclinic instability of a slowly varying zonal flow, Part 2. J.Atmos. Sci., 32, 2094-2102.

Green, J.S.A., 1960: A problem in baroclinic stability. Quart.J.Roy.Met.Soc., 86, 237-51.

Green, J.S.A., 1970: Transfer properties of the large-scale eddies, and the general circulation of the atmosphere. Quart.J.Roy.Met.Soc., 96, 157-184.

Green, J.S.A., 1977: The weather during July 1976: Some dynamical considerations of the drought. Weather, 32, 120-126.

Held, I.M., 1975: Momentum transport by quasi-geostrophic eddies. J.Atmos.Sci., 32, 1494-1497.

Held, I.M., 1978: The vertical scale of an unstable baroclinic wave and its importance for eddy heat flux parameterizations. J.Atmos.Sci., 35, 572-576.

Hollingsworth, A., 1975: Baroclinic instability of a simple flow on the sphere. Quart.J.Roy. Meteor.Soc., 101, 495-528.

Hollingsworth, A., Arpe,K., Tiedtke,M., Capaldo, M., Savijärvi, H., Akesson, O. and Woods, J.A., 1979: Comparison of Medium Range Forecasts made with two parameterization schemes. ECMWF Technical Report No. 13, 214 pp.

Hollingsworth, A., Simmons, A.J. and Hoskins, B.J., 1976: The effect of spherical geometry on momentum transports in simple baroclinic flows. Quart.J.Roy.Meteor.Soc., 102, 901-911.

Holopainen, E.O., 1978: On the dynamic forcing of the long-term mean flow by the large-scale Reynolds' stresses in the atmosphere. J.Atmos.Sci., 35, 1596-1604.

Hoskins, B.J., 1975: The geostrophic momentum approximation and the semi-geostrophic equations. J.Atmos.Sci., 32, 233-242.

Hoskins, B.J., 1976: Baroclinic waves and frontogenesis. Part I: Introduction and Eady waves. Quart. J.Roy.Meteor:Soc., 102, 103-122.

Hoskins, B.J. and Bretherton, F.P., 1972: Atmospheric frontogenesis models: mathematical formulation and solution. J.Atmos.Sci., 29, 11-37.

Hoskins, B.J., Draghici, I. and Davies, H.C., 1978: A new look at the -equation. Quart.J.Roy.Meteor. Soc., 104, 31-38.

Hoskins, B.J. and Simmons, A.J., 1975: A multi-layer spectral model and the semi-implicit method Quart.J.Roy.Meteor.Soc., 101, 637-655.

Hoskins, B.J. and West, N.V., 1979: Baroclinic waves and frontogenesis. Part II: Uniform potential vorticity jet flows-cold and warm fronts. J. Atmos.Sci., 36, in press.

Krishnamurti, T.N., Molinari, J., Pan, H.-L. and Wong, V., 1977: Downstream amplification and formation of monsoon disturbances. Mon.Wea.Rev., 105, 1281-1297.

Kuo, H., 1949: Dynamic instability of two-dimensional nondivergent flow in a barotropic atmosphere. J.Meteor., 6, 105-122.

Kuo, H., 1951: Dynamical aspects of the general circulation and the stability of zonal flow. Tellus, 3, 268-284.

Lau, N.-C., 1978: On the three-dimensional structure of the observed transient eddy statistics of the Northern Hemisphere wintertime circulation. J.Atmos.Sci., 35, 1900-1923.

Lau, N.-C., 1979a: The structure and energetics of transient disturbances in the Northern Hemisphere wintertime circulation. J.Atmos. Sci., 36, 982-995.
1979b: The observed structure of tropospheric stationary waves and the local balances of vorticity and heat. J.Atmos. Sci., 36, 996-1016.

Lintzen, R.S. and Farrel, B., 1979: Personal communication.

Mansfield, D., 1974: Polar lows: the development of baroclinic disturbances in cold air outbreaks. Quart.J.Roy.Meteor.Soc., 100, 541-554.

McIntyre, M.E., 1970: On the non-separable parallel flow instability problem. J.Fluid Mech., 40, 273-306.

McIntyre, M.E., 1972: Baroclinic instability of an idealized model of the polar night jet. Quart.J.Roy.Meteor.Soc., 98, 165-174.

Miles, J.W., 1964: A note on Charney's model of zonal-wind instability. J.Atmos.Sci., 21, 451-452.

Merkine, L.-O., 1977: Convective and absolute instability of baroclinic eddies. Geophys.Astrophys. Fluid Dynamics, 9, 129-157.

Moura, A.D. and Stone, P.H., 1976: The effects of spherical geometry on baroclinic instability. J.Atmos.Sci., 33, 602-616.

Namias, J. and Clapp, P.F., 1944: Studies of the motion and development of long waves in the westerlies. J.Meteor., 1, 57-77.

Newell, R.E., Kidson, J.W., Vincent, D.G. and Boer, G.J., 1972: The general circulation of the tropical atmosphere, and interactions with extratropical latitudes, Vol.1. The MIT Press, 258 pp.

1974: The general circulation of the tropical atmosphere, and interactions with extratropical latitudes, Vol.2. The MIT Press, 371 pp.

Newton, C.W., Phillips, N.A., Carson, J.E. and Bradbury, D.L., 1951: Structure of shear lines near the tropopause in summer. Tellus, 3, 154-171.

Ogura, Y. and Phillips, N.A., 1962: Scale analysis of deep and shallow convection in the atmosphere. J. Atmos.Sci., 19, 173-179.

Oort, A.H. and Rasmusson, E.R., 1971: Atmospheric circulation statistics. NOAA Prof. Pap. 5. (US Govt. Printing Office, Stock No. 0317-0045, c 55.25:5.)

Palmen, E. and Newton, C.W., 1969: Atmospheric circulation systems. Academic Press, 603 pp.

Pedlosky, J., 1964a: The stability of currents in the atmosphere and the ocean. Part I. J.Atmos. Sci., 21, 201-19.

1964b: The stability of currents in the atmosphere and the ocean. Part II. J.Atmos. Sci., 21, 342-53.

1964c: An initial value problem in the theory of baroclinic instability. Tellus, 16, 12-17.

Pedlosky, J., 1972: Limit cycles and unstable baroclinic waves. J.Atmos.Sci., 29, 53-63.

Petterssen, S., 1956: Weather Analysis and Forecasting. Second Edition, Vol. 1. McGraw-Hill, New York, 426 pp.

Phillips, N.A., 1954: Energy transformations and meridional circulations associated with simple baroclinic waves in a two-level, quasi-geostrophic model. Tellus, 6, 273-86.

Rossby, C.-G., 1945: On the propagation of frequencies and energy in certain types of oceanic and atmospheric waves. J.Meteor., 2, 187-204.

Sawyer, J.S., 1956: The vertical circulation at meteorological fronts and its relation to frontogenesis. Proc.R.Soc., A, 234, 346-362.

Simmons, A.J., 1974: The meridional scale of baroclinic waves.J.Atmos.Sci., 31, 1515-1525.

Simmons, A.J., 1977a: A note on the instability of the African easterly jet. J.Atmos.Sci., 34, 1670-1674.

1977b: Baroclinic instability in the summer mesosphere. Quart.J.Roy.Met. Soc., 103, 211-215.

Simmons, A.J. and Hoskins, B.J., 1975: A comparison of spectral and finite-difference simulations of a growing baroclinic wave. Quart.J.Roy.Meteor.Soc., 101, 551-565.

Simmons,A.J. and Hoskins, B.J., 1976: Baroclinic instability on the sphere:Normal modes of the primitive and quasi-geostrophic equations. J.Atmos.Sci., 33, 1454-1477.

Simmons, A.J. and Hoskins, B.J., 1977: Baroclinic instability on the sphere. Solutions with a more realistic tropopause. J.Atmos. Sci., 34, 581-588.

Simmons, A.J. and Hoskins, B.J., 1978: The life cycles of some nonlinear baroclinic waves. J.Atmos.Sci., 35, 414-432.

Simmons, A.J. and Hoskins, B.J., 1979: The downstream and upstream development of unstable baroclinic waves. J.Atmos.Sci., 36, in press.

Simons, T.J., 1972: The nonlinear dynamics of cyclone waves. J. Atmos.Sci., 29, 38-52.

Staley, D.O and Ball, R.L., 1977: On the wavelength of maximum baroclinic instability. J.Atmos. Sci., 34, 1679-1688.

Stone, P.H., 1966: Frontogenesis by horizontal wind deformation fields. J.Atmos.Sci., 23, 455-465.

Stone, P.H., 1969: The meridional structure of baroclinic waves. J.Atmos.Sci., 26, 376-89.

Stone, P.H., 1978: Baroclinic adjustment. J.Atmos.Sci., 35, 561-571.

Thacker, W.C., 1976: Spatial growth of Gulf Stream meanders. Geophys.Fluid Dynamics, 7, 271-295.

Tokioka, T., 1973: A stability study of medium-scale disturbances with inclusion of convective effects. J.Meteor.Soc.Japan, 51, 1-9.

Warn, H., 1976: Baroclinically unstable modes of a two-layer model on the sphere. J.Atmos. Sci., 33, 1478-1498.

White, A.A., 1977: Modified quasi-geostrophic equations using geometric height as vertical coordinate. Quart.J.Roy.Meteor.Soc., 103, 383-396.

Williams, R.T., 1967: Atmospheric frontogenesis: A numerical experiment. J.Atmos.Sci., 24 627-641.

Williams, R.T., 1968: A note on quasi-gesotrophic frontogenesis. J.Atmos.Sci., 25, 1157-1159.

Williams, R.T. and Plotkin, J., 1968: Quasi-geostrophic frontogenesis. J.Atmos.Sci., 25, 201-206.

Yeh, T.-C., 1949: On energy dispersion in the atmosphere. J.Meteor., 6, 1-16.